

**HILIC-MS ANALYSIS OF PROTEIN GLYCOSYLATION USING
NONPOROUS SILICA**

by

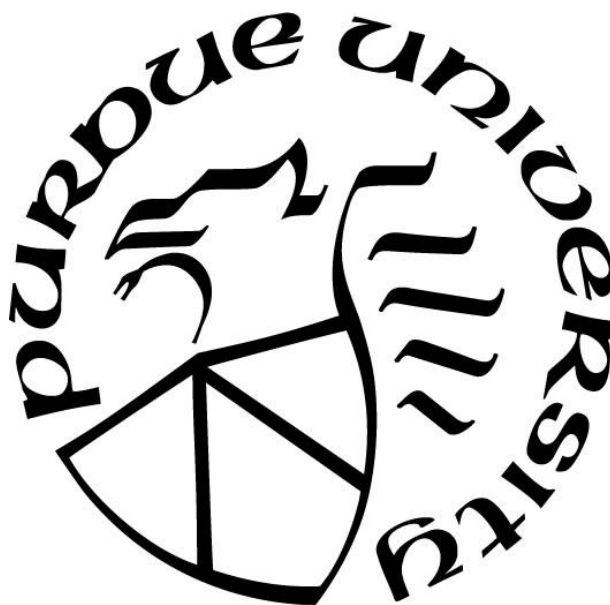
Rachel Elizabeth Jacobson

A Dissertation

Submitted to the Faculty of Purdue University

In Partial Fulfillment of the Requirements for the degree of

Doctor of Philosophy



Department of Chemistry

West Lafayette, Indiana

December 2018

THE PURDUE UNIVERSITY GRADUATE SCHOOL
STATEMENT OF DISSERTATION APPROVAL

Dr. Mary Wirth, Chair

Department of Chemistry

Dr. Peter Kissinger

Department of Chemistry

Dr. Chittaranjan Das

Department of Chemistry

Dr. Abram Axelrod

Department of Chemistry

Approved by:

Dr. Christine Hyrcyna

Head of the Departmental Graduate Program

To my grandmother

ACKNOWLEDGMENTS

First, I would like to express my gratitude to my research advisor, Professor Mary Wirth, for her support during my time at Purdue. She had faith in my future abilities as a scientist by accepting me into her lab, supported me financially with grant monies, trusted me with the training and mentorship of her lab members, taught me to think more critically with regards to experimental design and literature, and has held up high standards for me during my training.

Thank you also to my thesis committee members, Prof. Peter Kissinger, Prof. Chitta Das, and Prof. Abram Axelrod, for their time and efforts supporting my graduate research.

I would also like to acknowledge my collaborators during my PhD studies. These include Yiyang Zhou, Alexis Huckabee, Edwin Alzate, Charlie Bupp, and Yunqian Zou from the Wirth lab and Taylor Zhang, Bingchuan Wei, Wendy Sandoval, and Guanghui Han from Genentech. I have been fortunate to have productive collaborations and fruitful discussions with regards to our shared scientific endeavors.

Thank you to the Wirth lab members past and present who have inspired, assisted, and supported me through my time in the lab. Special thanks to Alexis for her mentorship and training in lab; Charlie, Edwin, Yiyang, John, Jonathan, and Yunqian for their collaboration and support. Thank you also to Leye, Xiang, Brian, Ao, Nick, Gavin, Ximo, Tamika, Tyrel, Cameron, Yun, and Aaron for your advice, support, and encouragement.

I have been well-funded during my time at Purdue. Thank you to the Chemistry department for my positions as a teaching assistant and graduate assistant. Thank you also to Genentech for sponsoring my research. Finally, thank you to the National Institutes of Health for a Traineeship.

Last but certainly not least, I would like to thank my friends and family. First, to my incredibly supportive husband and love of my life Vince. My mother, Shelley, especially with regards to holding down the fort at home. My brother, Josh, and sister-in

law Harmonie who bring me happiness and remind me I'm not crazy. My grandparents on both sides of the family, who supported me both personally and financially through high school and college. My father, Paul, who loves to brag to his coworkers about his daughter getting her PhD. To my in-laws, Mary Jean, Dave, and Evan, for your comfort and support. Thank you all for your love and encouragement through my research and life. I am blessed to have you.

ABBREVIATIONS

A	Eddy diffusion term in Van Deemter equation
AAm	Acrylamide
ACN	Acetonitrile
AFP	Alfa-fetoprotein
AGET	Activators Generated by Electron Transfer
ATRP	Atom Transfer Radical Polymerization
B	Longitudinal diffusion term in Van Deemter equation
C	Mass transfer term in Van Deemter equation
CE	Capillary electrophoresis
CpB	Carboxypeptidase B
CQA	Critical quality attribute
DFA	Difluoroacetic acid
D_m	Analyte's diffusion coefficient in the mobile phase
d_p	Particle diameter
DTT	Dithiothreitol
ESI	Electrospray ionization
FA	Formic acid
FDA	Food and Drug Administration
Fab	Antigen-binding fragment
(Fab') ₂	Antigen-binding fragment
Fc	Fragment crystallizable region
Fd'	Heavy chain portion of the Fab fragment
FPP	Fully porous particles
FWHM	Full width half maximum
H	Plate height
HIC	Hydrophobic interaction chromatography
HILIC	Hydrophilic interaction liquid chromatography
HPLC	High performance liquid chromatography
IdeS	Immunoglobulin-degrading enzyme from <i>Streptococcus pyogenes</i>
IEF	Isoelectric focusing
IEX	Ion-exchange chromatography
IgG	Immunoglobulin G
IPA	Isopropyl alcohol
k'	Retention factor
L	Column length
LCMS	Liquid chromatography – mass spectrometry
mAb	Monoclonal antibody

MALDI	Matrix assisted laser desorption/ionization
mCl	Trimethylchlorosilane
mBC	((Chloromethyl) phenylethyl) dimethylchlorosilane
Me ₆ TREN	Tris[2-(dimethylamino)ethyl]amine
MS	Mass Spectrometry
N	Number of theoretical plates
NME	New molecular entity
NP	Normal phase
NPP	Nonporous particles
PAAm	Polyacrylamide
PSA	Prostate specific antigen
PTM	Post translational modification
RBF	Round bottom flask
RPLC	Reversed phase liquid chromatography
R _s	Resolution (chromatographic figure of merit)
SEM	Scanning electron microscope
SI	Surface initiated
SPP	Superficially porous particles
tBC	(Chloromethyl)phenylethyl- trichlorosilane
tCl	Methyltrichlorosilane
TEM	Transmission electron microscope
TFA	Trifluoroacetic acid
TIC	Total Ion Count
t _R	Retention time
t ₀	Dead time
UHPLC	Ultra high performance liquid chromatography
W	Peak width
W _{1/2}	Full width half maximum
W _B	Width of peak at base
α	Selectivity (chromatographic figure of merit)
γ	Obstruction factor
ν	Linear flow rate (of mobile phase through column)
λ	Packing factor of column

TABLE OF CONTENTS

ACKNOWLEDGMENTS	4
ABBREVIATIONS	6
CHAPTER 1. INTRODUCTION	20
1.1 Protein chromatography	20
1.1.1 Importance of protein chromatography	20
1.1.2 Basics of chromatography	20
1.1.3 Challenges and quirks of protein chromatography	26
1.1.4 Advances in protein chromatography	27
1.2 Glycosylation analysis	28
1.2.1 Current methods for glycosylation analysis	28
1.3 Hydrophilic interaction liquid chromatography.....	32
1.3.1 Basics of HILIC	32
1.3.2 HILIC for glycoprotein separation	33
1.4 Thesis overview	34
1.5 Figures.....	35
1.6 References	37
CHAPTER 2. PREPARATION AND USE OF NONPOROUS, SILYLATED, SILICA NANOPARTICLES FOR UHPLC COLUMN PACKING.....	41
2.1 Abstract	41
2.2 Unique Properties of Nonporous Silica Particles for Various Applications.....	41
2.3 Use of nonporous silica nanoparticles in chromatography	42
2.3.1 Discussion on use of nonporous particles.....	42
2.4 Thermal Treatment of Nonporous Silica	43

2.4.1	Purpose of calcination and annealing	43
2.4.2	Calcination and annealing procedures	43
2.5	Rehydroxylation of Annealed Silica	44
2.5.1	Purpose of rehydroxylation.....	44
2.5.2	Rehydroxylation Procedure	44
2.6	Silane Modification of Silica	44
2.6.1	Purpose of silanization.....	44
2.6.2	Silanization procedure	45
2.7	AGET ATRP Modification of Initiator Bearing Silica Particles	46
2.7.1	Purpose of AGET ATRP modification.....	46
2.7.2	AGET ATRP procedure	46
2.8	Conclusion	48
2.9	Figures.....	49
2.10	References	51
CHAPTER 3. DEVELOPMENT AND OPTIMIZATION OF IN SITU AGET ATRP FOR PRODUCTION OF POLYACRYLAMIDE HILIC COLUMNS		54
3.1	Introduction: Value and limitations of a polyacrylamide stationary phase	54
3.2	Previous development of AGET ATRP reaction for production of polyacrylamide HILIC HPLC columns.....	55
3.3	Surface initiated AGET ATRP reaction for producing stationary phase.....	56
3.4	Longer polyacrylamide chains decrease dependence on TFA.....	56
3.5	Monochlorosilanes vs trichlorosilanes for initiating polymerization	57
3.6	Loading capacity of PAAm column and commercial column.....	58
3.6.1	Column length and shape affects loading capacity.....	58
3.6.2	Particle size affects loading capacity and resolution	61
3.7	Comparing PAAm to commercial column	62

3.8	Conclusions.....	62
3.9	Figures and Tables	63
1.1	References.....	81
CHAPTER 4. UHPLC HILIC-MS FOR SEPARATION OF GLYCOSYLATED IGG1 FRAGMENTS		82
4.1	Abstract.....	82
4.2	Introduction.....	82
4.2.1	Monoclonal antibodies in the pharmaceutical industry	82
4.3	Method	86
4.3.1	HPLC column preparation.....	86
4.3.2	Sample preparation	87
4.3.3	HILIC and HILIC-MS	88
4.4	Results and Discussion	89
4.4.1	Necessity of digestion and reduction	89
4.4.2	Digestion and reduction time optimization.....	90
4.4.3	PAAm column and necessity of TFA	91
4.4.4	HILIC separation and MS peak identification.....	91
4.4.5	Deglycosylated Fc peak	93
4.4.6	Implementation	93
4.5	Conclusions.....	94
4.6	References.....	95
4.7	Figures and Table.....	100
CHAPTER 5. GLYCOPEPTIDE BIOMARKERS ENRICHED AND SEPARATED WITH HILIC		113
5.1	Introduction.....	113
5.1.1	Usefulness of AFP glycan determination in hepatocellular carcinoma.....	113

5.1.2	Solid phase extraction (SPE) HILIC with nonporous particles	113
5.2	Method	115
5.2.1	Production of HILIC-SPE beads	115
5.2.2	Preparation of Ribonuclease B peptides	115
5.2.3	Preparation of AFP peptides	116
5.2.4	Enrichment of peptides with HILIC-SPE	116
5.2.5	Separation and detection of AFP glycopeptides with HILIC-UV and HILIC-MS	117
5.3	Results and discussion	117
5.3.1	HILIC separation of Ribonuclease B peptides	117
5.3.2	HILIC-MS of Ribonuclease B peptides	118
5.4	Conclusion and future work	118
5.5	Tables and figures	120
5.6	References	134
CHAPTER 6. FUTURE DIRECTIONS		136
6.1	New HILIC monomer for improved stability and altered functionality	136
6.2	Increasing surface area in column to improve loading capacity	136
6.3	Ion-exchange on silica-polymer hybrid column with low silanol activity	136
6.4	Elucidation of water layer surrounding HILIC stationary phase	137
6.5	Figures	139
6.6	References	140
PUBLICATIONS		147
VITA		143

LIST OF TABLES

Table 3.1: Comparing reproducibility of packing trichlorosilane and monochlorosilane initiator particles. Injection peak width and dead time for a 2 μ L packed with 100% acetonitrile injection. Data presented as mean \pm standard deviation of a 3-column set for each type of particles.	63
Table 3.2: Comparison of standard 5 cm PAAm column and PAAm conical column by varying mass injected of Ribonuclease B, then calculating asymmetry of the major peak. Both columns were produced using an <i>ex situ</i> AGET ATRP polymerization on 1 μ m nominal size particles.....	63
Table 3.3: Comparison of standard PAAm 5 cm, 1 μ m d_p column and a Waters Acquity Amide glycoprotein 10 cm column by varying mass injected of Ribonuclease B, then calculating asymmetry of the major peak.	64
Table 3.4: Comparison of PAAm 3 cm columns of varying particle size, 0.75, 1.0, and 1.5 μ m d_p nonporous particles were tested with varying mass injected of Ribonuclease B, then calculating asymmetry of the major peak. Since the free volume of the 1.5 μ m column was tested to be slightly greater than the 1.0 or .75 μ m columns, two flow rates were tested in an attempt to make fairer comparisons: the same flow rate as the other columns (100 μ L/min), and an adjusted flow rate (129 μ L/min) to match the greater free volume.....	65
Table 4.1: Peak identification by HILIC-MS. The glycan structures and expected masses, in addition to the observed masses of the Fc/2-glycan fragments are detailed.....	100
Table 5.1: PeptideCutter output showing peptide sequence from Ribonuclease B digestion with high specificity α -chymotrypsin. ^{18,19} In bold, red type is the glycosylated asparagine (N) at position 60.	120
Table 5.2: PeptideCutter output showing peptide sequence resulting from AFP digestion with trypsin. In bold, red type is the glycosylated asparagine (N) at position 251. Note that this peptide has only 8 amino acids on the chain. Table continues on next two pages as well.	121
Table 5.3: Comparison of theoretical and experimental glycopeptide masses of Ribonuclease B chymotrypsin digest, including glycan composition.	123

LIST OF FIGURES

Figure 1.1: Graph showing the increase in the number of biologic NME's over the past 7 years. This emphasizes the value of improving analytical techniques for biological drugs.²35

Figure 1.2: Depiction of fully porous particles, “core-shell” or superficially porous particles, and nonporous particles and the potential paths an analyte could take on its route through the particle. A) Fully porous particles have the longest potential route, ultimately broadening peaks as the analyte molecules take different routes. B) Superficially porous particles minimize the risk of analytes remaining in the pores longer than identical analyte molecules, by reducing the paths an analyte can take. C) Nonporous particles have no pores in the particle and will therefore not allow analytes to interact with any surface other than the external shell of stationary phase.36

Figure 2.1: Chemical structure of trichlorosilanes used for AGET ATRP initiators. A) ((chloromethyl)phenylethyl)trichlorosilane B) methyltrichlorosilane.....49

Figure 2.2: Chemical structure of monochlorosilanes used for AGET ATRP initiators. A) ((chloromethyl)phenylethyl)dimethylchlorosilane B) trimethylchlorosilane.49

Figure 2.3: Diagram showing packing and modification setups. For packing, the reservoir was filled with a particle slurry and pushed through a union into the column. For modification, the reservoir was filled with a reaction solution and flowed through the column packed with initiator particles. During packing, the reservoir and column setup was sonicated to improve packing homogeneity.50

Figure 3.1: Chemical degradation of polyacrylamide as a result of hydrolysis, resulting in the acrylamide monomer to convert to acrylic acid. The amide is hydrolyzed into a carboxylic acid, changing selectivity.66

Figure 3.2: Comparison of two HILIC separations performed on columns produced with A) monochlorosilane and B) trichlorosilane initiators. A significant difference is not seen between the two separations. The absorbance difference is due to a more sensitive detector used for the monochlorosilane particles.....66

Figure 3.3: Comparison of A) mushroom and B) brush polymer configurations. Both configurations entail unbranched polymer chains directly attached to the surface. The conformations are dependent on the density of the polymer chain tethered to the surface. The mushroom conformation is found when the distance s between individual chains is greater than $2x$ the polymer's radius r . The brush conformation occurs when the polymer

chains are packed together, therefore the polymer chains are extended to a length of L . This conformation occurs when s is less than $2r$. Given the polymer chains' ability to move, the volume that it is likely to occupy is shaded.^{5,9}67

Figure 3.4: Diagram of the polyacrylamide polymer chains and the hypothesized mechanism of hydrophilic partitioning to specifically retain the glycan, leaving the protein sterically hindered from interacting with the stationary phase. The mobile phase is a solution of acetonitrile, water, and acid modifier.67

Figure 3.5: Comparison of the methods and polymer structure of A) columns polymerized before packing and B) columns polymerized after packing.68

Figure 3.6: HILIC chromatograms of ribonuclease B for the best three columns produced with A) *ex situ* and B) *in situ* polymerization. Chromatograms for the remaining five columns produced by C) *ex situ* and D) *in situ* polymerization. The gradient was 75 to 60% ACN + 0.1% TFA in 20 min. 2 μ L of a 1 mg/mL solution of Ribonuclease B was injected. UV absorbance detected at 215 nm, column temperature 30°C, and flow rate of 100 μ L/min.69

Figure 3.7: HILIC data for ribonuclease B and the corresponding plots of backpressure during the gradient elutions. 40 runs were done for each panel, which show the runs for the 1st, 20th, and 40th runs. The flow rates listed regard the chromatographic separations. (A) HILIC for *ex situ* growth with a flow rate of 100 μ L/min and (B) the corresponding backpressure. (C) HILIC for *ex situ* growth with a flow rate of 150 μ L/min and (D) the corresponding backpressure. (E) HILIC for *in situ* growth with a flow rate of 100 μ L/min and (F) the corresponding backpressure. (G) HILIC for *in situ* growth with a flow rate of 150 μ L/min and (H) the corresponding backpressure. The gradient was the same as in Figure 3.6.70

Figure 3.8: Comparison between horizontal and vertical polymerization. A) Horizontal polymerization grows the polymer chain one monomer at a time on a surface. B) Vertical polymerization attaches a polymer chain to a surface.71

Figure 3.9: PAAm column 1 μ m d_p , $L = 5$ cm, 15% gradient change in 30 min, A = H₂O + acid, B = ACN + acid, 50 μ L/min, 0.5 μ g Ribonuclease B injection 1 mg/mL in 75% ACN, A) 70 minute AGET ATRP polymerized column with conditions 0.1% TFA with gradient 75-60%, B) 70 minute AGET ATRP polymerized column with conditions 0.1% FA + 0.025% TFA with gradient 70-55%, C) 55 minute AGET ATRP polymerized column with conditions 0.1% TFA with gradient 75-60% D) 55 minute AGET ATRP polymerized column with conditions 0.1% FA + 0.025% TFA with gradient 70-55%72

Figure 3.10: A PAAm nonporous column has a maximum capacity of around 0.5 μg before resolution rapidly deteriorates for HILIC separations. A) 0.5 μg B) 2 μg C) 10 μg Ribonuclease B sample injection. Injection sample was in 80% ACN + 0.1% TFA. Gradient 1-minute stacking at 75% ACN followed by 75 to 60% ACN in 20 minutes. Both mobile phases 0.1% TFA acid modifier. 30°C column temperature. 620 nm particle diameter.....73

Figure 3.11: A Waters Acquity glycoprotein Amide column has a maximum capacity between 2 and 10 μg before overloading occurs for the largest peak for HILIC separations. A) 0.5 μg B) 2 μg C) 10 μg Ribonuclease B sample injection. Injection sample was in 80% ACN + 0.1% TFA. Gradient 30 seconds of stacking at 85% ACN followed by 67 to 60% ACN in 20 minutes. Both mobile phases 0.1% TFA acid modifier. 30°C column temperature.74

Figure 3.12: Comparison of ribonuclease B loading capacities taken on 2, 3, and 5 cm PAAm columns. The shorter columns exhibit peak fronting, indicative of overloading. .75

Figure 3.13: Comparison of 2 and 5 cm columns with varying injection mass. The shorter column is unable to match the resolution of the longer column, indicating that the longer length is necessary for a high-quality separation.75

Figure 3.14: A) Example of a linear adsorption isotherm, where the concentration of the solute adsorbed onto the stationary phase and the concentration of the solute in solution increase and decrease with one another at the same linear rate. B) The Langmuir isotherm, a nonlinear curve used to depict chromatographic deviation from the linear isotherm. C) Nonlinearity due to “overloading” ultimately results in retention times shifting and fronting or tailing peaks, as depicted in the chromatogram. As the mass injected increases, the retention time shifts forward, and fronting worsens. C’s depiction of an overloaded run is adapted from Dolan in LCGC.¹⁰76

Figure 3.15: A) Depiction of the conical column used. A separate cone-shaped stainless-steel fixture was placed at the head of a 30 mm column and packed with the column. B) A standard column used as a comparison 5 cm in length.76

Figure 3.16: Ribonuclease B separations performed on both the machined conical column and a standard column. A) Conical column zoomed in. B) Standard column zoomed in. C) Conical column showing entire separation. D) Standard column showing entire separation. Injection masses were varied to determine if the conical column resulted in improved loading capacity. It appears that loading capacity is slightly improved over the 5 cm column, judged by a lower amount of shifting in the retention time with increased injection mass.....77

Figure 3.17: Comparison of peak asymmetry for 0.75, 1.0, and 1.5 μm particle diameter columns. Ribo B was injected in varying masses and asymmetry of the largest peak calculated as a stand-in for peak capacity. Given the difficulty in measuring peak width of higher injection masses due to overlap with other peaks, another method was used to compare peak capacity as well (retention time shifting).78

Figure 3.18: Comparison of loading capacity of varying sized particles. Ribonuclease B was injected in varying masses onto columns, then the largest peak was analyzed for retention time changes. A) Change in retention time (min) B) Conversion of retention time (min) to retention volume (μL) as a fairer comparison of 1.5 μm dp column run at 129 $\mu\text{L}/\text{min}$. The 0.75 μm column shows the least change in retention as injection mass increases, while the 1.5 μm column shows the most change. Note that all columns, even the 0.75 μm particle diameter, shifts retention between 0.1 and 0.5 μg , showing that it is still overloaded.....79

Figure 3.19: PAAm column is superior for small sample masses compared to Waters column, the latter of which loses minor peaks due to broadening and does not separate leading minor peaks from the major glycoform. A) Nonporous PAAm column with 1-minute stacking at 75% ACN followed by 75 to 60% ACN gradient in 20 minutes. B) Waters Acquity glycoprotein Amide column. Both have an injection of 0.5 μg Ribonuclease B in 80% ACN + 0.1% TFA. Gradient 30 seconds of stacking at 85% ACN followed by 67 to 60% ACN in 20 minutes. Both have mobile phases 0.1% TFA acid modifier and 30°C column temperature.....80

Figure 4.1: Scheme comparing middle-down vs the gold standard of glycosylation analysis. A) In the gold standard, the enzymatic glycan release is slow, followed by labeling before fluorescence or MS detection. B) In the middle-down approach, releasing the Fc subunit is fast, needs no labeling, and can be detected via UV or MS immediately after digestion.....101

Figure 4.2: A more detailed scheme for middle-down production of IgG1 subunits. Fragments are generated by IdeS digestion below the hinge region, followed by DTT reduction of disulfide bonds. The released Fc/2 fragments bearing glycans are then ready for HILIC analysis.102

Figure 4.3: Comparison of varying acid modifiers in separation of digested and reduced IgG1 on long-chain polyacrylamide column. A) 0.1% TFA, 75 to 65 %B. B) 0.1% FA + 0.025% TFA, 75 to 65 %B. C) 0.5% FA, 57 to 47 %B. All run conditions were 10% ΔB in 20 min, 70 $\mu\text{L}/\text{min}$, 0.5 μg IgG1 digested and reduced injected in starting gradient, detection at 280 nm. Column was a 1 μm dp in-situ polyacrylamide HILIC column produced with a 70 min reaction time.....103

Figure 4.4: Comparison of digested and reduced IgG1 to unaltered IgG1 shows the latter elutes far after the subunits. A) Digested and reduced IgG1 B) Whole IgG1. Column is of a different particle size from the rest of the paper, $d_p = 620$ nm. Conditions 75 to 60% ACN in 20 min at 30°C, 1.4 μ g injection, 100 μ L/min, UV detection 215 nm.....104

Figure 4.5: Relative peak area recovery of IgG1 Fc glycoforms in HILIC-HPLC-UV. A 15 min reduction of IgG1 provides 4x greater recovery than the unreduced IgG1, despite both being cleaved from the Fab fragment by IdeS. Note that the reduced IgG1 has an outlier of low recovery; this outlier is the first run of the set which seems to be causing the low recovery.....105

Figure 4.6: A) Peak heights and errors for varying times of digestion with IdeS. B) Peak heights and errors for varying times of reduction with DTT, after digestion with IdeS. The peaks are as labeled in Figure 3A. The height of each peak is represented as the percentage of total Fc/2 glycoforms in the sample. The error bars represent the 95% CI based on three replicate reactions, each followed by HILIC separation and quantitation by peak area.106

Figure 4.7: HILIC chromatograms using UV detection at 215 nm for IgG1 Fc/2 fragments prepared as in scheme from Figure 1 A) Commercial column (Waters Acquity Amide Glycoprotein 2.1 mm x 150 mm), with conditions 70 to 63% ACN in 20 min at 30°C, 4 μ g injection, 200 μ L/min. B) Same as panel A but absorbance is zoomed 10x. C) Polyacrylamide brush layer HILIC column (2.1 mm x 5 mm), with conditions 75 to 65% ACN in 20 min at 30°C, 1 μ g injection, 100 μ L/min. D) Same as panel C but absorbance is zoomed 10x. For both columns, 0.1% TFA was used as the mobile phase additive. ..107

Figure 4.8: A) HILIC-MS of the Fc/2 glycoforms of the pharmaceutical grade IgG1 using the polyacrylamide brush layer HILIC column, with the labels identifying each of the glycans. B) Discovered glycan structures based on MS identification.....108

Figure 4.9: The deconvoluted mass spectra for all peaks labeled in the chromatogram of Figure 4.8A, except for peaks 4,5.109

Figure 4.10: Raw mass spectra of the 8 peaks, separated via HILIC as seen in the chromatogram of Figure 4.8A, showing the charge distributions and their m/z range from the electrospray process. These were used to generate the deconvoluted mass spectra presented in the paper.109

Figure 4.11: A) Deconvoluted mass spectrum for overlapped peaks 4 and 5, showing presence of the expected Man5 peak and a G0F peak with a C-terminal lysine. The overlap with peak 3 gives the large single from G0F. B) Initial chromatogram (black) and chromatogram after enzymatic removal of the C-terminal lysine using CpB (red),

confirming the presence of G0F+Lys in the initial chromatogram at this peak position.	110
Figure 4.12: Digested and reduced IgG1 separated in HILIC, with A) treated with PNGase F to remove the glycosylation from the Fc fragment and B) no treatment with PNGase F. In the PNGase F treated chromatogram, the deglycosylated Fc elutes as a separate peak. The glycosylated Fc has not disappeared entirely from the chromatogram, indicating an incomplete digestion.	111
Figure 4.13: HILIC chromatograms of IdeS and PNGase F digested and DTT reduced IgG1 with A) MS and B) UV detection. The difference in weight between 23783 and 25198 is consistent with the G0 glycan which confirms the loss of the glycan.	111
Figure 4.14: Scheme depicting a rapid, automated workflow for on-site analysis during biomanufacture to ensure correct glycosylation.	112
Figure 5.1: Depiction of a procedure used for cartridge SPE.	124
Figure 5.2: HILIC separations of ribonuclease B glycopeptides varying solvent modifier. PAAm 750 nm dp lab-produced column was used for separations. A) UV Absorbance at 215 nm wavelength, 0.1% TFA. B) UV absorbance at 215 nm, 0.1% FA + 0.025% TFA. Gradient stacked for 1 min at 95% ACN, then 95-60% ACN in 40 minutes, then 5 minutes of rinsing at 60% ACN before returning to 95% ACN for reconditioning. Flow rate was 50 μ L/min for both separations.	125
Figure 5.3: HILIC separations of Ribonuclease B glycopeptides varying solvent modifier. Waters Acquity Glycoprotein 100 mm HILIC column was used for separations. A) UV Absorbance at 215 nm wavelength, 0.1% TFA. The reason for the baseline increase at the end of the run is the change in UV absorbance at the end of the gradient. Later experiments the time was extended to circumvent this issue. B) UV absorbance at 215 nm, 0.1% FA + 0.025% TFA. Gradient stacked for 1 min at 95% ACN, then 95-60% ACN in 40 minutes, then 5 minutes of rinsing at 60% ACN before returning to 95% ACN for reconditioning. Flow rate was 100 μ L/min for both separations.	126
Figure 5.4A: HILIC-MS of ribonuclease B glycopeptides by peak using the lab-produced PAAm column. MS TIC chromatogram from 800-1400 m/z, 0.1% FA + 0.025% TFA, 95-60% ACN in 40 minutes, 50 μ L/min.....	127
Figure 5.5A: HILIC-MS of ribonuclease B glycopeptides by peak using the Waters Acquity column. A) MS TIC chromatogram from 800-1400 m/z, 0.1% FA + 0.025% TFA, 95-60% ACN in 40 minutes, 100 μ L/min.	131

Figure 6.1: Scheme showing hydrolysis of polyacrylamide on silica surface. The amide group on polyacrylamide is hydrolyzed to a hydroxyl group, producing a copolymer of acrylamide and acrylic acid on the surface.139

Figure 6.2: Comparison of the monomer used in this work and the new monomer currently being tested for improved stability in HILIC stationary phases. A) Acrylamide
B) N-hydroxymethylacrylamide139

CHAPTER 1. INTRODUCTION

1.1 Protein chromatography

1.1.1 Importance of protein chromatography

Biologics are the fastest growing segment among novel pharmaceutical actives and will only increase with a greater number of biosimilars coming onto the market.^{1,2} Figure 1.1 shows the increase in FDA approvals of biologic new molecular entities (NMEs) from 2011-2017. Since proteins and other biological molecules are produced by cellular machinery, an inherently imprecise process, these products will be heterogeneous. Furthermore, heterogeneity can be introduced during the purification process, storage, or stress conditions (temperature, light, chemical modifications).³ Protein heterogeneity has a great effect on function, stability, immunogenicity, and clearance; therefore it is necessary to control these processes.^{4,5} The control process must first begin, however, with characterization.⁶ Chromatography can aid in this analysis, including providing orthogonal information to mass spectrometry (MS). As biologics continue to increase in number of regulatory approvals, chromatography is expected to be used in their characterization.

1.1.2 Basics of chromatography

Chromatography is a broad range of techniques used to fractionate molecules in a mixture by their differing properties. The molecules separated are analytes, and the mixture is a sample. The sample is dissolved in the mobile phase, which carries the analytes through the packed bed. In liquid chromatography, which is the focus of this dissertation, the mobile phase is a liquid and the stationary phase is a solid. The constituents of the sample travel through the mobile phase at different rates, depending on their attraction to the stationary phase. The method used in this dissertation is column chromatography, where the mobile phase moves through the stationary phase packed in a cylindrical column. Silica particles are modified to produce a stationary phase and packed

inside the column, producing a packed bed. To observe the physical separation of the analytes, a detector is placed at the end of the column. Detection techniques include mass spectrometry, UV absorbance, and fluorescence.

1.1.2.1 Figures of merit in chromatography

A chromatographic separation can be judged by a variety of metrics including resolution, column efficiency, selectivity, retention time, and peak broadening. These figures of merit are not independent of one another but are useful descriptions of specific separation mechanisms. A wide range of conditions can affect these metrics and can be changed to improve the separation.

1.1.2.1.1 Resolution

Resolution (R_s) is a description of how far apart two peaks are in a separation, calculated in Equation 1, where t_{RB} is the retention time of analyte B, t_{RA} is the retention time of analyte A, W_A is the peak width of analyte A, and W_B is the peak width of analyte B. The equality on the right can be used to calculate R_s from a chromatogram. To show a mathematical relationship between resolution, the analyte retention factors, efficiency, and selectivity, use the center equality as follows where N is the number of theoretical plates, α is a selectivity term equaling k_2/k_1 , k_1 is the retention factor for analyte 1, and k_2 is the retention factor for analyte 2.

$$R_s = \left(\frac{\sqrt{N}}{4} \right) \left(\frac{\alpha - 1}{\alpha} \right) \left(\frac{k_2}{k_2 + 1} \right) = \frac{2[t_{RB} - t_{RA}]}{W_A + W_B} \quad (1)^7$$

As discovered in (1), resolution is dependent on column efficiency, and the interplay between the column and the analyte (selectivity and retention). These properties are explained in more detail below.

1.1.2.1.2 Retention factor

The retention factor (k') is the ratio of the analyte's retention time on the column to the dead time (t_0) shown in Equation (2):

$$k' = \frac{t_R - t_0}{t_0}$$

(2)

A high k' value tells us that the analyte is well retained, spending a long time interacting with the stationary phase. There are several ways to adjust the retention of an analyte, falling into two categories: switching out the column to one with a different stationary phase or adjusting solvent strength of the mobile phase. Changing the ratio of solvents A and B in the mobile phase will affect the retention, as will selecting a different solvent.

1.1.2.1.3 Selectivity

One of the most powerful tools to affect selectivity is changing the column stationary phase. Changing the pH, adding an ion-pairing reagent, or adding salts can affect ionizable groups on the analyte or stationary phase – further affecting selectivity. The selectivity factor α describes how well two analytes can be separated on a specific column due to the differences in each analyte's interactions. The selectivity factor shows the relationship between the analytes' distribution constants K or their retention factors k' , shown in (3):

$$\alpha = \frac{K_B}{K_A} = \frac{k'_B}{k'_A}$$

(3)

1.1.2.1.4 Efficiency

Peak efficiency describes the dispersion as the analyte travels through the HPLC system and column. These dispersion effects cause the original injection to take on a Gaussian peak shape upon detection. The plate number (N) describes the amount of broadening the HPLC column and system has added to the peak, ultimately describing the quality of column performance. Equation 4 shows the calculation for plate number, where t_R is retention time, w_b is the width of the peak at the base, and $w_{1/2}$ is full width at half max (FWHM).⁸

$$N = 16 \left(\frac{t_R}{w_b} \right)^2 = 5.54 \left(\frac{t_R}{w_{1/2}} \right)^2$$

(4)

The higher the number of theoretical plates, the more sample components could be separated under these conditions. Furthermore, more plates result in narrower peaks. A related concept, plate height (H) or “height equivalent to a theoretical plate” (HETP), is shown in Equation (5) where L is column length. Since H is inversely proportional to N, the shorter the plate height, the more efficient the separation.

$$H = \frac{L}{N}$$

(5)

Efficiency is most related to the physical factors inside the column. Particle size, packing quality, and column dimensions all play a role to determine efficiency. Furthermore, extra-column parameters such as injection volume and dead volume (detector cell, tubing, unions) affect efficiency as well, usually in a deleterious context. Finally, the flow rate affects column efficiency in a variety of ways, which can be discussed by the Van Deemter equation.

1.1.2.2 Van Deemter equation

A chromatographic separation can be judged by a variety of metrics including resolution, peak broadening, peak shape, and speed. A wide range of conditions can affect these metrics and can be changed to improve the separation. The Van Deemter equation can be used to explain and predict the effects of changing the flow rate⁷.

$$H = A + \frac{B}{v} + Cv$$

(6)

In (6), H is the plate height, a measure of efficiency. Kinetic factors that affect the plate height are eddy diffusion (A-term), longitudinal diffusion (B-term), and the analyte’s resistance to mass transfer (C-term). These factors are specific to an individual column and analyte. The plate height is also dependent on the linear flow rate (v) of the mobile

phase through the column. Finally, the plate height has a contribution from the instrument.

Going into more detail, eddy diffusion results from multiple potential pathways the analyte can take through the packed bed. Since the analyte must zig-zag through the particles, some analytes will travel a longer distance than others (as an analogy, look up a YouTube video of Plinko and watch as a ball dropping can travel many different paths on its way to the bottom). The A-term can be further broken down into the following determining variables: λ (packing factor) and d_p (particle diameter). The A-term is independent of flow rate in this equation.

$$A = 2\lambda d_p \quad (7)$$

The B-term, longitudinal diffusion, can be determined from the analyte's diffusion coefficient in the mobile phase (D_m) and the obstruction factor for analyte diffusion (γ). The term captures zone broadening as a result of diffusion through the column. Faster flow rates can lessen the effects of zone broadening as it gives the analyte less time to diffuse. Furthermore, large molecules (for example proteins) cause this factor to be smaller due to a smaller D_m .

$$\frac{B}{v} = \frac{2\gamma D_m}{v} \quad (8)$$

The analyte's resistance to mass transfer (C-term) is subdivided into three processes: intraparticle mass transfer (C_p), mobile phase mass transfer (C_m), and stationary phase mass transfer (C_s):

$$C = C_p + C_m + C_s$$

Intraparticle mass transfer describes the analyte's time spent inside a particle (Equation (9)), since the analyte stops progressing linearly through the column once it becomes trapped inside a pore. The analyte solely moves through the particle and returns to the mobile phase flow via diffusion. Therefore, it increases linearly with flow rate v , since the analytes not in the pore continue moving through the column. The function of the retention factor k' (shown as $f_p(k')$) describes diffusion in and out of the porous

medium and obstruction by solid particles.⁹ Also contributing to intraparticle mass transfer are the square of the particle diameter d_p , and the mobile phase diffusion coefficient D_m .⁷ It should be noted that in the case of nonporous particles as in this thesis, this term is eliminated.

$$C_p = \frac{f_p(k')d_p^2}{D_m}v$$

(9)

Contributing to mobile phase mass transfer (Equation 10) are a function of the retention factor k' (shown as $f_m(k')$), the square of the particle diameter d_p , and the mobile phase diffusion coefficient D_m .⁷ It can be best explained as zone broadening due to an unequal flow profile across the column. Since flow is faster in the center of the column and fastest in the center of the interstitial space between particles, some analytes will be going faster and others slower.

$$C_m = \frac{f_m(k')d_p^2}{D_m}v$$

(10)

Stationary phase mass transfer describes the desorption rate of the analyte on/off of the stationary phase (Equation 11). Broadening occurs when the adsorbed fraction is left behind by the analytes in the mobile phase. Occurring on a large scale, this produces a Gaussian peak shape that continues to broaden with the number of interactions the analytes have with the stationary phase. However, C_s 's effects can be lessened at low flow rates.

$$C_s = \frac{f_s(k')d_p^2}{D_s}v$$

(11)

Once expanded, the Van Deemter now looks like this (12:

$$H = 2\lambda d_p + \frac{2\gamma D_m}{v} + \left(\frac{f_p(k')d_p^2}{D_m}\right)v + \left(\frac{f_m(k')d_p^2}{D_m}\right)v + \left(\frac{f_s(k')d_p^2}{D_s}\right)v$$

(12)

1.1.3 Challenges and quirks of protein chromatography

Liquid chromatography of dyes and small molecules has been performed for over 100 years.¹⁰ However, it is only recent technological advances that have allowed for fast liquid chromatography of proteins. Proteins are much larger than dyes and traditional small molecule drugs, producing different challenges. Tertiary and quaternary protein structures can decompose or be denatured outside of their biological location (e.g. aqueous, buffered solution). Transmembrane proteins are especially vulnerable, due to their exposed hydrophobic regions and will aggregate and precipitate from aqueous solution.¹¹ In some chromatographic situations, this denaturization is planned (e.g. organic mobile phase or added denaturant) or expected. In others, steps are taken to minimize denaturing by using salt buffers to maintain structure (e.g. hydrophobic interaction chromatography or HIC). A denatured protein would be linear or less “spherical,” and have more exposed hydrophobic groups. In contrast, a properly folded protein would keep its hydrophilic external character. Note that these characteristics would result in very different chromatographic retention despite being the same protein. Therefore, consideration of tertiary and quaternary structure must be taken in chromatography of proteins.

Another challenge of characterizing biological molecules is heterogeneity produced by post-translational modifications (PTMs). As an organism’s mechanism of changing protein structure and function in response to external or internal stimuli, PTM characterization is highly important for both protein drugs and diagnostic purposes.¹² While small molecule drugs do have chirality and impurities as sources of heterogeneity, it is nowhere near the scale of a protein drug’s PTMs. Furthermore, a protein’s PTMs are much smaller compared to the whole macromolecule compared to a small molecule’s potential impurities. Also, silica must be sufficiently annealed and polymerized to avoid silanols from interacting strongly with proteins and broadening peaks indiscriminately.

Finally, large molecules such as proteins have a low diffusion coefficient in solution, which can be detrimental to efficiency with fully porous particles. The reason is

that analytes inside the pores do not move linearly with the flow rate but rely on their diffusion in the mobile phase to move around and back out of the pore again. However, a poorly diffusing molecule can enter the pore and get “lost” in the porous particle, broadening peaks and reducing efficiency. To solve this problem, two solutions have been found relying on similar principles: reducing or eliminating the pores. Superficially porous particles with wide pores are shown to improve the efficiency of protein separations with minimal loss of sample loading capacity.¹³ Nonporous particles which eliminate the pores altogether are also shown to improve efficiency of protein separations.^{14–16}

1.1.4 Advances in protein chromatography

1.1.4.1 Silica purity and stationary phases

Advances in silica purity have crossed over from the fiber-optics industry. Silica particles have decreased in size and improved in homogeneity as manufacturers improve their methods. High pressure pumps have allowed very stable column packing and faster HPLC. Finally, advances in materials science and polymer chemistry have improved stationary phase design for greater specificity and fewer indiscriminate interactions (i.e. silanol).

1.1.4.2 Particle morphology affects analyte interaction with stationary phase

There are three types of silica particles used in packed bed media: fully porous, superficially porous (or “core-shell”), and nonporous (Figure 1.2). Fully porous particles were the traditional media used for packed beds in chromatography and are still the most widely used. There are a wide range of pore sizes and particle diameters available. For large molecules such as proteins, wider pores ($\sim 300\text{\AA}$) are used so as to not restrict access to the entire porous structure; for small molecules, smaller pores are preferred for their surface area ($\sim 100\text{\AA}$).¹³

Superficially porous particles were first introduced by Advanced Materials Technology's (AMT) Kirkland, DeStefano, and Langlois.^{17,18} This technology became widely available after a court ruling that AMT must withdraw their patent application for producing the particles. Superficially porous particles are more efficient than fully porous

particles of a similar size as well since the paths an analyte could take are fewer and more similar to each other. This results in a lower C term, ultimately lowering plate height.

Finally, nonporous particles are a niche column type, most commonly used for separation of proteins in UHPLC or capillaries. These columns have improved packing, more uniform particle shape and size, and smoother particle surface – leading to improved efficiency even over superficially porous particles. This efficiency improvement results from a minimized A-term and lower C-term than either variety of porous particles. However, nonporous particles also have lower loading capacity and higher back pressure compared to other morphologies, limiting their usage to small sample mass and low flow rates.

1.2 Glycosylation analysis

1.2.1 Current methods for glycosylation analysis

Glycosylation is a critical quality attribute (CQA) of therapeutic proteins such as monoclonal antibodies (mAbs), since even a difference in a single sugar monomer of the glycan can affect biological activity.¹⁹ In 2016 and 2017, 96% (24/25) of FDA approvals of biological NME's were glycosylated. In the same two years, 21/25 were mAbs with the breakdown being 18 IgG1 and 3 IgG4 variants.²⁰ As mAbs continue to dominate biologic drug trials and approvals, it is important to continue improving analytical techniques to identify and monitor microheterogeneity including glycosylation. During therapeutic glycoprotein development, complementary methods are usually used to determine glycosylation site, structure, and abundance.^{21,22} This is due to the lack of a “gold standard” that answers all questions necessary for regulatory purposes.²⁰ Therefore, multiple methods are employed based on the strength of the technique for a specific attribute. For example, site determination and deglycosylated fraction is possible with glycopeptide and intact glycoprotein analysis, but not at the glycan level.

1.2.1.1 Glycan (bottom-up)

N-linked glycans can be cleaved from the protein via PNGase, followed by derivatization to aid in detection. Derivatization is necessary for fluorescence or UV based detection methods and can be beneficial to CE and MS by adding charge to the

molecule. 2-AB (2-aminobenzamide) is commonly used for HILIC with fluorescence detection.²³ A database for 2-AB is available to determine the structure of glycans given their elution position in HILIC.²⁴ 2-AA (2-aminobenzoic acid) is another versatile label for HPLC or capillary electrophoresis (CE) separations, used for fluorescence, UV, or MS detection. 2-AA has one negative charge, improving CE separation and MS sensitivity. PA (2-aminopyridine) is another label with an HPLC elution database available, however is more tedious due to a necessary purification step for commercially produced PA.^{25,26} The fluorescent APTS (1-aminopyrene-3,6,8-trisulfonic acid) is used for capillary electrophoresis, providing three negative charges.²⁷

Derivatization is not necessary for MS detection, but is commonly performed to stabilize sialic acid residues, enhance signal, and aid in structure determination.^{26,28} Derivatives for MS analysis include hydrazide, permethylation, and the reductive amination techniques described above.²⁶ Ionization of the glycan (conjugated or native) is mainly performed using MALDI (matrix assisted laser desorption/ionization) or ESI (electrospray ionization). MALDI, while considered a “soft” ionization technique, causes dissociation of labile glycosidic bonds under standard vacuum conditions.²⁹ This affects native and reductively aminated glycans with sialic acid, uronic acid, sulfate, phosphate, and fucose residues.³⁰ Permethylation (replacement of hydrogens with methyl groups on hydroxyl, amine, and carboxyl groups) can improve stability of the residues aforementioned, allowing for MALDI to be performed without the dissociation of sialic acid residues.^{26,29} ESI is a softer ionization technique, with no sialic acid dissociation in native or conjugated glycans.³⁰ Furthermore, ESI can be used on-line with chromatography. An attractive combination for glycan analysis consists of native glycans separated by HILIC, followed by ESI-MS to minimize sample preparation. Tandem MS without chromatography is possible for glycan analysis, however, isomers may not be distinguishable.³⁰ For reference, currently the fastest available system for glycan cleavage and derivatization is the GlycoWorks RapiFluor-MS N-glycan kit, which advertises 30 minutes for sample preparation.³¹

1.2.1.2 Glycopeptide (bottom-up)

Glycopeptides are short amino acid chains with glycans still attached to the chain. Trypsin (or another promiscuous enzyme) digestion of a glycoprotein retains valuable structural information about the location of the glycan on the protein. Since many antibodies contain N-linked glycans on their Fab fragment, the ability to easily distinguish glycan location is highly relevant. Identity and relative abundances of each glycoform can still be determined with glycopeptide analysis. MALDI-MS and nanoLC coupled to ESI-MS are both common methods to identify glycan composition and attachment on the peptide level.^{29,30}

2-AB (2-aminobenzamide) is commonly used for HILIC with fluorescence detection.²³ A database for 2-AB is available to determine the structure of glycans given their elution position in HILIC.²⁴ 2-AA (2-aminobenzoic acid) is another versatile label for HPLC or capillary electrophoresis (CE) separations, used for fluorescence, UV, or MS detection. 2-AA has one negative charge, improving CE separation and MS sensitivity. PA (2-aminopyridine) is another label with an HPLC elution database available, however is more tedious due to a necessary purification step for commercially produced PA.^{25,26} The fluorescent APTS (1-aminopyrene-3,6,8-trisulfonic acid) is used for capillary electrophoresis, providing three negative charges.²⁷

Derivatization is not necessary for MS detection, but is commonly performed to stabilize sialic acid residues, enhance signal, and aid in structure determination.^{26,28} Derivatives for MS analysis include hydrazide, permethylation, and the reductive amination techniques described above.²⁶ Ionization of the glycan (conjugated or native) is mainly performed using MALDI (matrix assisted laser desorption/ionization) or ESI (electrospray ionization). MALDI, while considered a “soft” ionization technique, causes dissociation of labile glycosidic bonds under standard vacuum conditions.²⁹ This affects native and reductively aminated glycans with sialic acid, uronic acid, sulfate, phosphate, and fucose residues.³⁰ Permethylation (replacement of hydrogens with methyl groups on hydroxyl, amine, and carboxyl groups) can improve stability of the residues aforementioned, allowing for MALDI to be performed without the dissociation of sialic acid residues.^{26,29} MALDI can be an attractive option for high-throughput analysis, since the derivatization can be performed concurrently, followed by fast ionization and

detection. However, MALDI is best used with smaller molecules and proteins, and has a lower mass accuracy than other methods.

ESI is a softer ionization technique, with no sialic acid dissociation in native or conjugated glycans.³⁰ Furthermore, ESI can be used on-line with chromatography. An attractive combination for glycan analysis consists of native glycans separated by HILIC or porous graphitized carbon, followed by ESI-MS to minimize sample preparation. Tandem MS is possible for glycan analysis, however, isomers may not be distinguishable.³⁰ For reference, currently the fastest available commercial system for glycan cleavage and derivatization is the GlycoWorks RapiFluor-MS N-glycan kit, which advertises 30 minutes for sample preparation.³¹

1.2.1.3 Glycopeptide (bottom-up)

Glycopeptides are short amino acid chains with glycans still attached to the chain. Trypsin (or another promiscuous enzyme) digestion of a glycoprotein retains valuable structural information about the location of the glycan on the protein. Since many antibodies contain N-linked glycans on their Fab fragment, the ability to easily distinguish glycan location is highly relevant. Identity and relative abundances of each glycoform can still be determined with glycopeptide analysis. Enrichment using a HILIC-tip is often used in glycopeptide analysis due to the low abundance of glycopeptides compared to non-glycosylated peptides in the sample.³² Furthermore, the short peptide chain does not provide enough UV absorbance for quantitation.

MALDI-MS and nanoLC coupled to ESI-MS are both common methods to identify glycan composition and attachment on the peptide level.^{29,30} MALDI can be an attractive option for high-throughput analysis of many samples, since a trypsin digest and cleanup steps can be performed concurrently, followed by fast ionization and detection.³²

1.2.1.4 Glycoprotein (top-down) and fragmented glycoprotein (middle-down)

Intact glycoproteins can be analyzed directly to determine glycan structures, abundances, and location. Common methods include HPLC, CE, MS, and IEF. LC-ESI-MS is a technique commonly used in HILIC mode for glycoprotein analysis, but other modes including reversed-phase (RPLC) and size exclusion chromatography (SEC) have

been used as well.^{22,33–35} Furthermore, charge-based separations such as isoelectric focusing (IEF)^{36,37}, capillary electrophoresis (CE)^{36,38–40}, and ion-exchange chromatography (IEX)^{40,41} have been used to separate silylated from non-silylated species due to its charge.

To increase MS sensitivity for mAbs, it is common to add fragmentation techniques in the sample preparation steps.²¹ Reduction of disulfide bonds with DTT (dithiothreosine) or TCEP (tris(2-carboxyethyl)phosphine) is used to separate the light chains and heavy chains. This has the added effect of exposing the glycan, necessary if chromatography is used in tandem. To further increase MS sensitivity, additional fragmentation can be performed along with reduction including enzyme digestion with IdeS or papain, both of which cleave the heavy chain into two parts.

1.3 Hydrophilic interaction liquid chromatography

1.3.1 Basics of HILIC

Hydrophilic interaction liquid chromatography (HILIC) is a separation mode used for polar analytes. HILIC is valuable for highly polar analytes poorly retained in the more common reverse phase mode (RP). HILIC is similar to (and is sometimes considered a variant of) normal phase chromatography (NP), both utilizing a polar stationary phase and an organic mobile phase. However, HILIC uses a water-organic gradient for elution, while NP uses two organic solvents with differing levels of polarity. Furthermore, the HILIC separation mechanism is more complicated than NP. Considering the popularity and analytical power of HPLC-MS systems, HILIC is a valuable tool as a MS compatible chromatography mode.³³

HILIC stationary phases can be divided into two types: bare silica and bonded. Polar bonded phases are derivatized onto a solid support surface, and can be neutral, charged, or zwitterionic. Common examples of bonded phases used in HILIC include diol, amino, amide, cyano, and alkylamide.⁴²

HILIC mode can be considered mixed-mode, deriving selectivity from hydrophilic partitioning, hydrogen bonding, and electrostatic interactions.^{43,44} Choice of stationary phase and solvent conditions affect the extent of each selection mode.⁴⁵ For

example, zwitterionic sulfoalkylbetaine bonded phases strongly adsorb water. In HILIC mode, this water becomes part of the stationary phase, controlling selectivity through hydrophilic partitioning and hydrogen bonding.⁴⁶ Ion exchange interactions also affect retention on zwitterionic stationary phases. Common choices for HILIC separations are acids such as trifluoroacetic acid (TFA) and formic acid (FA), but salts can also be used as an added method to control retention and selectivity.⁴⁷

The neutral HILIC surface used in this paper is a dense brush layer of polyacrylamide. The surface is designed to exclude protein interactions with the aqueous layer, but to allow small glycan moieties to partition into the water layer. TFA is used as a buffer modifier in our separations as well, to lower the pH and act as an ion-pair for the charged protein. For MS detection, Formic acid (FA) or difluoroacetic acid (DFA) is used instead of TFA.

1.3.2 HILIC for glycoprotein separation

HPLC of glycans was first seen in the literature in 1985,⁴⁸ prior to the popularization of HILIC in 1990.⁴³ Alpert also was the first in the literature to apply HILIC to the separation of glycans in 1994.⁴⁹ From there, the next significant advance in glycan separation did not occur until 2011, when Tetaz and coworkers separated an intact protein by glycoform.³³ From this point, interest in HILIC of intact glycoproteins has exploded due to site-specific analysis and ease of sample preparation, especially compared to glycan-level analysis. More recent papers show a variety of commercial columns used for both glycoprotein, with no clear market leader. HILIC columns used for intact glycoprotein separations include but are not limited to: TSKgel Amide-80 (Tosoh Bioscience, Japan), ZIC-HILIC (SeQuant, Germany), PolyHYDROXYETHYL A (PolyLC, Columbia, MD), XBridge BEH Amide (Waters, Milford, MA), Acquity UPLC Glycoprotein BEH Amide (Waters), and AdvanceBio Glycan Mapping (Agilent Technologies, Santa Clara, CA).^{33,50–52} Commercial columns used for HILIC vary significantly in particle morphology and stationary phase design.

1.4 Thesis overview

The objective of this research is to develop and apply a HILIC UHPLC stationary phase that allows for separation of intact glycoproteins. In Chapter 1 I give an overview of the problems of current glycosylation profiling with regards to biotherapeutics, and my strategy to separate the intact glycoprotein with HILIC. Chapter 2 describes the methods used to produce the nonporous packing material and stationary phase. In Chapter 3 I describe previous work in developing a HILIC polyacrylamide stationary phase, and further improvements I have made. Chapter 4 describes development of an assay in collaboration with Genentech of therapeutic mAb glycosylation. In Chapter 5, I show HILIC-MS of digested ribonuclease B as a beginning step to analyze glycosylated biomarkers.

1.5 Figures

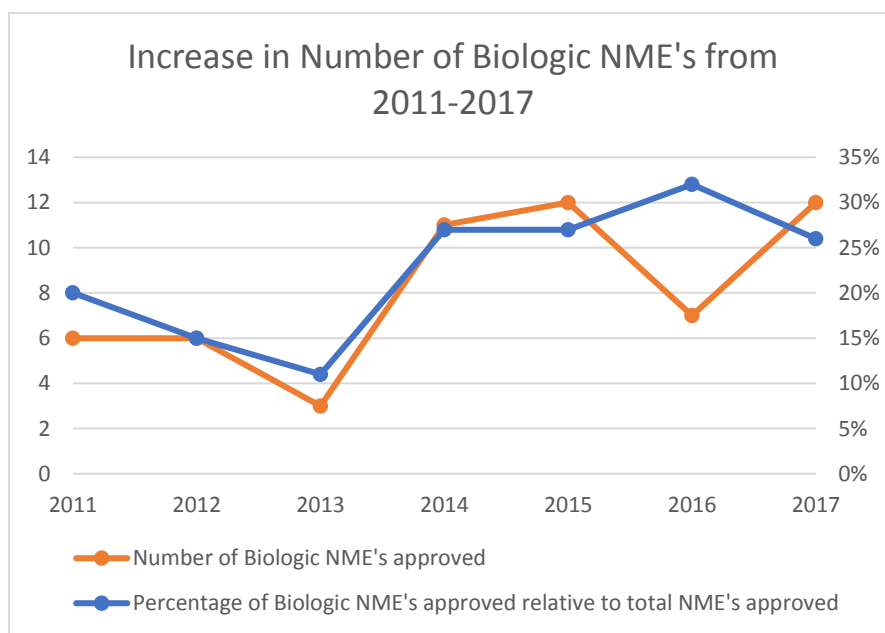


Figure 1.1: Graph showing the increase in the number of biologic NME's over the past 7 years. This emphasizes the value of improving analytical techniques for biological drugs.²

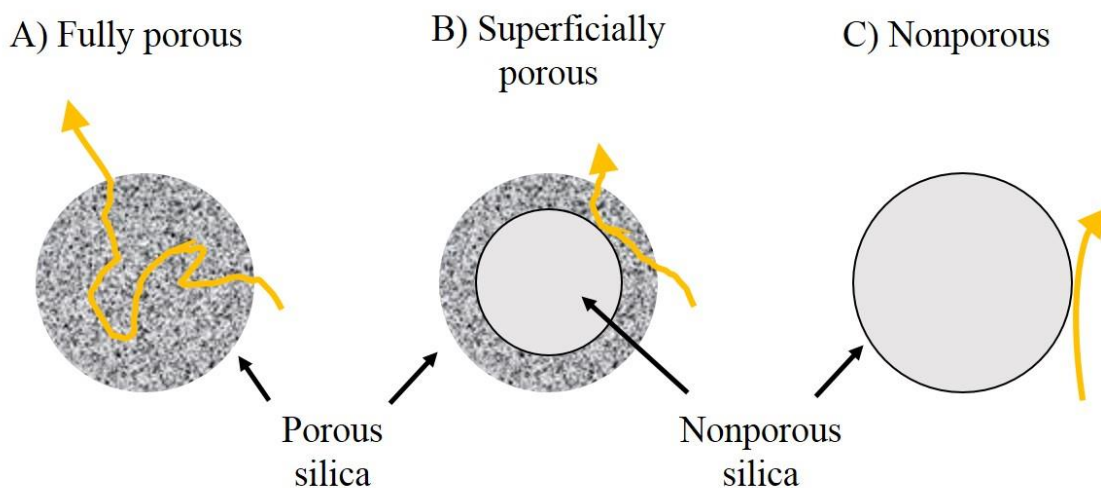


Figure 1.2: Depiction of fully porous particles, “core-shell” or superficially porous particles, and nonporous particles and the potential paths an analyte could take on its route through the particle. A) Fully porous particles have the longest potential route, ultimately broadening peaks as the analyte molecules take different routes. B) Superficially porous particles minimize the risk of analytes remaining in the pores longer than identical analyte molecules, by reducing the paths an analyte can take. C) Nonporous particles have no pores in the particle and will therefore not allow analytes to interact with any surface other than the external shell of stationary phase.

1.6 References

1. Center for Drug Evaluation and New Drugs at FDA: CDER's New Molecular Entities and New Therapeutic Biological Products. Available at: <https://www.fda.gov/Drugs/DevelopmentApprovalProcess/DrugInnovation/default.htm>. (Accessed: 7th September 2018)
2. Mirasol, F. Biologic NMEs Maintain Strong Presence in 2017 Drug Approvals. *BioPharm International* (2018). Available at: <http://www.biopharminternational.com/biologic-nmes-maintain-strong-presence-2017-drug-approvals>. (Accessed: 7th September 2018)
3. Liu, H., Gaza-Bulseco, G., Faldu, D., Chumsae, C. & Sun, J. Heterogeneity of Monoclonal Antibodies. *J. Pharm. Sci.* **97**, 2426–2447 (2008).
4. Farley, A. R. & Link, A. J. Chapter 40 Identification and Quantification of Protein Posttranslational Modifications. in *Methods in Enzymology* **463**, 725–763 (Elsevier, 2009).
5. Walsh, C. T., Garneau-Tsodikova, S. & Gatto, G. J. Protein Posttranslational Modifications: The Chemistry of Proteome Diversifications. *Angew. Chem. Int. Ed.* **44**, 7342–7372 (2005).
6. Berkowitz, S. A., Engen, J. R., Mazzeo, J. R. & Jones, G. B. Analytical tools for characterizing biopharmaceuticals and the implications for biosimilars. *Nat. Rev. Drug Discov.* **11**, 527–540 (2012).
7. Skoog, D. A., Holler, F. J. & Nieman, T. A. *Principles of Instrumental Analysis*. (Saunders College Publishing, 1998).
8. Theory_Of_HPLC_Chromatographic_Parameters.pdf.
9. Rogers, B. A. *et al.* Submicrometer Particles and Slip Flow in Liquid Chromatography. *Anal. Chem.* **87**, 2520–2526 (2015).
10. Berezkin, V. G. Biography of Mikhail Semenovich Tswett and translation of Tswett's preliminary communication on a new category of adsorption phenomena. *Chem. Rev.* **89**, 279–285 (1989).
11. Lodish, H. *et al.* Purifying, Detecting, and Characterizing Proteins. (2000).
12. Prabakaran, S., Lippens, G., Steen, H. & Gunawardena, J. Post-translational modification: nature's escape from genetic imprisonment and the basis for dynamic information encoding. *Wiley Interdiscip. Rev. Syst. Biol. Med.* **4**, 565–583 (2012).
13. Schuster, S. A., Wagner, B. M., Boyes, B. E. & Kirkland, J. J. Wider Pore Superficially Porous Particles for Peptide Separations by HPLC. *J. Chromatogr. Sci.* **48**, 566–571 (2010).

14. Wirth, M. J. Mass transport in sub-2- μ m high-performance liquid chromatography. *J. Chromatogr. A* **1148**, 128–130 (2007).
15. Malkin, D. S., Wei, B., Fogiel, A. J., Staats, S. L. & Wirth, M. J. Submicrometer Plate Heights for Capillaries Packed with Silica Colloidal Crystals. *Anal. Chem.* **82**, 2175–2177 (2010).
16. Rogers, B. J. & Wirth, M. J. Obstructed Diffusion in Silica Colloidal Crystals. *J. Phys. Chem. A* **117**, 6244–6249 (2013).
17. Kirkland, J. J., Schuster, S. A., Johnson, W. L. & Boyes, B. E. Fused-core particle technology in high-performance liquid chromatography: An overview. *J. Pharm. Anal.* **3**, 303–312 (2013).
18. AGILENT TECHNOLOGIES, INC., Plaintiff, v. JOSEPH J. KIRKLAND, JOSEPH J. DESTEFANO, TIMOTHY J. LANGLOIS, and ADVANCED MATERIALS TECHNOLOGY, INC., Defendants., 2010 Del. Ch. LEXIS 34. Available at: <https://advance.lexis.com/open/document/lpadocument/?pdmfid=1000522&crid=dXJuOmNvbnRlbnRJdGVtOjdYWU0tMzlnMmC1ZQjBNLUiwMDAtMDAwMDAtMDA&pddocfullpath=%2Fshared%2Fdocument%2Fcases%2Furn%3AcontentItem%3A7XYM-39M0-YB0M-B000-00000-00&pdcomponentid=5077>. (Accessed: 28th August 2018)
19. Mellstedt, H. Clinical considerations for biosimilar antibodies. *Eur. J. Cancer Suppl.* **11**, 1–11 (2013).
20. O’Flaherty, R., Trbojević-Akmačić, I., Greville, G., Rudd, P. M. & Lauc, G. The sweet spot for biologics: recent advances in characterization of biotherapeutic glycoproteins. *Expert Rev. Proteomics* **15**, 13–29 (2018).
21. Zhang, L., Luo, S. & Zhang, B. Glycan analysis of therapeutic glycoproteins. *mAbs* **8**, 205–215 (2016).
22. Domínguez-Vega, E. *et al.* High-resolution glycoform profiling of intact therapeutic proteins by hydrophilic interaction chromatography-mass spectrometry. *Talanta* **184**, 375–381 (2018).
23. Ivarsson, M., Villiger, T. K., Morbidelli, M. & Soos, M. Evaluating the impact of cell culture process parameters on monoclonal antibody N-glycosylation. *J. Biotechnol.* **188**, 88–96 (2014).
24. Royle, L. *et al.* HPLC-based analysis of serum N-glycans on a 96-well plate platform with dedicated database software. *Anal. Biochem.* **376**, 1–12 (2008).
25. Taniguchi, N. *et al.* *Experimental Glycoscience: Glycobiology*. (Springer Science & Business Media, 2009).

26. Ruhaak, L. R. *et al.* Glycan labeling strategies and their use in identification and quantification. *Anal. Bioanal. Chem.* **397**, 3457–3481 (2010).
27. Chen, F.-T. A. & Evangelista, R. A. Profiling glycoprotein N-linked oligosaccharide by capillary electrophoresis. *Electrophoresis* **19**, 2639–2644 (1998).
28. Bones, J., Mittermayr, S., O'Donoghue, N., Guttman, A. & Rudd, P. M. Ultra Performance Liquid Chromatographic Profiling of Serum N-Glycans for Fast and Efficient Identification of Cancer Associated Alterations in Glycosylation. *Anal. Chem.* **82**, 10208–10215 (2010).
29. Wada, Y. *et al.* Comparison of the methods for profiling glycoprotein glycans--HUPO Human Disease Glycomics/Proteome Initiative multi-institutional study. *Glycobiology* **17**, 411–422 (2007).
30. Leymarie, N. & Zaia, J. Effective Use of Mass Spectrometry for Glycan and Glycopeptide Structural Analysis. *Anal. Chem.* **84**, 3040–3048 (2012).
31. Lauber, M. A. *et al.* Rapid Preparation of Released N-Glycans for HILIC Analysis Using a Labeling Reagent that Facilitates Sensitive Fluorescence and ESI-MS Detection. *Anal. Chem.* **87**, 5401–5409 (2015).
32. Yang, X. *et al.* Ultrafast and high-throughput N-glycan analysis for monoclonal antibodies. *mAbs* **8**, 706–717 (2016).
33. Tetaz, T., Detzner, S., Friedlein, A., Molitor, B. & Mary, J.-L. Hydrophilic interaction chromatography of intact, soluble proteins. *J. Chromatogr. A* **1218**, 5892–5896 (2011).
34. Janin-Bussat, M.-C. *et al.* Cetuximab Fab and Fc N-Glycan Fast Characterization Using IdeS Digestion and Liquid Chromatography Coupled to Electrospray Ionization Mass Spectrometry. in *Glycosylation Engineering of Biopharmaceuticals* (ed. Beck, A.) **988**, 93–113 (Humana Press, 2013).
35. Zhang, Z., Pan, H. & Chen, X. Mass spectrometry for structural characterization of therapeutic antibodies. *Mass Spectrom. Rev.* **28**, 147–176 (2009).
36. Zhao, S. S. & Chen, D. D. Y. Applications of capillary electrophoresis in characterizing recombinant protein therapeutics: CE and CEC. *ELECTROPHORESIS* **35**, 96–108 (2014).
37. Reichel, C. & Thevis, M. Gel electrophoretic methods for the analysis of biosimilar pharmaceuticals using the example of recombinant erythropoietin. *Bioanalysis* **5**, 587–602 (2013).
38. de Kort, B. J., de Jong, G. J. & Somsen, G. W. Profiling of erythropoietin products by capillary electrophoresis with native fluorescence detection: CE and CEC. *ELECTROPHORESIS* **33**, 2996–3001 (2012).

39. Haselberg, R., de Jong, G. J. & Somsen, G. W. Low-Flow Sheathless Capillary Electrophoresis–Mass Spectrometry for Sensitive Glycoform Profiling of Intact Pharmaceutical Proteins. *Anal. Chem.* **85**, 2289–2296 (2013).
40. Thakur, D. *et al.* Profiling the Glycoforms of the Intact α Subunit of Recombinant Human Chorionic Gonadotropin by High-Resolution Capillary Electrophoresis–Mass Spectrometry. *Anal. Chem.* **81**, 8900–8907 (2009).
41. Schiestl, M. *et al.* Acceptable changes in quality attributes of glycosylated biopharmaceuticals. *Nat. Biotechnol.* **29**, 310–312 (2011).
42. Buszewski, B. & Noga, S. Hydrophilic interaction liquid chromatography (HILIC)—a powerful separation technique. *Anal. Bioanal. Chem.* **402**, 231–247 (2012).
43. Alpert, A. J. Hydrophilic-interaction chromatography for the separation of peptides, nucleic acids and other polar compounds. *J. Chromatogr. A* **499**, 177–196 (1990).
44. Hemström, P. & Irgum, K. Hydrophilic interaction chromatography. *J. Sep. Sci.* **29**, 1784–1821 (2006).
45. Fu, Q. *et al.* Carbohydrate separation by hydrophilic interaction liquid chromatography on a ‘click’ maltose column. *Carbohydr. Res.* **345**, 2690–2697 (2010).
46. Jandera, P. Stationary and mobile phases in hydrophilic interaction chromatography: a review. *Anal. Chim. Acta* **692**, 1–25 (2011).
47. Alpert, A. J. Effect of salts on retention in hydrophilic interaction chromatography. *J. Chromatogr. A* **1538**, 45–53 (2018).
48. Blanken, W. M., Bergh, M. L. E., Koppen, P. L. & van den Eijnden, D. H. High-pressure liquid chromatography of neutral oligosaccharides: Effects of structural parameters. *Anal. Biochem.* **145**, 322–330 (1985).
49. Alpert, A. J. *et al.* Hydrophilic-interaction chromatography of complex carbohydrates. *J. Chromatogr. A* **676**, 191–202 (1994).
50. Rinaldi, F. *et al.* Application of a rapid HILIC-UV method for synthesis optimization and stability studies of immunogenic neo -glycoconjugates. *J. Pharm. Biomed. Anal.* **144**, 252–262 (2017).
51. Tengattini, S. *et al.* Hydrophilic interaction liquid chromatography-mass spectrometry as a new tool for the characterization of intact semi-synthetic glycoproteins. *Anal. Chim. Acta* **981**, 94–105 (2017).
52. Periat, A. *et al.* Potential of hydrophilic interaction chromatography for the analytical characterization of protein biopharmaceuticals. *J. Chromatogr. A* **1448**, 81–92 (2016).

CHAPTER 2. PREPARATION AND USE OF NONPOROUS, SILYLATED, SILICA NANOPARTICLES FOR UHPLC COLUMN PACKING

2.1 Abstract

Chapter 2 provides an overview to the packed bed used in this work. I have included this section since nonporous nanoparticles are uncommon chromatographic media for UHPLC columns. However, with the trend of increasing UHPLC instrument pressures due to shrinking particle size, nonporous nanoparticles are gaining interest. The value of nonporous nanoparticles is realized with improved resolution and recovery, especially with regards to large protein separations. These separations are becoming more common as biomarkers and therapeutics, with only recent interest from column manufacturers to produce columns designed for protein separations. The various methods used to produce the packed bed are included in this chapter as well.

2.2 Unique Properties of Nonporous Silica Particles for Various Applications

Nonporous silica particles are used in a variety of applications including photonics/optics¹, chemical sensors², and chromatographic separation media³⁻⁵. These applications, among many others, take advantage of the favorable properties of silica particles. Colloidal crystals can be formed from silica spheres, forming a highly ordered and face centered cubic (fcc) structure. Methods of producing silica spheres result in a narrow particle size range. These monodisperse particles can self-assemble into close packed structures, aiding in many applications.⁶ As a result of these unique properties, nonporous silica particles are often used as a solid support. The advantage of the fcc structure has been shown in capillary packing³, thin films⁶, and membranes.⁷ Furthermore, silica has a high thermal conductivity, excellent for dispersing heat caused by friction and limiting the temperature gradient within a packed structure.⁸ Finally, the ability to tailor the surface through silanization of hydroxyl groups is a huge advantage. The particles may then be used, or further polymerized to tailor the characteristics of the surface.

2.3 Use of nonporous silica nanoparticles in chromatography

2.3.1 Discussion on use of nonporous particles

Traditional chromatography media are composed of porous silica particles packed into beds. Fully porous particles have the longest potential route, ultimately broadening peaks as the analyte molecules take different routes. Superficially porous particles minimize the risk of analytes remaining in the pores longer than identical analyte molecules, by reducing the paths an analyte can take. Nonporous particles have no pores in the particle and will therefore not allow analytes to interact with any surface other than the external shell of stationary phase. The movement of analyte inside a pore depends on pore diameter and analyte diffusion through the stagnant mobile phase. Slow analyte diffusion in the absence of flow causes peak broadening. Slow diffusion is most common in large molecules such as proteins, so nonporous particles have the most potential efficiency gain over porous particles in the cases of proteins and other large molecules.⁹

Also of interest in protein separations is the ability to increase flow rate with little change in efficiency.^{10,11} As previously mentioned, slow analyte diffusion in the absence of flow (while in the stagnant mobile phase in the pores) causes peak broadening. By eliminating the pores, the change in efficiency as a result of flow rate is no longer limited by the analyte in the pores, but the analytes' movement through the interstitial space and the on/off kinetics between the analyte and the stationary phase.¹² Nonporous particles are therefore much more amenable to faster flow rates.^{13,14}

Nonporous particles also shine in their overall homogeneity and production quality. Furthermore, the packing procedure does not introduce the presence of fines, a common problem in commercial porous columns causing clogging and heterogeneous paths.¹⁵ Size distribution of nonporous particles is much narrower than fully porous particles, as FPP typical particle diameter RSD is 10-20%¹⁶, but NPP is 8% (SupSil Premium, used in this thesis)¹⁷. Size heterogeneity has a large effect on separation efficiency of large molecules, therefore this should be minimized as much as possible.¹⁸

Small quantities (i.e. sub- μ g) of biomolecule are especially good targets for the use of nonporous particles. Given limited quantities of analyte in biopsies for biomarker analysis or biologics manufacture, these applications are easy to find. Nonporous particles have both a positive and negative attribute with regard to analyte quantity. The

positive is that quantitative recovery of analyte is possible with nonporous particles since molecules cannot get “stuck” in the pores.¹⁹ The negative is that due to their relatively low surface area of the stationary phase, nonporous columns exhibit a lower loading capacity when compared to their porous cousins.

2.4 Thermal Treatment of Nonporous Silica

2.4.1 Purpose of calcination and annealing

Calcination and annealing steps are performed prior to the modification of the particles. Calcination at 600 °C shrinks the spheres by driving out organic compounds and solvents used in the Stöber process of silica particle production. By “preshrinking” the particles, cracks in the packed bed are prevented due to sphere shrinkage. Furthermore, the refractive index is comparable to fused (solid) silica, which shows that the densities are similar.¹ Next, the particles are annealed at 1050 °C, which melts the outer surface to smooth roughness and pores, strengthens the surface, and decreases the number of isolated silanols on the surface.^{20,21}

2.4.2 Calcination and annealing procedures

Approximately 10-20 grams of silica particles (Superior Silica, Mesa, AZ) were placed in a covered crucible for 12 hours for calcination at 600 °C. Particle diameters from 100 -2000 nm were used in this thesis, most commonly 750, 1000, or 1500 nm nominal size. Once cool, particles were crushed in the crucible with a spatula, then funneled into a 500 mL round bottom flask (RBF). Ethanol (200 mL, 100%) was added to the flask and sonicated for 2 hours, or until all particles were suspended. After suspension, the particle slurry was centrifuged in 50 mL conical tubes at 6500 rpm for 5 minutes. Ethanol was decanted, and conical tubes were placed in a vacuum oven at 60 °C for 20 minutes or until dry. Particles were returned to the crucible and calcination steps were repeated twice. After the third calcination, the particles were not cooled, but the temperature was ramped to 1050 °C for 3 hours of annealing. The particles were then allowed to cool, crushed in the crucible with a spatula, and funneled into a 500 mL RBF. Ethanol (200 mL, 100%) was added to the flask, and sonicated overnight to suspend particles. The particle slurry was centrifuged in 50 mL conical tubes at 6500 rpm for 5

minutes. Ethanol was decanted and conical tubes were placed in a vacuum oven at 60 °C for 20 minutes or until dry.

2.5 Rehydroxylation of Annealed Silica

2.5.1 Purpose of rehydroxylation

Rehydroxylation requires boiling silica particles in a strong acid for an extended period of time. The previous annealing step condensed surface silanols to siloxane bonds, so rehydroxylation is necessary to restore silanols for silanization.²² Furthermore, rehydroxylation prior to silanization maximizes the hydrolytic and mechanical stability of the bonded phase.²³

2.5.2 Rehydroxylation Procedure

Annealed silica particles (6 grams) were suspended in 150 mL water in a 500 mL RBF under sonication for at least 2 hours. Once well suspended, 150 mL concentrated nitric acid was added. The RBF was placed in a sand bath at 350°C to reflux with stir bar overnight (minimum of 8 hours). If more or fewer particles were necessary to rehydroxylate, up to 2 grams of silica particles could be added per 100 mL total volume of nitric acid solution. The reaction was cooled while stirring. When cool, slurry was poured from the flask to 50 mL conical tubes. Tubes were centrifuged at 6500 rpm for 4 minutes. Liquid was decanted, and tubes were refilled with ultrapure water. Tubes were vortexed until particles resuspended. Particles were rinsed a minimum of twice more, until pH was approximately equal to that of ultrapure water. Particles were placed in a 60 °C vacuum oven until dry. Particles were used immediately in the next reaction or resuspended in water to preserve particle hydroxylation.

2.6 Silane Modification of Silica

2.6.1 Purpose of silanization

Silanes are used commercially as coupling agents²⁴, protective films²⁵, and surface property modifiers.²⁶ In this work, trichlorosilanes, and monochlorosilanes are used for covalent attachment of a halogen (Cl) for surface initiated AGET ATRP. Silanes

are also used directly as stationary phases bound to the silica surface. Trichlorosilanes form a crosslinked monolayer on the silica surface which minimizes silanol activity. This is highly valuable for separations where the silane acts as stationary phase. However, with a second polymer layer acting as the stationary phase the effects of silanols are minimal. Using monochlorosilanes simplifies the reaction but requires the use of an amine catalyst and heating.²⁷

2.6.2 Silanization procedure

2.6.2.1 Trifunctional benzyl chloride initiator

Dry toluene (200 mL) and rehydroxylated particles (2 grams) are added to a round bottom flask with septum. The particles are suspended via sonication. The silanes (chloromethyl)phenylethyl-trichlorosilane (4 mL; shown in Figure 2.1, Gelest, Morrisville, PA) and methyl trichlorosilane (200 μ L; shown in Figure 2.2, Gelest) are mixed in a small amount of dry toluene and added via syringe to the flask, limiting exposure to air and water. The reaction occurs for 3 hours with a nitrogen balloon attached to the septum. After completion, the reaction solution is poured into conical tubes, centrifuged, and decanted. This process is repeated three times to rinse the silanes from the particles. Particles are dried in a 60 °C vacuum oven.

2.6.2.2 Monofunctional benzyl chloride initiator

In this thesis, if not otherwise specified, the monofunctional benzyl chloride reaction was used for producing initiator particles. Rehydroxylated particles were prepared as previously described. The rehydroxylated particles (2 grams) were added to a 250 mL round bottom flask and suspended in dry toluene with sonication and magnetic stirring. The flask is purged with nitrogen. When suspended, ((chloromethyl) phenylethyl) dimethylchlorosilane (3.2 mL or 2% v/v; shown in Figure 2.2, Gelest) and butylamine (200 μ L or 0.1% v/v, Sigma Aldrich, Saint Louis, MO) were added to the flask via syringe. The reaction was refluxed for 1 hour at 80°C. Next, trimethylchlorosilane (200 μ L or 0.1% v/v; shown in Figure 2.2, Gelest) is added via syringe and the reaction continues for 2 hours. After completion, the particles were rinsed thrice in dry toluene and dried in a 60 °C vacuum oven for 1 hour.

2.7 AGET ATRP Modification of Initiator Bearing Silica Particles

2.7.1 Purpose of AGET ATRP modification

Hydrophilic interaction liquid chromatography requires a polar stationary phase. To produce a highly polar polymer phase on the surface of the particles, horizontal polymerization was employed to form a brush layer of polyacrylamide. The hydrophilic nature of the acrylamide attracts water to surround each particle, providing an ideal polar stationary phase. Surface initiated AGET ATRP is specifically used to produce a dense brush layer. The high density of the brush layer excludes protein interactions with the water, but allows small glycan moieties to partition into the water layer.²⁸ AGET ATRP is also controllable, enabling shell thickness to be tuned.²⁹

2.7.2 AGET ATRP procedure

2.7.2.1 *Ex situ*

For *ex situ* polymerization, a 3:1 solution of water: isopropyl alcohol (IPA) was prepared. In a round bottom flask (RBF), 4.4 grams of acrylamide and 0.5 grams of benzyl chloride particles were suspended via sonication in 20 mL water/IPA solution. Ice was added to the water bath to keep temperature at 4 °C. A septum was placed over the top of the reaction without a needle. Two solutions were then prepared in separate 1-dram vials. Solution A contained 40.0 mg copper (II) chloride solid in 2.5 mL water/IPA, with 80 µL (Tris[2(dimethylamino)ethyl]amine) added. Solution B contained 20.0 g sodium ascorbate in 2.5 mL water/IPA. When particles were fully suspended, solution A was added to the flask followed by solution B via syringe. Immediately after solution B was added, the reaction timer began for 55 minutes. After the reaction, the mixture was poured into a 50 mL conical tube and rinsed three times with water. The resulting acrylamide particles were placed in a vacuum desiccator at room temperature to dry.

Once dry, 154 mg of acrylamide particles were suspended in 2.5 mL of water and packed into a 3 cm stainless steel column using a Lab Alliance 1500 HPLC packing pump (Lab Alliance, Syracuse, NY). Figure 2.3 shows the packing setup. The reservoir was filled with a particle slurry and pushed through a union into the column at 17 kPSI. The reservoir and column were sonicated during the packing process.

2.7.2.2 *In situ*

For the *in situ* reaction, 154 mg of benzyl chloride silica particles were packed into a 3 cm stainless steel column (IDEX, Lake Forest, IL). A 3:1 solution of water: isopropyl alcohol (IPA) was prepared. Water/IPA was used to condition the benzyl chloride column by using a packing pump to rinse at a flow rate of 100 $\mu\text{L}/\text{minute}$. A partial amount of the above free particle reaction was prepared, using identical concentrations but lower quantities. 880 mg of acrylamide was added to 4 mL water/IPA solution, which results in about 4.8 mL. For solution A, 8.0 mg of copper (II) chloride was added to 500 μL of water/IPA solution with 16 μL (Tris[2(dimethylamino)ethyl]amine). For solution B, 4.0 mg of sodium ascorbate was added to 500 μL of water/IPA solution. When ready to start the reaction, solution A was added to the acrylamide solution, followed by solution B and mixed well. The reservoir was emptied, and the reaction solution was added immediately. The reaction apparatus was reattached to the pump and the flow begins at 200 $\mu\text{L}/\text{minute}$ until blue appears from the bottom of the column, indicating that reaction mixture flowed to the end of the column. The flow rate was lowered to 100 $\mu\text{L}/\text{minute}$ for 55 minutes. After the reaction was complete, the column was hooked directly to the pump and rinsed for a minimum of 30 minutes at 50 $\mu\text{L}/\text{minute}$.

2.7.2.3 *In situ* stopped flow

An alternate reaction method was stopping the flow but allowing the reaction to continue. Briefly, after the reaction solution is added to the reservoir, the reaction apparatus was reattached to the pump and the flow begins at 200 $\mu\text{L}/\text{minute}$ until the blue reaction solution appears from the bottom of the column. The flow rate was lowered to 100 $\mu\text{L}/\text{minute}$ for 5 minutes, then the flow was turned off for 65 minutes. After the flow was turned off, the bottom of the column was covered with parafilm to prevent oxygen from reaching the reactant solution. When the reaction was complete, the column was connected directly to the pump and rinsed for a minimum of 30 minutes at 50 $\mu\text{L}/\text{minute}$.

2.8 Conclusion

The steps required to produce a functional nonporous HILIC column have been honed over my time at Purdue and many researchers before me. The value of nonporous nanoparticles is realized with improved resolution and recovery, especially with regards to large protein separations. These separations are becoming more common with the low sample availability in analysis of biomarkers and biologics. The HILIC columns produced with these methods are used in the following chapters.

2.9 Figures

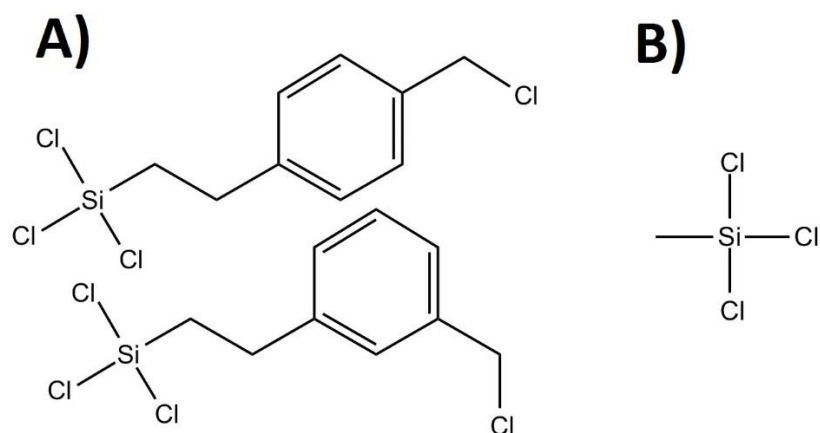


Figure 2.1: Chemical structure of trichlorosilanes used for AGET ATRP initiators. A) ((chloromethyl)phenylethyl)trichlorosilane B) methyltrichlorosilane.

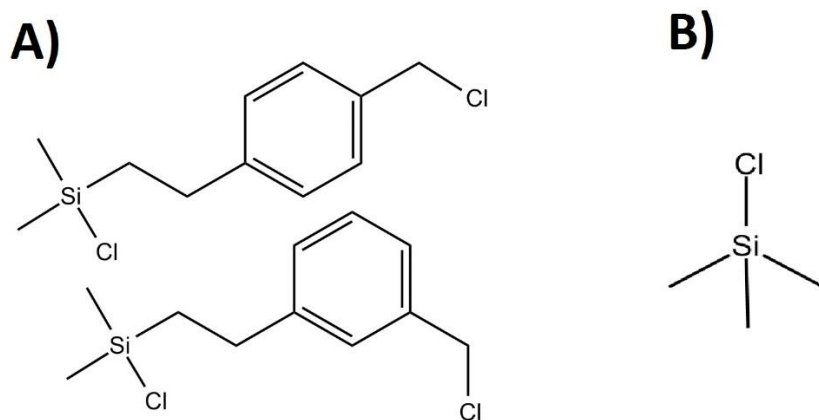


Figure 2.2: Chemical structure of monochlorosilanes used for AGET ATRP initiators. A) ((chloromethyl)phenylethyl)dimethylchlorosilane B) trimethylchlorosilane.

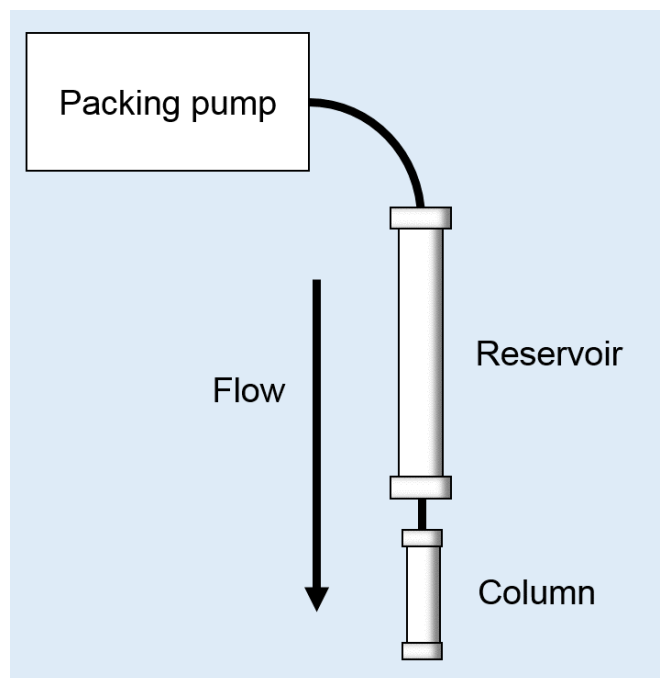


Figure 2.3: Diagram showing packing and modification setups. For packing, the reservoir was filled with a particle slurry and pushed through a union into the column. For modification, the reservoir was filled with a reaction solution and flowed through the column packed with initiator particles. During packing, the reservoir and column setup was sonicated to improve packing homogeneity.

2.10 References

1. Chabanov, A. A., Jun, Y. & Norris, D. J. Avoiding cracks in self-assembled photonic band-gap crystals. *Appl. Phys. Lett.* **84**, 3573 (2004).
2. Lu, G. *et al.* Fabrication of Metal-Organic Framework-Containing Silica-Colloidal Crystals for Vapor Sensing. *Adv. Mater.* **23**, 4449–4452 (2011).
3. Birdsall, R. E., Koshel, B. M., Hua, Y., Ratnayaka, S. N. & Wirth, M. J. Modeling of protein electrophoresis in silica colloidal crystals having brush layers of polyacrylamide: Microfluidics and Miniaturization. *ELECTROPHORESIS* **34**, 753–760 (2013).
4. Xiao, D., Le, T. V. & Wirth, M. J. Surface Modification of the Channels of Poly(dimethylsiloxane) Microfluidic Chips with Polyacrylamide for Fast Electrophoretic Separations of Proteins. *Anal. Chem.* **76**, 2055–2061 (2004).
5. Wirth, M. J. Mass transport in sub-2- μm high-performance liquid chromatography. *J. Chromatogr. A* **1148**, 128–130 (2007).
6. Gao, W., Rigout, M. & Owens, H. Self-assembly of silica colloidal crystal thin films with tuneable structural colours over a wide visible spectrum. *Appl. Surf. Sci.* **380**, 12–15 (2016).
7. Surface-Modified Silica Colloidal Crystals: Nanoporous Films and Membranes with Controlled Ionic and Molecular Transport - Accounts of Chemical Research (ACS Publications). Available at: <http://pubs.acs.org/doi/full/10.1021/ar400157w>. (Accessed: 2nd September 2016)
8. Cahill, D. G. & Pohl, R. O. Thermal conductivity of amorphous solids above the plateau. *Phys. Rev. B* **35**, 4067 (1987).
9. Duncan, J. K., Chen, A. J. & Siebert, C. J. Performance evaluation of non-porous versus porous ion-exchange packings in the separation of proteins by high-performance liquid chromatography. *J. Chromatogr.* **397**, 3–12 (1987).
10. Maa, Y. & Horváth, C. Rapid analysis of proteins and peptides by reversed-phase chromatography with polymeric micropellicular sorbents. *J. Chromatogr. A* **445**, 71–86 (1988).
11. Lee, W.-C. Protein separation using non-porous sorbents. *J. Chromatogr. B. Biomed. Sci. App.* **699**, 29–45 (1997).
12. Yu, J. & El Rassi, Z. High Performance Liquid Chromatography of Small and Large Molecules with Nonporous Silica-Based Stationary Phases. *J. Liq. Chromatogr. Relat. Technol.* **20**, 183–201 (1997).

13. Liao, J.-L. & Hjertén, S. High-performance liquid chromatography of proteins on compressed, non-porous agarose beads. *J. Chromatogr. A* **457**, 175–182 (1988).
14. Hjertén, S. & Liao, J. High-performance liquid chromatography of proteins on compressed, non-porous agarose beads. *J. Chromatogr. A* **457**, 165–174 (1988).
15. Billen, J., Gzil, P., Vervoort, N., Baron, G. V. & Desmet, G. Influence of the packing heterogeneity on the performance of liquid chromatography supports. *J. Chromatogr. A* **1073**, 53–61 (2005).
16. Gritti, F. & Guiochon, G. Mass transfer kinetics, band broadening and column efficiency. *J. Chromatogr. A* **1221**, 2–40 (2012).
17. Products. *Superior Silica* Available at: <http://superiorsilica.com/products/>. (Accessed: 13th September 2018)
18. Lukács, D. & Horváth, K. IMPACT OF SIZE HETEROGENEITY OF CORE-SHELL PACKING MATERIALS ON CHROMATOGRAPHIC SEPARATION OF LARGE BIOMOLECULES. 5
19. Yamasaki, Y., Kitamura, T., Nakatani, S. & Kato, Y. Recovery of proteins and peptides with nanogram loads on non-porous packings. *J. Chromatogr. A* **481**, 391–396 (1989).
20. Newby, J. J., Legg, M. A., Rogers, B. & Wirth, M. J. Annealing of silica to reduce the concentration of isolated silanols and peak tailing in reverse phase liquid chromatography. *J. Chromatogr. A* **1218**, 5131–5135 (2011).
21. Van Le, T., Ross, E. E., Velarde, T. R. C., Legg, M. A. & Wirth, M. J. Sintered Silica Colloidal Crystals with Fully Hydroxylated Surfaces. *Langmuir* **23**, 8554–8559 (2007).
22. Wirth, M. J., Le, T. V. & Zheng, S. Hardening of ordered films of silica colloids. (2010).
23. Köhler, J., Chase, D. B., Farlee, R. D., Vega, A. J. & Kirkland, J. J. Comprehensive characterization of some silica-based stationary phase for high-performance liquid chromatography. *J. Chromatogr. A* **352**, 275–305 (1986).
24. Plueddemann, E. P. Silane adhesion promoters in coatings. *Prog. Org. Coat.* **11**, 297–308 (1983).
25. De Graeve, I., Franquet, A., Le Pen, C., Terryn, H. & Vereecken, J. 1 - Silane films for the pre-treatment of aluminium: film formation mechanism and curing. in *Innovative Pre-Treatment Techniques to Prevent Corrosion of Metallic Surfaces* 1–18 (Woodhead Publishing, 2007). doi:10.1533/9781845693688.1

26. Kulkarni, S. A., Ogale, S. B. & Vijayamohanan, K. P. Tuning the hydrophobic properties of silica particles by surface silanization using mixed self-assembled monolayers. *J. Colloid Interface Sci.* **318**, 372–379 (2008).
27. Kaas, R. L. & Kardos, J. L. The interaction of alkoxy silane coupling agents with silica surfaces. *Polym. Eng. Sci.* **11**, 11–18 (1971).
28. Zhang, Z., Wu, Z. & Wirth, M. J. Polyacrylamide brush layer for hydrophilic interaction liquid chromatography of intact glycoproteins. *J. Chromatogr. A* **1301**, 156–161 (2013).
29. Min, K., Jakubowski, W. & Matyjaszewski, K. AGET ATRP in the Presence of Air in Miniemulsion and in Bulk. *Macromol. Rapid Commun.* **27**, 594–598 (2006).

CHAPTER 3. DEVELOPMENT AND OPTIMIZATION OF IN SITU AGET ATRP FOR PRODUCTION OF POLYACRYLAMIDE HILIC COLUMNS

3.1 Introduction: Value and limitations of a polyacrylamide stationary phase

Various types of stationary phases have been previously developed for HILIC, as described in Chapter 1. The mobile phase used for these columns is usually a combination of acetonitrile and water, to force the polar compounds onto the hydrophilic stationary phase. Some researchers have reported attempting to replace acetonitrile with other organic solvents such as ethanol, methanol, or acetone.¹⁻³ The purpose is to more easily dissolve and elute more polar molecules. However, when using a more polar solvent, the stationary phase must be more polar than current offerings, otherwise weak retention will occur. A recent development in polyacrylamide columns from outside the Wirth lab tested alcohols as mobile phases and found that the high hydrophilicity of the polyacrylamide phase allowed for even alcohols as the weak (organic) solvent, due to the large enough difference in hydrophilicity between the stationary and mobile phases.⁴

However, there are two main limitations to this stationary phase. First, the polyacrylamide is not stable under elevated temperatures. As a result, HILIC separations cannot be performed above 30 °C with the columns. Second, the polyacrylamide chemically degrades via hydrolysis over time, resulting in poor separations after approximately 1-2 months after polymerization. Edwin Alzate confirmed this via IR spectroscopy, illustrating that changes occur to the NH₂ group over time (Figure 3.1). Therefore, columns must be made immediately before a separation and are not ideal targets for commercialization despite their superior separations. This chapter describes the development and optimization in our lab to produce and improve polyacrylamide HILIC columns. These include changes to the silane initiators, column packing, and AGET ATRP reaction.

3.2 Previous development of AGET ATRP reaction for production of polyacrylamide HILIC HPLC columns

A recap of previous work is presented to bring the readers up to speed on development of polyacrylamide columns. Atom transfer radical polymerization (ATRP) of acrylamide onto nonporous particles produced a brush layer of polyacrylamide chains. The trichlorosilane initiators described in chapter 2 were covalently bound to the surface to contain the polymer growth to the surface. A brush regime was shown to be especially valuable for separating glycoproteins; which occurs when surface-bound polymer chains are so closely packed, the polymer does not curl in on itself close to the surface (Figure 3.3).⁵ It was hypothesized that the glycan would partition between the polymer chains to interact with the aqueous layer, but the protein would remain sterically inhibited from interacting (Figure 3.4).⁶ Polyacrylamide proved itself to be an excellent stationary phase for both capillary electrophoresis⁷ and HILIC⁸.

Dr. Charu Yerneri developed the AGET ATRP reaction for polyacrylamide columns, building on work by previous students who had produced these columns via ATRP.^{8,9} ATRP and its reactants are highly air-sensitive, requiring a Schlenk line and a glove box to perform. The use of AGET ATRP allows for small amounts of oxygen to be present in the flask before the reaction starts. As long as the container is airtight, the ascorbate simply reduces the oxygen present before the reaction begins. The AGET ATRP reaction Dr. Yerneri pioneered to produce polyacrylamide columns was performed in a flask, horizontally polymerizing acrylamide monomers onto the initiator-bearing silica surface.

The next improvement, *in situ* AGET ATRP, was accomplished by Dr. Alexis Huckabee and myself. Typical column production had been to attach the silane initiator to the silica particle, perform the AGET ATRP reaction in a flask, then pack the particles into a column. The *in-situ* method is as follows: attach the silane initiator to the silica particle, then pack the initiator particles into the column, and finally pump the AGET ATRP reaction solution into the column to polymerize the acrylamide to the surface (Figure 3.5). By packing the initiator-bearing silica particles in the stainless-steel column before the reaction, column-to-column reproducibility improved. Furthermore, the column was able to complete at least 100% more runs before performance worsened (40

runs vs more than 100 runs).¹⁰ Finally, higher chromatographic resolution was observed with HILIC separation of ribonuclease B. The higher resolution and stability for the columns produced by an *in-situ* reaction is explained by the packing of hard contacts between particles rather than the soft, compressible polyacrylamide layer.

3.3 Surface initiated AGET ATRP reaction for producing stationary phase

Surface initiated AGET ATRP, or SI AGET ATRP, is used in this work for two main reasons: 1) Control over location and chain length, and 2) Denser chain growth. We used horizontal polymerization in contrast to vertical polymerization since dense chains are needed and can be added monomer-by-monomer (Figure 3.8). The reaction is performed using initiator-bearing silica particles with the polymerization reagents in solution. Growth begins after the ascorbate reduces all the dissolved oxygen in solution. From there, the reaction continues until A) The monomer runs out, B) Ascorbate has been completely oxidized, or C) The reagents are rinsed from the initiator particles.

3.4 Longer polyacrylamide chains decrease dependence on TFA

HILIC is an efficient method for glycan separation and is MS-compatible as well. However, for glycoproteins, HILIC has lower resolution and often uses less MS-compatible solvents such as TFA or salts. TFA is used as a mobile phase modifier for HILIC of glycoproteins due to its strong acidity—necessary to neutralize silanols on the silica surface. When using TFA in the mobile phase, however, MS sensitivity is lost since its anion forms adducts with proteins. MS-compatible modifiers such as formic acid (FA) or difluoroacetic acid (DFA) are potential substitutes, but the pKa of both acids is much higher than TFA, leaving some of the acidic silanols unpaired. A potential solution for this issue is to screen the silanol's charge with a thicker PAAm layer, which can extend past the Debye layer and render the presence of silanols a moot concern.

Figure 3.9 shows such an experiment by testing a longer PAAm layer (70-minute AGET ATRP) and comparing to the normal layer (55-minute AGET ATRP). Previous studies have shown a linear relationship between reaction time and polymer growth, so a longer time of polymerization is equivalent to a longer polymer chain.⁹ First, compare

Figure 3.9 A and B, which show the 55-minute column run with 0.1% TFA and 0.1% FA + 0.025% TFA as the mobile phase additive, respectively. Note the loss of resolution with a decrease in TFA. Next, compare C and D, which show the 70-min column run under the same mobile phase additives. A similar resolution can be attained for both the “high TFA” and the “low TFA” mobile phases with the longer polymer chain.

One caveat must be made, however, and that is the reduced flow rate required for the longer polymer chain column. This is due to the polymer layer extending into the pore and reducing the accessible volume, increasing back pressure. Future work into longer polymer chains must use at least 1500 nm nominal d_p or the columns will likely prove difficult to handle.

3.5 Monochlorosilanes vs trichlorosilanes for initiating polymerization

A set of three columns for both monochlorosilane and trichlorosilane initiator particles were produced, for a total of six columns. The method from chapter 2 was followed for both silanization and in situ AGET ATRP. Since this work was performed before switching particle sizes, 750 nm nominal sized particles were used on 3 cm columns using a 75-min stopped-flow reaction.

Table 3.1 shows the difference in homogeneity and void volume for both trichlorosilane columns and monochlorosilane columns. A set of three columns was used for determining the mean and standard deviation. While the monofunctional columns had slightly smaller void volumes and peak widths, the differences among columns varies more than for the trifunctional columns. The resolution does not significantly change and is well within the standard deviation of individual columns of either method alone (Figure 3.2). As long as the silanol activity is minimized through mobile phase additives or PAAm chain length, the surface is sufficiently hydrated, and the PAAm chains have similar densities, I would expect that resolution would be similar. These results show that there is no change between monochlorosilanes and trichlorosilanes used as initiators for AGET ATRP.

Since acetonitrile (used for hydrophobic particles) did not suspend the monofunctional particles as well as the trifunctional particles, John Biechele-Speziale recommended an alternative of suspending the hydrophobic particles in 0.5% TWEEN in

H₂O instead. Furthermore, Tween-20 in water is far more environmentally friendly than acetonitrile, toluene, or blends of isopropyl alcohol and heptane (other solvents used for packing hydrophobic particles in our lab). The downside is that this method requires >10 minutes of rinsing the packing solvent out of the column before performing in-column polymerization.

3.6 Loading capacity of PAAm column and commercial column

An observation was made that more sample could be injected onto a Waters 10 cm Acquity Amide glycoprotein column than the PAAm column produced in this lab. To determine the extent of the difference in loading capacity, Ribonuclease B was injected onto each column at varying sample masses. The chromatogram's main peak was analyzed for asymmetry, where A_s is asymmetry, b is the width of the second half of the peak at 1/10 the height, and a is the width of the first half of the peak at 1/10 the height:

$$A_s = \frac{b}{a} \quad (13)$$

Therefore, if $A_s = 1$, the peak is Gaussian and symmetrical. If $A_s > 1$, the peak is narrower at the beginning of the peak than at the end, which means there is some overloading of the column.

Table 3.3 shows peak asymmetry of both the PAAm and the Waters column at varying injection masses. While the Waters column exhibits no asymmetry at 0.5 μ g Ribonuclease B, the PAAm column shows an asymmetry of 1.9. Furthermore, by 10 μ g, the Waters' asymmetry is 2.5 and PAAm is at 4.1. This shows that the initial observation

was correct that less can be injected onto the PAAm column without overloading compared to the Waters column.

3.6.1 Column length and shape affects loading capacity

In the previous section, it was found that despite the small particle size, our nonporous nanoparticles have a relatively small loading capacity ($\sim 0.5 \mu\text{g}$) compared to commercially available core-shell or fully porous particles of larger size. This section seeks to uncover the properties underlying this issue and recommend potential solutions.

Column “overloading” results from the analyte on the stationary phase reaching a nonlinear portion of the adsorption isotherm. This ultimately means that the concentration of the solute adsorbed onto the stationary phase and the concentration of the solute in solution increase and decrease with one another at the same linear rate. The Langmuir curve is commonly used as a model to depict chromatographic deviation from the linear isotherm. This nonlinearity ultimately results in retention times shifting and fronting or tailing peaks (Figure 3.14).¹¹

A potential solution is increasing the surface area inside the column. By increasing the number of chromatographic sites available to interact with the analyte, the separation should return to the linear isotherm. Common ways to do this are: 1) decreasing particle size, 2) using a wider or longer column, or 3) using a pore size or morphology better suited to the analyte. However, these solutions each have their drawbacks. Decreasing particle size is accompanied by an increase in back pressure, which is significant for our 820 nm d_p particles. A longer column also will require higher pressures. While a wider column would decrease back pressure required, it would also decrease sensitivity due to the larger mobile phase volumes used. Finally, nonporous particles are used in this work due to their superior homogeneity, which reduces the A term, and their ability to provide a stable framework for the growth of PAAm.

The first subsection tests nonporous PAAm columns of varying lengths to compare resolution and loading capacity. The second subsection tests a cone-shaped inlet to the column, where the volume at the head of the column is larger, potentially providing a greater area for stacking.

3.6.1.1 Loading capacity and resolution improve with increasing column length

As expected by theory, efficiency is proportional to the length of the column.¹² Equation 14 describes the relationship between column efficiency (plate number), column length, and particle size. Column length is in millimeters, and particle size is in μm . One could consider that both column length and particle size are directly proportional to the stationary phase's surface area. With this in mind, plate height improves with increasing surface area inside the column.

$$N \propto \frac{L}{d_p}$$

(14)

There are a few practical limitations to the basic theory. Changes in particle size and column length often change other factors such as packing quality and particle homogeneity. Furthermore, increasing column length increases the analyte's retention time in the column, worsening the effects of diffusion. The goal in this section is to determine the effects of particles' surface area on the loading capacity of polyacrylamide columns.

3.6.1.2 Conical column head improves loading capacity

We also tested increasing the surface area by widening part of the column. A special fitting was machined out of stainless steel to match the column. The fitting was attached to the head of the column and packed at the same time. The schematic in Figure 3.15 depicts both a typical column and the conical column. Overall, this change resulted in a 40% greater particle surface area inside the conical column compared to the typical cylindrical column.

Looking at Figure 3.16B, the typical cylindrical column exhibits asymmetrical peaks and the retention time shifts forward as the injection mass increases. From this, we can conclude the column is overloaded even at $2\ \mu\text{g}$. The difference in retention time between $0.5\ \mu\text{g}$ and $10\ \mu\text{g}$ injected onto the column is 1.4 minutes, with no gradient changes. The conical column (Figure 3.16A) also shows asymmetrical peaks and retention time shifts. However, the difference in retention time between $0.5\ \mu\text{g}$ and $10\ \mu\text{g}$

is half, or 0.7 minutes. The 2- μ g injection onto the conical column also appears to be symmetrical, unlike the 2- μ g injection for the cylindrical column.

These data lead me to conclude that the conical column provides some improvement to loading capacity. Quantitatively, the 40% increase in surface area appears to provide a proportionate 50% improvement in loading capacity (based on change in retention time). Considering the gains in loading capacity due to surface area, it would be reasonable to expect further gains due to surface area increases. Since a noted issue is maximum loading capacity of around 0.5 μ g, I consider surface area increases to be especially important for our column going forward. This could take the form of a decrease in particle size, increase in column width, increase in column length, or a reworked conical column incorporating an even greater increase in column width only at the head of the column. Future work on this project is intended and included in Chapter 6: Future Directions.

3.6.2 Particle size affects loading capacity and resolution

As noted in chapter 1, smaller particle size improves homogeneity of the column packing, ultimately improving resolution. Unfortunately, smaller particles also increase back pressure, as expected from the Kozeny-Carman equation:

$$P = \frac{180L\eta\langle v \rangle(1 - \epsilon)^2}{D_p^2\epsilon^2} \quad (15)$$

Particle diameters ranging from 750 – 1500 nm (before thermal treatment) best balance back pressure and surface area for 3 and 5 cm column lengths. In the past, I have observed particle diameters below 750 nm increase the back pressure during the *in-situ* modification beyond the maximum UHPLC pressure for a given flow rate. Furthermore, 2000 nm particle diameter columns do not have sufficiently large surface area for separation, resulting in poor resolution, even if longer columns are packed. Since I have shown with the conical column that loading capacity improves with greater surface area inside the column, I tested the effects of particle size as well, since a decrease in particle size is an increase in surface area and vice versa.

To determine the effect of particle size on loading capacity and resolution, columns were packed with 0.75, 1.0, and 1.5 μm nominal diameter nonporous particles. Experiments by former students have shown a roughly 20% decrease in diameter after calcination, annealing, and silanization – so the true sizes are 0.62, 0.82, and 1.2 μm respectively. Ribonuclease B was injected at varying masses (0.1 μg – 10 μg) and asymmetry of the largest peak was calculated.

Table 3.4 and shows the results of this experiment, showing a general increase in asymmetry within a single column's series as injection mass increases. Unfortunately, widths of larger injection mass peaks were difficult to measure since significant peak overlap occurred. Therefore, a second method, retention time shifting, was used in conjunction to compare loading capacity.

Figure 3.18 shows A) Change in retention time (min) and B) Conversion of retention time (min) to retention volume (μL) as a fairer comparison of 1.5 μm dp column run at 129 $\mu\text{L}/\text{min}$. The 0.75 μm column shows the least change in retention volume as injection mass increases (97 μL), followed by the 1.0 μm column at 148 μL . The 1.5 μm column shows the most change at 196 μL . Note that all columns, even the 0.75 μm particle diameter, shifts retention between 0.1 and 0.5 μg , showing that it is still overloaded.

3.7 Comparing PAAm to commercial column

Figure 3.19 compares resolution of the PAAm column to the Waters column. The PAAm column is superior for small sample masses compared to Waters column. The PAAm column shows two peaks at the beginning of the chromatogram, and a small peak at the end of the chromatogram. In the Waters column, these minor peaks are not visible due to peak broadening. Furthermore, several other peaks are split in the PAAm column but are indistinguishable from a single peak in the Waters column.

3.8 Conclusions

This chapter has been focused on two areas: the nonporous particles and the polyacrylamide brush layer. Nonporous particles, while good for improving efficiency in protein separations, often have a low loading capacity compared to their porous and superficially porous cousins. I found that increasing the surface area inside the column proportionally improves loading capacity. This ultimately provides an avenue for minimizing the issue: testing higher surface area columns. The second area of research focuses on polyacrylamide, which has excellent stationary phase properties due to its hydrophilicity and brush conformation. By increasing chain length of the polyacrylamide, the dependence of resolution on TFA is diminished, allowing for MS-compatible separations without compromise.

3.9 Figures and Tables

Table 3.1: Comparing reproducibility of packing trichlorosilane and monochlorosilane initiator particles. Injection peak width and dead time for a 2 μL packed with 100% acetonitrile injection. Data presented as mean \pm standard deviation of a 3-column set for each type of particles.

	Monofunctional	Trifunctional
t_0	$51 \pm 4 \mu\text{L}$	$53 \pm 3 \mu\text{L}$
2σ (peak width)	$9 \pm 3 \mu\text{L}$	$10 \pm 2 \mu\text{L}$

Table 3.2: Comparison of standard 5 cm PAAm column and PAAm conical column by varying mass injected of Ribonuclease B, then calculating asymmetry of the major peak. Both columns were produced using an *ex situ* AGET ATRP polymerization on 1 μm nominal size particles.

Experiment	Mass Injected (μg)	$A_s = b/a$
Standard column	0.5	1.5
	2	2.2
	5	3.1
	10	3.5
Conical column	0.5	1.3
	2	1.4
	5	2.2
	10	2.3

Table 3.3: Comparison of standard PAAm 5 cm, 1 μm d_p column and a Waters Acquity Amide glycoprotein 10 cm column by varying mass injected of Ribonuclease B, then calculating asymmetry of the major peak.

Experiment	Mass Injected (μg)	$A_s = b/a$
PAAm	0.5	1.9
	2	3.6
	10	4.1
Waters	0.5	1
	2	1.3
	10	2.5

Table 3.4: Comparison of PAAm 3 cm columns of varying particle size, 0.75, 1.0, and 1.5 μm d_p nonporous particles were tested with varying mass injected of Ribonuclease B, then calculating asymmetry of the major peak. Since the free volume of the 1.5 μm column was tested to be slightly greater than the 1.0 or .75 μm columns, two flow rates were tested in an attempt to make fairer comparisons: the same flow rate as the other columns (100 $\mu\text{L}/\text{min}$), and an adjusted flow rate (129 $\mu\text{L}/\text{min}$) to match the greater free volume.

Particle diameter	Flow Rate	Mass Injected (μg)	As = b/a
1.5 μm	129 $\mu\text{L}/\text{min}$	10	3.9
		5	1.4
		2	1.4
		0.5	1.4
		0.1	1.0
1.0 μm	100 $\mu\text{L}/\text{min}$	10	3.3
		5	3.9
		2	2.9
		0.5	1.7
		0.1	1.0
0.75 μm	100 $\mu\text{L}/\text{min}$	10	3.7
		5	2.5
		2	2.2
		0.5	1.9
		0.1	1.9

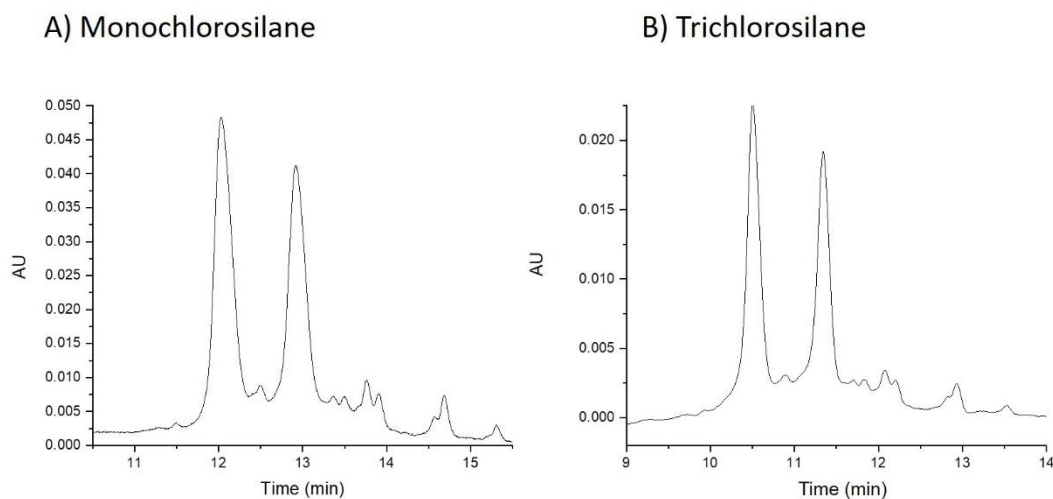
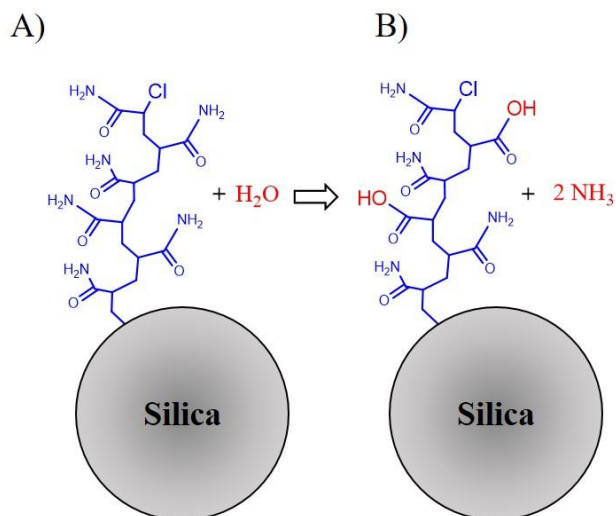


Figure 3.2: Comparison of two HILIC separations performed on columns produced with A) monochlorosilane and B) trichlorosilane initiators. A significant difference is not seen between the two separations. The absorbance difference is due to a more sensitive detector used for the monochlorosilane particles.

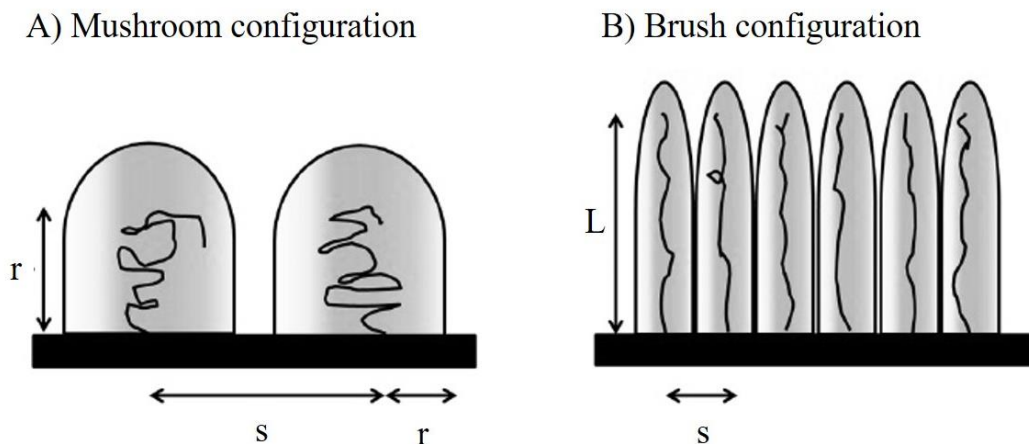


Figure 3.3: Comparison of A) mushroom and B) brush polymer configurations. Both configurations entail unbranched polymer chains directly attached to the surface. The conformations are dependent on the density of the polymer chain tethered to the surface. The mushroom conformation is found when the distance s between individual chains is greater than $2 \times$ the polymer's radius r . The brush conformation occurs when the polymer chains are packed together, therefore the polymer chains are extended to a length of L . This conformation occurs when s is less than $2r$. Given the polymer chains' ability to move, the volume that it is likely to occupy is shaded.^{5,9}

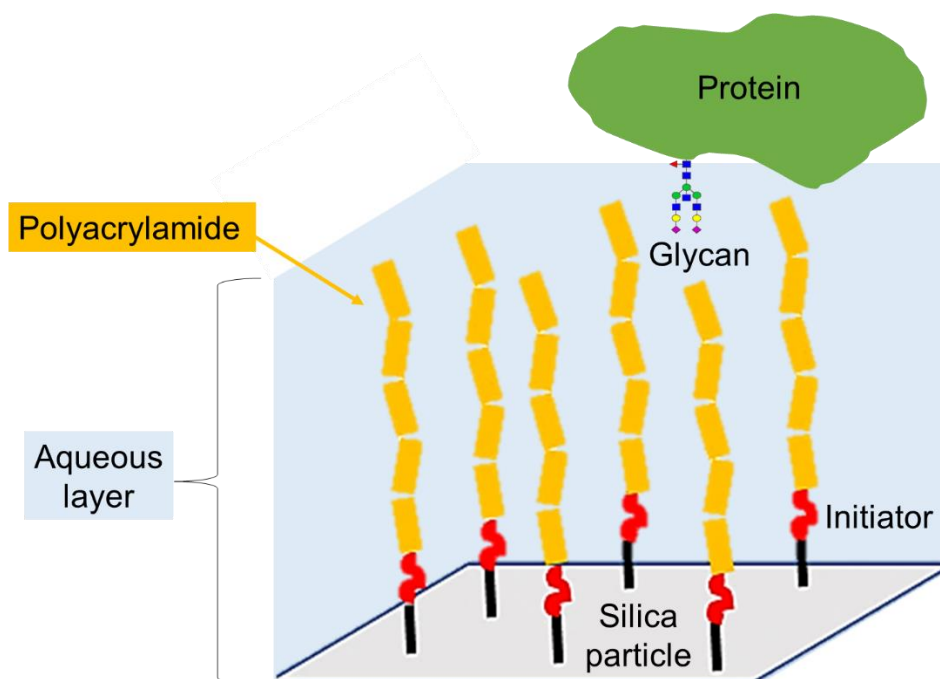


Figure 3.4: Diagram of the polyacrylamide polymer chains and the hypothesized mechanism of hydrophilic partitioning to specifically retain the glycan, leaving the protein sterically hindered from interacting with the stationary phase. The mobile phase is a solution of acetonitrile, water, and acid modifier.

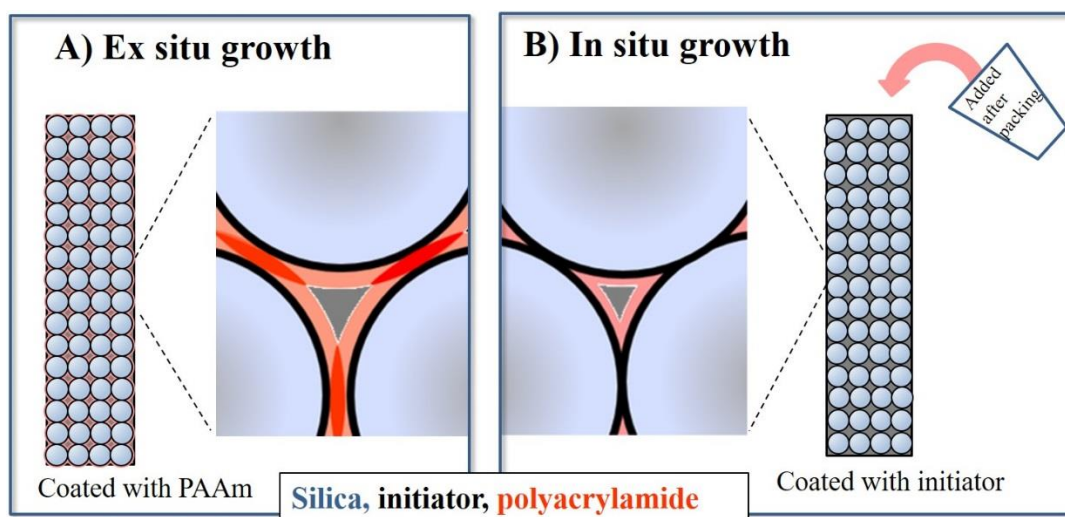


Figure 3.5: Comparison of the methods and polymer structure of A) columns polymerized before packing and B) columns polymerized after packing.

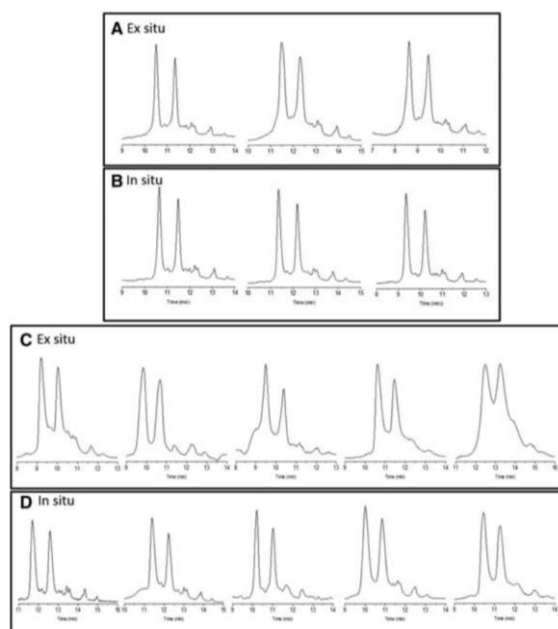


Figure 3.6: HILIC chromatograms of ribonuclease B for the best three columns produced with A) *ex situ* and B) *in situ* polymerization. Chromatograms for the remaining five columns produced by C) *ex situ* and D) *in situ* polymerization. The gradient was 75 to 60% ACN + 0.1% TFA in 20 min. 2 μ L of a 1 mg/mL solution of Ribonuclease B was injected. UV absorbance detected at 215 nm, column temperature 30°C, and flow rate of 100 μ L/min.

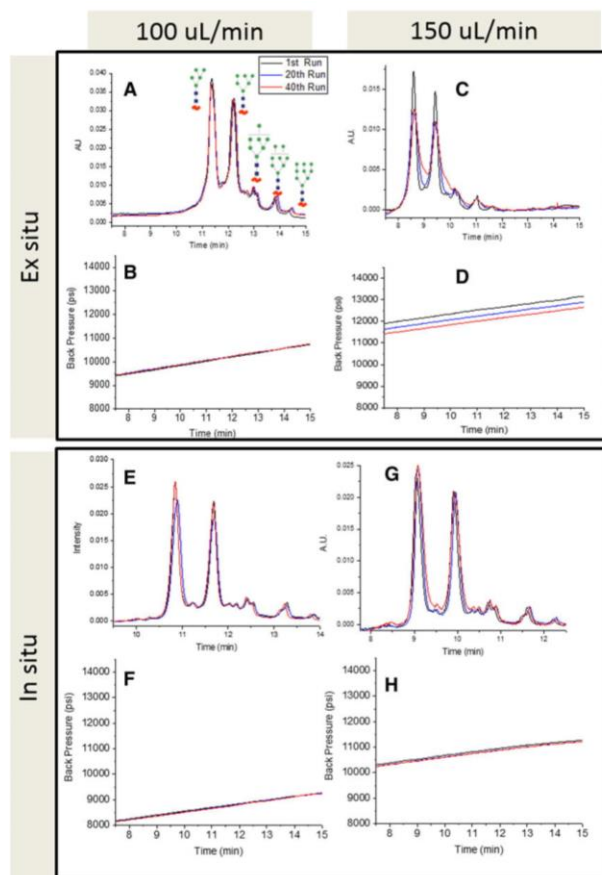
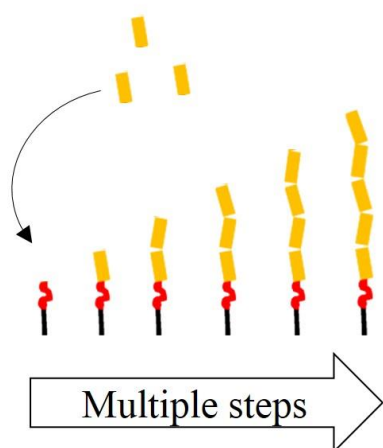


Figure 3.7: HILIC data for ribonuclease B and the corresponding plots of backpressure during the gradient elutions. 40 runs were done for each panel, which show the runs for the 1st, 20th, and 40th runs. The flow rates listed regard the chromatographic separations. (A) HILIC for ex situ growth with a flow rate of 100 $\mu\text{L}/\text{min}$ and (B) the corresponding backpressure. (C) HILIC for ex situ growth with a flow rate of 150 $\mu\text{L}/\text{min}$ and (D) the corresponding backpressure. (E) HILIC for in situ growth with a flow rate of 100 $\mu\text{L}/\text{min}$ and (F) the corresponding backpressure. (G) HILIC for in situ growth with a flow rate of 150 $\mu\text{L}/\text{min}$ and (H) the corresponding backpressure. The gradient was the same as in Figure 3.6.

A) Horizontal polymerization



B) Vertical polymerization

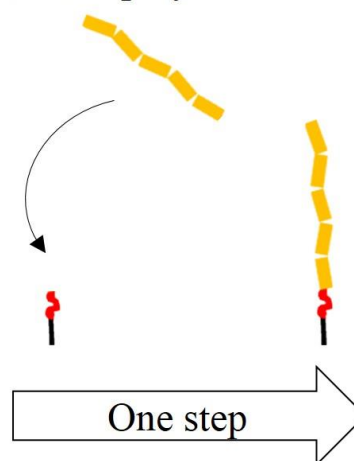


Figure 3.8: Comparison between horizontal and vertical polymerization. A) Horizontal polymerization grows the polymer chain one monomer at a time on a surface. B) Vertical polymerization attaches a polymer chain to a surface.

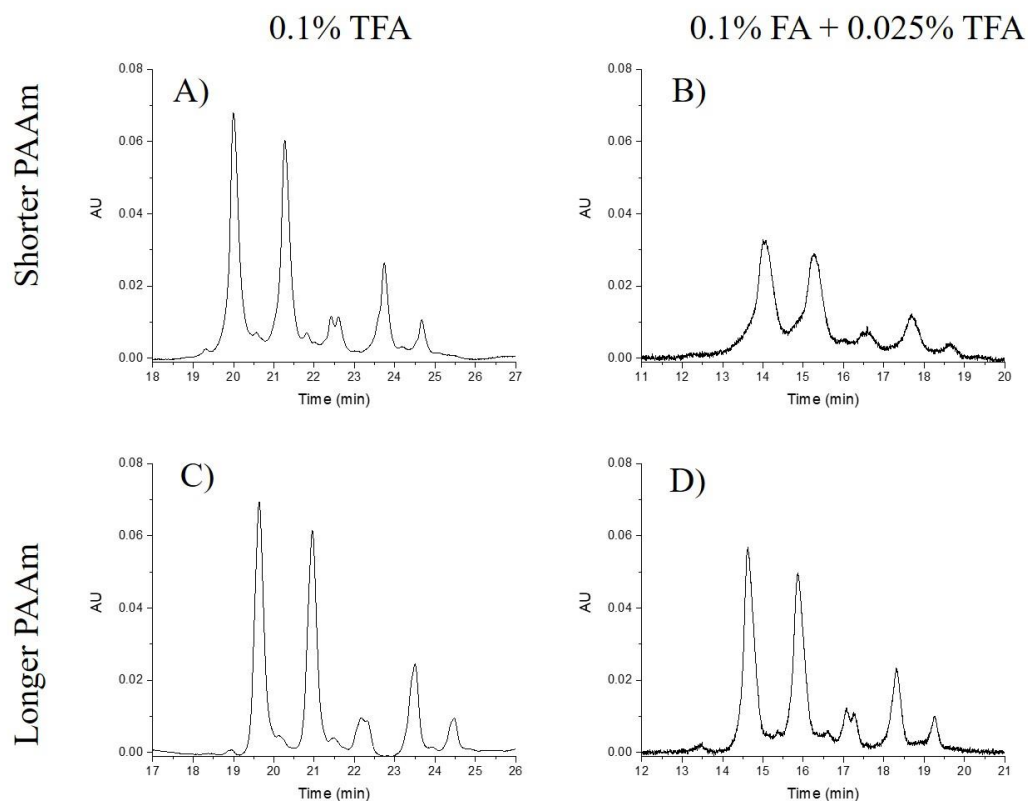


Figure 3.9: PAAm column 1 μm d_p , $L = 5$ cm, 15% gradient change in 30 min, A = H_2O + acid, B = ACN + acid, 50 $\mu\text{L}/\text{min}$, 0.5 μg Ribonuclease B injection 1 mg/mL in 75% ACN, A) 70 minute AGET ATRP polymerized column with conditions 0.1% TFA with gradient 75-60%, B) 70 minute AGET ATRP polymerized column with conditions 0.1% FA+ 0.025% TFA with gradient 70-55%, C) 55 minute AGET ATRP polymerized column with conditions 0.1% TFA with gradient 75-60% D) 55 minute AGET ATRP polymerized column with conditions 0.1% FA + 0.025% TFA with gradient 70-55%

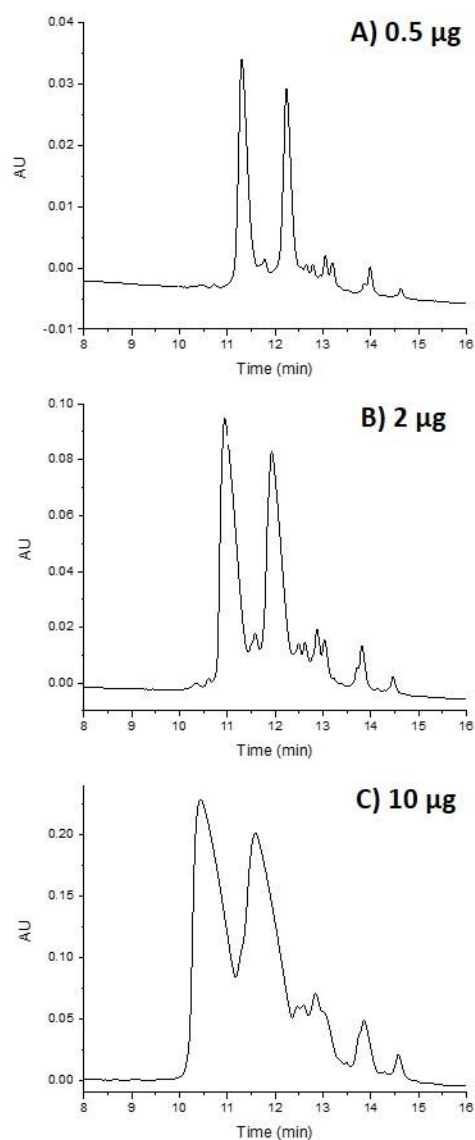


Figure 3.10: A PAAm nonporous column has a maximum capacity of around 0.5 μg before resolution rapidly deteriorates for HILIC separations. A) 0.5 μg B) 2 μg C) 10 μg Ribonuclease B sample injection. Injection sample was in 80% ACN + 0.1% TFA. Gradient 1-minute stacking at 75% ACN followed by 75 to 60% ACN in 20 minutes. Both mobile phases 0.1% TFA acid modifier. 30°C column temperature. 620 nm particle diameter.

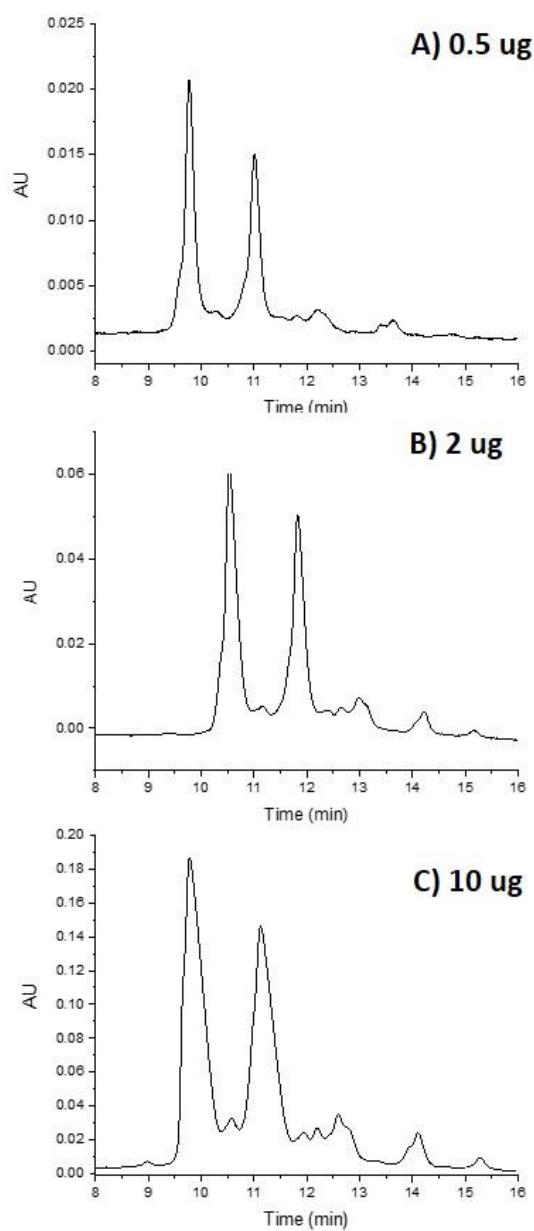


Figure 3.11: A Waters Acquity glycoprotein Amide column has a maximum capacity between 2 and 10 μg before overloading occurs for the largest peak for HILIC separations. A) 0.5 μg B) 2 μg C) 10 μg Ribonuclease B sample injection. Injection sample was in 80% ACN + 0.1% TFA. Gradient 30 seconds of stacking at 85% ACN followed by 67 to 60% ACN in 20 minutes. Both mobile phases 0.1% TFA acid modifier. 30°C column temperature.

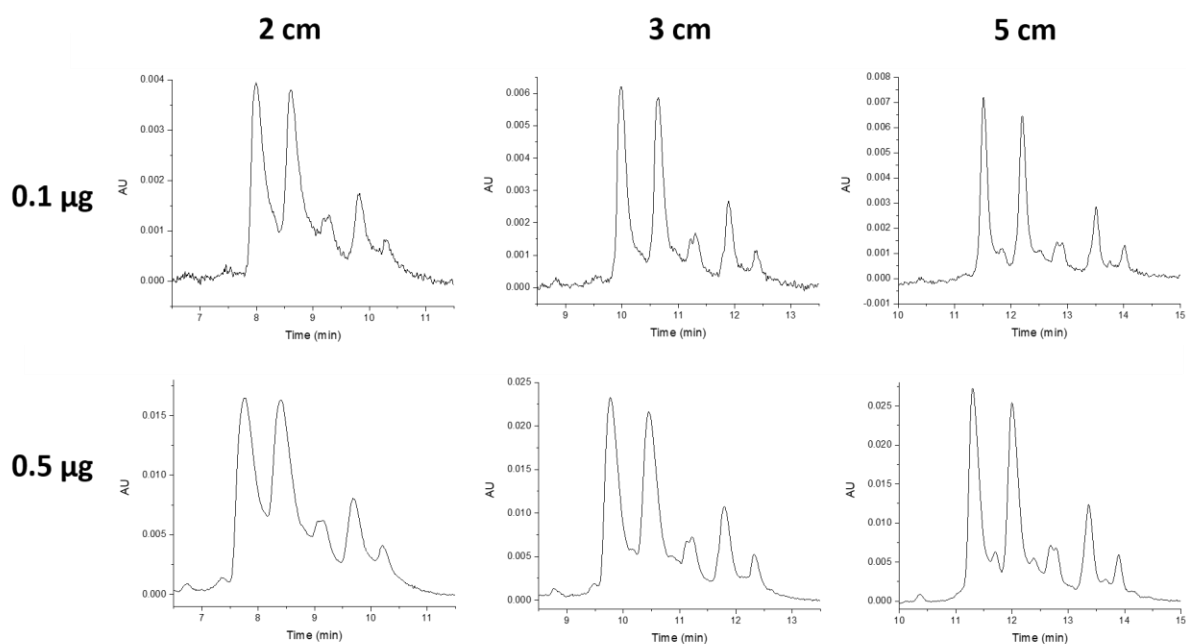


Figure 3.12: Comparison of ribonuclease B loading capacities taken on 2, 3, and 5 cm PAAm columns. The shorter columns exhibit peak fronting, indicative of overloading.

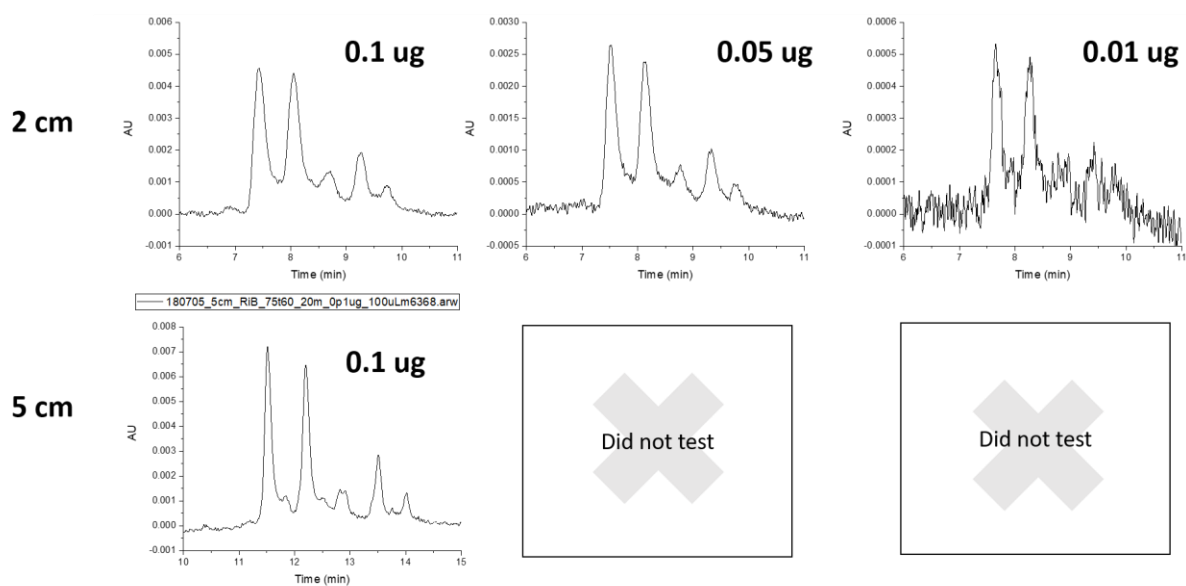


Figure 3.13: Comparison of 2 and 5 cm columns with varying injection mass. The shorter column is unable to match the resolution of the longer column, indicating that the longer length is necessary for a high-quality separation.

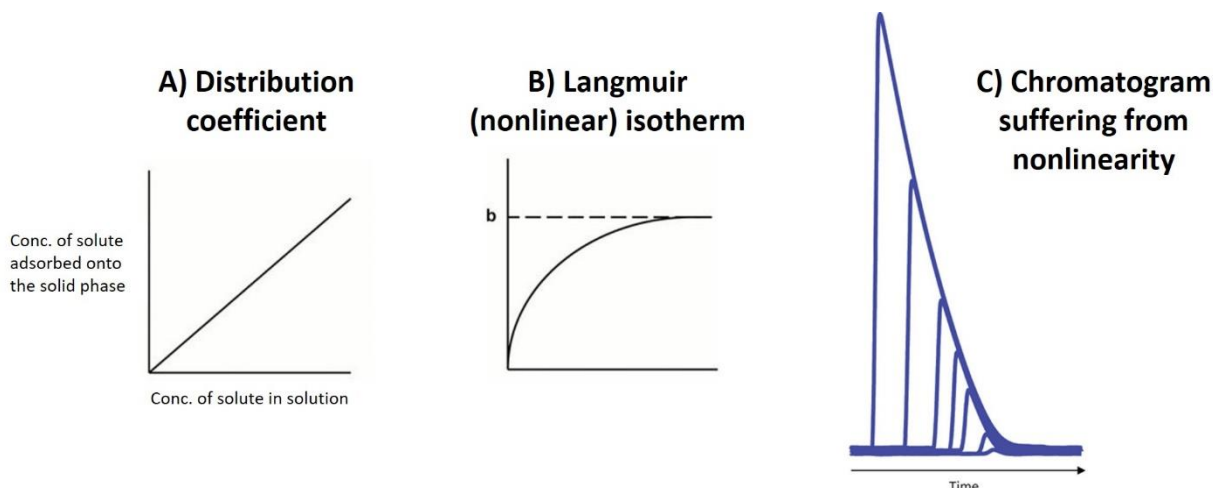
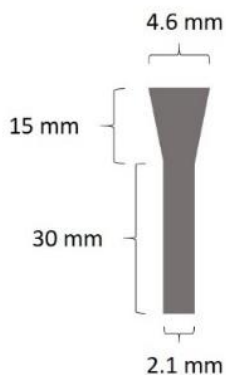


Figure 3.14: A) Example of a linear adsorption isotherm, where the concentration of the solute adsorbed onto the stationary phase and the concentration of the solute in solution increase and decrease with one another at the same linear rate. B) The Langmuir isotherm, a nonlinear curve used to depict chromatographic deviation from the linear isotherm. C) Nonlinearity due to “overloading” ultimately results in retention times shifting and fronting or tailing peaks, as depicted in the chromatogram. As the mass injected increases, the retention time shifts forward, and fronting worsens. C’s depiction of an overloaded run is adapted from Dolan in LCGC.¹⁰

A) Conical column (4.5 cm length including cone)



B) Standard column (5 cm length)

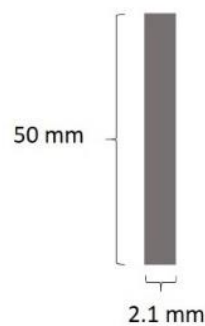


Figure 3.15: A) Depiction of the conical column used. A separate cone-shaped stainless-steel fixture was placed at the head of a 30 mm column and packed with the column. B) A standard column used as a comparison 5 cm in length.

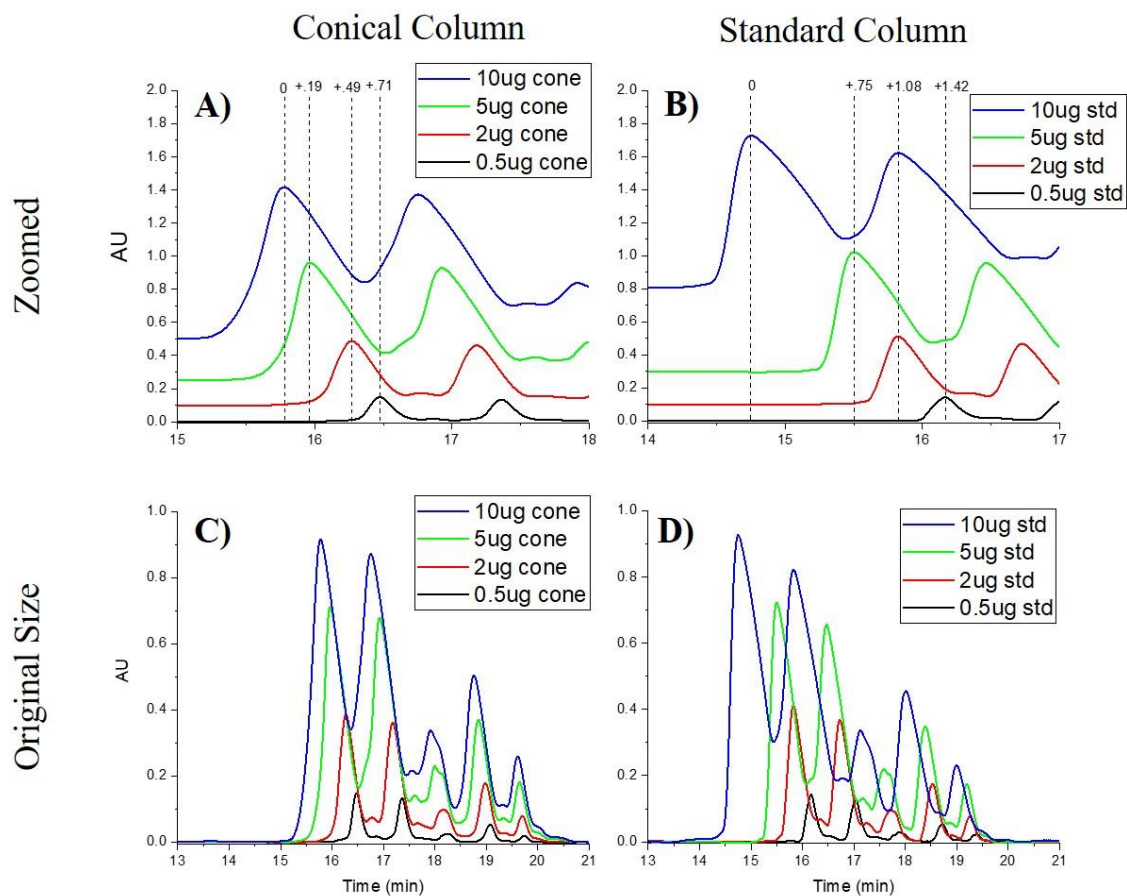


Figure 3.16: Ribonuclease B separations performed on both the machined conical column and a standard column. A) Conical column zoomed in. B) Standard column zoomed in. C) Conical column showing entire separation. D) Standard column showing entire separation. Injection masses were varied to determine if the conical column resulted in improved loading capacity. It appears that loading capacity is slightly improved over the 5 cm column, judged by a lower amount of shifting in the retention time with increased injection mass.

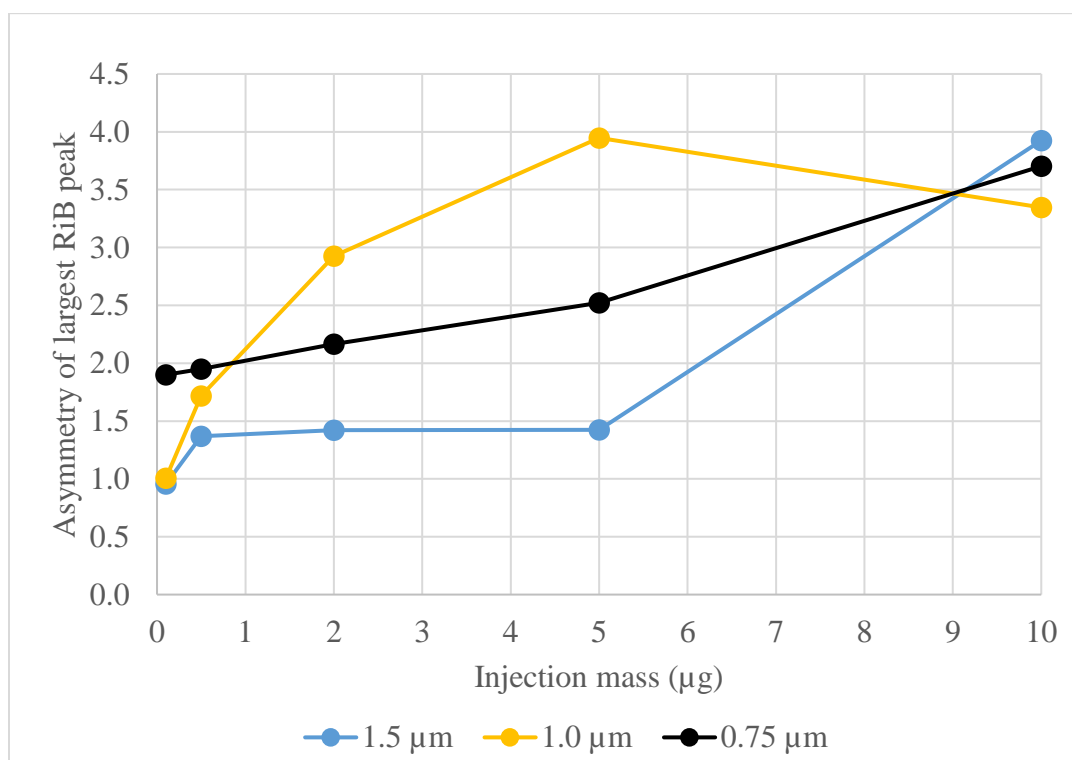
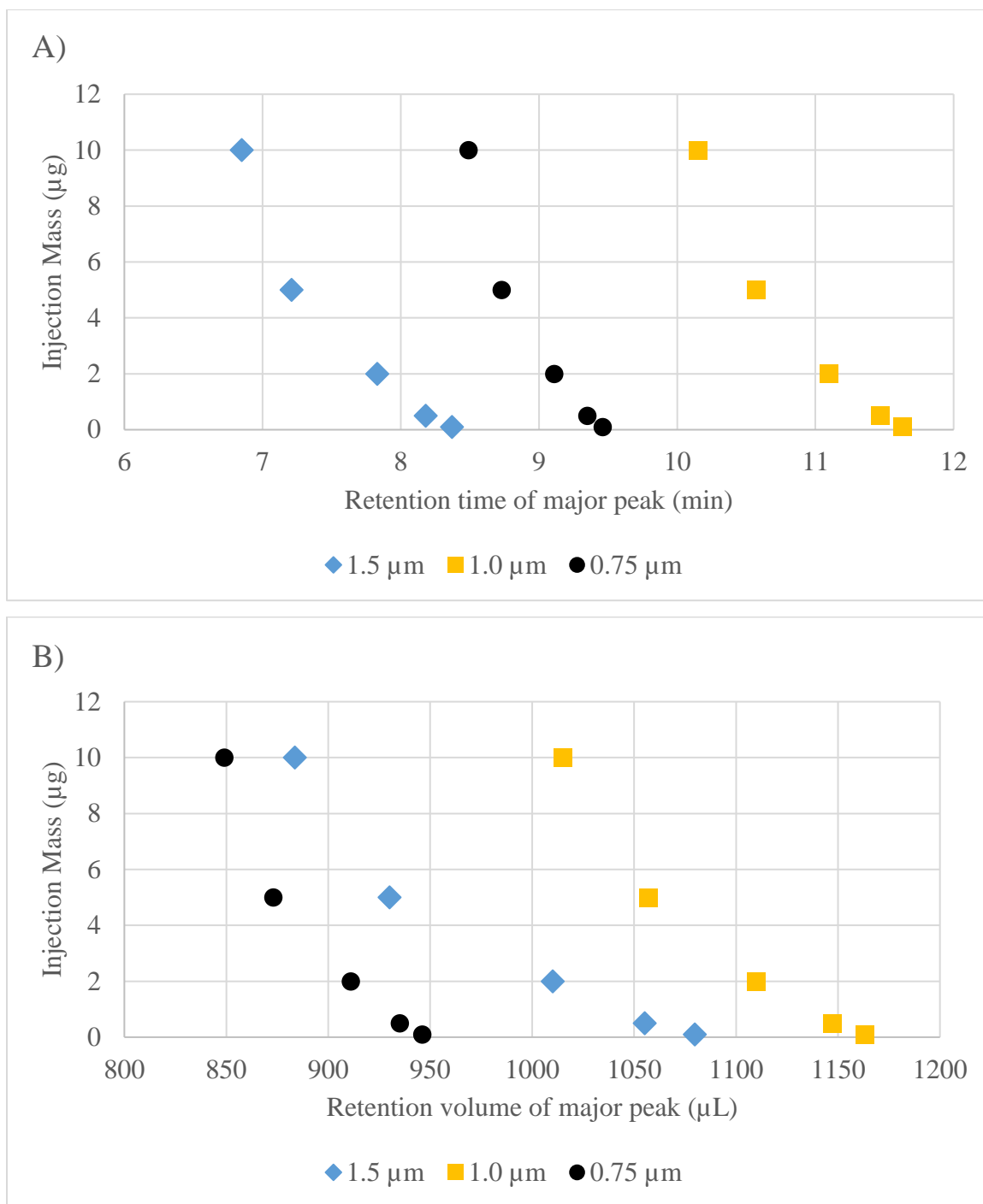


Figure 3.17: Comparison of peak asymmetry for 0.75, 1.0, and 1.5 μm particle diameter columns. Ribo B was injected in varying masses and asymmetry of the largest peak calculated as a stand-in for peak capacity. Given the difficulty in measuring peak width of higher injection masses due to overlap with other peaks, another method was used to compare peak capacity as well (retention time shifting).



the 0.75 μm particle diameter, shifts retention between 0.1 and 0.5 μg , showing that it is still overloaded.

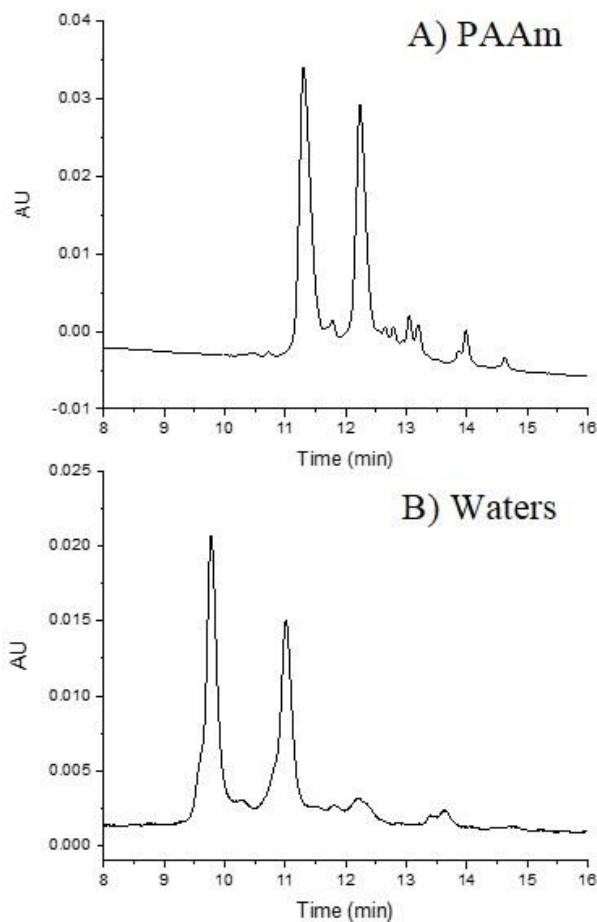


Figure 3.19: PAAm column is superior for small sample masses compared to Waters column, the latter of which loses minor peaks due to broadening and does not separate leading minor peaks from the major glycoform. A) Nonporous PAAm column with 1-minute stacking at 75% ACN followed by 75 to 60% ACN gradient in 20 minutes. B) Waters Acquity glycoprotein Amide column. Both have an injection of 0.5 μg Ribonuclease B in 80% ACN + 0.1% TFA. Gradient 30 seconds of stacking at 85% ACN followed by 67 to 60% ACN in 20 minutes. Both have mobile phases 0.1% TFA acid modifier and 30°C column temperature.

3.10 References

1. Melnikov, S. M., Höltzel, A., Seidel-Morgenstern, A. & Tallarek, U. How Ternary Mobile Phases Allow Tuning of Analyte Retention in Hydrophilic Interaction Liquid Chromatography. *Anal. Chem.* **85**, 8850–8856 (2013).
2. Hao, Z. *et al.* Separation of amino acids, peptides and corresponding Amadori compounds on a silica column at elevated temperature. *J. Chromatogr. A* **1147**, 165–171 (2007).
3. Li, R., Zhang, Y., Lee, C. C., Liu, L. & Huang, Y. Hydrophilic interaction chromatography separation mechanisms of tetracyclines on amino-bonded silica column. *J. Sep. Sci.* **34**, 1508–1516 (2011).
4. Cai, J. *et al.* A polyacrylamide-based silica stationary phase for the separation of carbohydrates using alcohols as the weak eluent in hydrophilic interaction liquid chromatography. *J. Chromatogr. A* **1524**, 153–159 (2017).
5. Backmann, N. *et al.* Sensing surface PEGylation with microcantilevers. *Beilstein J. Nanotechnol.* **1**, 3–13 (2010).
6. Wu, Z. Intact protein separations by using slip flow with nano-liquid chromatography-mass spectrometry. (Purdue University, 2014).
7. Birdsall, R. E., Koshel, B. M., Hua, Y., Ratnayaka, S. N. & Wirth, M. J. Modeling of protein electrophoresis in silica colloidal crystals having brush layers of polyacrylamide: Microfluidics and Miniaturization. *ELECTROPHORESIS* **34**, 753–760 (2013).
8. Zhang, Z., Wu, Z. & Wirth, M. J. Polyacrylamide brush layer for hydrophilic interaction liquid chromatography of intact glycoproteins. *J. Chromatogr. A* **1301**, 156–161 (2013).
9. Yernerli, C. Utilizing advanced polymerization techniques for simplifying polymer grafting from silica colloidal crystal substrates. (Purdue University, 2014).
10. Huckabee, A. G. *et al.* In-column bonded phase polymerization for improved packing uniformity. *J. Sep. Sci.* **40**, 2170–2177 (2017).
11. Giddings, J. C., Grushka, E. & Brown, P. R. *Advances in Chromatography*. **28**, (Marcel Dekker, 1989).
12. Snyder, L. R., Kirkland, J. J. & Dolan, J. W. *Introduction to modern liquid chromatography*. (John Wiley & Sons, Inc., 2010).
13. Dolan, J. W. Overload in Liquid Chromatography. Available at: <http://www.chromatographyonline.com/overload-liquid-chromatography-0?pageID=1>. (Accessed: 16th August 2018)

CHAPTER 4. UHPLC HILIC-MS FOR SEPARATION OF GLYCOSYLATED IGG1 FRAGMENTS

4.1 Abstract

Glycosylation is a critical quality attribute of therapeutic mAbs. The current assay for glycan profiling is laborious and time consuming, involving glycan cleavage and labeling. A fast, automated assay for mAb glycoprofiling would enable real-time monitoring of glycosylation events during the manufacturing process. This research details such an assay for monoclonal IgG1, with a total assay time of 35 minutes, readily amenable to automation. Sample preparation requires IdeS digestion followed by reduction in the same vessel, and then analysis by HPLC. The glycosylated Fc/2 fragment is released after a rapid proteolytic digestion by IdeS and subsequent reduction. Direct injection of this solution into an HPLC column, the Fc/2 fragments of the two most abundant glycans, G0F and G1F, are quantified. Crucial to this protocol is the HPLC column, which performs hydrophilic interaction liquid chromatography (HILIC) using a bonded phase of linear polyacrylamide chains on nonporous silica particles for higher resolution of the glycoforms. Glycoform detection and assignment is achieved using inline mass spectrometry (HILIC-MS). The entire analysis requires only 35 minutes and is readily applicable to automated real-time monitoring of the bioprocess.

4.2 Introduction

4.2.1 Monoclonal antibodies in the pharmaceutical industry

In the mid-1970s, hybridoma technology was developed by Köhler and Milstein. This technology allowed for the manufacture of monoclonal antibodies with predefined specificity in an immortal cell line.¹ Since this discovery, mAbs have rapidly gained use in both diagnosis and therapy. Recombinant DNA technology has advanced production beyond antibodies from non-human (generally murine) hosts, reducing immunogenicity with chimeric and humanized mAbs. More recently, transgenic mice expressing human antibodies and phage display libraries produce fully human mAbs without a human subject.

4.2.1.1 Microheterogeneity and critical quality attributes

Monoclonal antibodies, by definition, have been derived from a single clone of B cells and are monospecific. However, a therapeutic mAb product can still be heterogeneous due to errors in amino acid sequence, variation in post-translational processing, and differences in glycosylation.^{2,3} Degradation and aggregation can occur during purification and storage, further lowering the similarities among antibody molecules. These minor variants within a single mAb preparation are often referred to as microheterogeneity. The final mAb product, therefore, is not a single antibody but a group of similar antibodies differing by N-glycosylation or other minor differences.

A critical quality attribute (CQA) is defined as “a physical, chemical, biological, or microbiological property or characteristic that should be within an appropriate limit, range, or distribution to ensure the desired product quality” by the ICH Q8(R2) guidance document produced by the FDA.⁴ Potential CQAs are identified during drug development as affecting bioactivity, pharmacokinetics, pharmacodynamics, safety, and immunogenicity. CQAs must be highly controlled during the manufacturing process to ensure a safe and effective treatment.

4.2.1.2 Biological and regulatory impact of monoclonal antibody glycosylation

Glycan structures impact the efficacy and safety of a mAb drug, as such, it is considered a CQA of whole mAb and Fc fusion protein drugs.⁵ Cellular effector functions induced by various classes of FcγR are vital for immune system regulation and defense. These FcγR-induced functions turn the body's immune defenses against the mAb drug's target. X-ray crystallography data has determined that the glycan interacts non-covalently with the CH2 domain of the Fc.⁶ Interaction sites on the Fc for FcγRI, FcγRII, FcγRIII and C1q effector ligands are strongly dependent on the non-covalent interactions between the carbohydrate and the Fc for their proper formation. Effector mechanisms using these specific ligands are reduced or eliminated if the IgG molecule lacks a glycan on the Fc at Asn297.⁷

As an example, imagine a cancer mAb drug with 95% glycosylated forms and 5% aglycosylated forms. Since FcγR has a far lower affinity for aglycosylated Fc, the antibody product would not be as effective in neutralizing the pathophysiological

function, inducing antibody-dependent cell-mediated cytotoxicity, or inducing complement-dependent cytotoxic activity of the cancer cell.^{8,9} Therefore, it is important to monitor the percentage of glycosylated versus aglycosylated antibody in a batch; otherwise, the drug may fluctuate in effectiveness from batch to batch.

4.2.1.3 Standard method for glycan identification is lengthy and laborious

We have established that it is important to characterize and control glycosylation variants of therapeutic mAbs because some variants can cause an immune reaction or have different biological activities.^{10,11} The standard method for glycan identification and quantification is lengthy and laborious, consisting of antibody denaturation, enzymatic cleavage of the glycan from the Fc region with an N-glycanase, time-consuming labeling by reaction of 2-aminobenzamide to the aldehyde end of the glycan at elevated temperature, followed by reduction of the Schiff base and clean-up, and separation via capillary electrophoresis or hydrophilic interaction liquid chromatography (HILIC).^{12–14} This analysis typically requires two days. If the assay could be performed in less than an hour, glycoforms could be characterized while the antibody is still being produced in the bioreactor, facilitating near real-time monitoring of glycosylation.^{15–18} This capability has not yet been attained.^{19–21}

To speed up the glycan analysis and reduce labor, a faster assay with fewer operational steps is needed.²² To this end, reagents for faster glycan release and faster labeling decreased the overall analysis time to 3.5 hours, mostly comprised of sample preparation time.²³ Most recently, the sample preparation time was decreased to 30 minutes by labeling without immobilization, cleaving in parallel with labeling, and recovering the released glycans by solid-phase extraction.²⁴ After release and diluting into organic solution, HILIC-MS analysis was done. While these approaches have greatly decreased analysis time, multiple steps are still involved that require human intervention.

A HILIC separation of glycoproteins without releasing the glycans would significantly speed up the assay. For an intact mAb, the glycans on the Fc subunit are on the interior of the antibody, preventing sufficient interaction between the glycans and the stationary phase.²⁵ A fast, low-labor sample preparation can be performed by using a middle-down approach of simply releasing and analyzing the glycosylated Fc/2

fragments. A scheme comparing the two approaches is in Figure 4.1. The enzyme for this release, IdeS, intrinsically digests at a much faster rate than the enzyme for release of the glycans, on the scale of minutes. Furthermore, the IdeS enzyme leaves each glycan with a naturally UV-active label: the Fc/2 fragment. This sample preparation also preserves structural information about where the glycans are attached and avoids interference from any Fab glycosylation. The scheme is depicted in Figure 4.2. Addition of dithiothreitol (DTT) reduces the disulfide bonds to break the Fab fragments into smaller pieces. The reduction is not inherently necessary, but slightly improves resolution in HILIC by removing the more strongly retained Fab fragment. The DTT can be added to the same vial after the IdeS reaction, avoiding any labor beyond dispensing which can be automated. This scheme for glycan analysis was demonstrated by Periat *et al.* in the context of evaluating the utility of HILIC,²² but what impedes its adoption is the low resolution of HILIC for intact glycoproteins, particularly the inability to resolve the isomers of the G1F glycan.

A recent advance in the resolution of HILIC for intact glycoproteins uses a bonded phase of linear polyacrylamide on submicron nonporous particles.^{26,27} Polyacrylamide has exceptional hydrophilicity,²⁸ and the polyacrylamide chains are closely spaced to exclude protein while allowing the small glycan moieties to partition into the hydrated polymer layer.²⁷ The polymer thickness mediates strong ionic interaction to charged silanols.²⁹ HILIC mobile phases are also amenable to mass spectrometry.³⁰ Mass spectrometry is a popular tool to characterize protein variants,^{31–34} structural changes^{35–39}, and heterogeneity with special emphasis on glycosylation.^{38,40–46} Currently, the strategies used to characterize mAb glycosylation may occur at the intact protein level under native or denaturing conditions, the glycopeptide level, or on the released glycans level. Herein we investigate the rate of the reduction and cleavage reactions, the resolution of the novel HILIC column, the identification of the glycoforms at Fc/2 fragments level by high resolution MS, and quantitation of the glycoforms of IgG1 with UV absorbance detection.

4.3 Method

Empty stainless-steel columns (2.1 mm I.D., 50 mm length), reservoirs (4.6 mm I.D., 150 mm length), and frits (0.5 μ m pore diameter) were purchased from IDEX (Middleboro, MA). Stainless steel tubing, ferrules, and internal nuts were purchased from Valco Instruments Co. Inc. (Houston, TX). Nonporous silica particles (1.0 μ m diameter) were purchased from Superior Silica (Mesa, AZ). Acrylamide, TWEEN-20, butylamine, and Ribonuclease B were purchased from Sigma-Aldrich (Saint Louis, MO). Copper (II) chloride (CuCl_2), Tris[2-(dimethylamino)ethyl]amine (Me_6TREN), sodium ascorbate, dithiothreitol (DTT), trifluoroacetic acid (TFA), formic acid (FA), acetonitrile (ACN), toluene, nitric acid, isopropyl alcohol (IPA), and ethanol were purchased from Thermo Fisher Scientific (Waltham, MA). Ultrapure water was prepared with an in-lab purifier from Millipore. Genentech, Inc. provided the pharmaceutical grade monoclonal antibody (South San Francisco, CA).

4.3.1 HPLC column preparation

Nonporous silica particles were placed in a covered crucible for 12 hours for calcination at 600 °C. Cooled particles were funneled into a round-bottom flask. Ethanol was added to the round-bottom flask and sonicated until all particles were suspended. The particle slurry was centrifuged in 50 mL conical tubes, decanted, and dried. Particles were returned to the crucible and calcination steps were repeated twice. After the third calcination, the particles were not cooled, but the temperature was increased to 1050 °C for 3 hours of annealing. Cooled particles were suspended in ethanol via sonication, then centrifuged, decanted, and dried in a 60°C vacuum oven. Annealed particles shrunk in size from 1000 nm to 830 nm, as determined by SEM.

Annealed silica particles were suspended in 50% nitric acid and refluxed with stir bar overnight. The cooled particles in suspension were centrifuged and rinsed with ultrapure water, until pH was neutral. Rehydroxylated particles were dried in a 60 °C vacuum oven. The dried rehydroxylated particles were added to a 250 mL RBF and suspended in dry toluene with sonication and magnetic stirring. When suspended, ((chloromethyl) phenylethyl) dimethylchlorosilane (2% v/v; Gelest, Inc., Morrisville, PA) and butylamine (0.1% v/v) were added to the flask, and the reaction refluxed for 3 hours.

After completion, the particles were rinsed three times in dry toluene and dried in a 60°C vacuum oven. The silane particles were suspended in 0.5% TWEEN-20 in H₂O, then packed into a 2.1 mm x 50 mm column using a Lab Alliance Series 1500 pump (Scientific Systems, Inc., State College, PA).

To form the polyacrylamide brush layer, acrylamide (4.4 g) was suspended in 20 mL of 3:1 H₂O:IPA v/v in a 50 mL conical tube. Solution A was prepared by dissolving CuCl₂ (40 mg) and Me₆TREN (80 µL) in 2.5 mL 3:1 H₂O:IPA. Solution B was prepared by dissolving sodium ascorbate (20 mg) in 2.5 mL 3:1 H₂O: IPA. Solutions A then B were dispensed into the conical tube. The resulting mixture was poured into the reservoir. The column packed with silane initiator particles was connected to the reservoir. The reaction solution from the reservoir was pumped into the column starting at a high flow rate (200 µL/min) until the reaction mixture dripped from the end of the column. The flow rate was then lowered to 100 µL/min for 5 minutes. After this time, the flow was stopped, and the column was capped. The column reaction proceeded without flow for 65 minutes. After this time, the column was rinsed with 1:1 H₂O:IPA for 30 minutes at 100 µL/min.

4.3.2 Sample preparation

4.3.2.1 IdeS digestion and DTT reduction

The IdeS enzyme was used to digest IgG1, cleaving below the hinge region into two Fc/2 fragments and one (Fab')₂ fragment (Figure 4.2).⁴⁷ Next, dithiothreitol was added to reduce the disulfide bonds in the (Fab')₂ subunit, producing two light chain and two Fd' fragments. For each IgG1 digestion, 90 µg of a pharmaceutical grade monoclonal antibody provided by Genentech, Inc. was incubated with 90 units of IdeS (FabRICATOR, Genovis AB, Lund, Sweden) in 50 mM Tris buffer, pH 8. The unit definition for IdeS as provided by the manufacturer is as follows: one unit digests ≥ 95% of 1 µg human IgG when incubated in 10 mM sodium phosphate, 137 mM NaCl, 2.7mM KCl pH 7.4 at 37 °C for 30 minutes. The final concentration of the antibody was 9 mg/mL for the digestion. The incubation proceeded at 37 °C for a variable, controlled time. For reduction, 2 µL of 500 mM DTT was added and incubation continued at 37 °C for a variable, controlled time. After adding the DTT, the concentration of the antibody

was 7.5 mg/mL. A pictorial description of the digestion and reduction process can be seen in Figure 4.2).

4.3.2.2 IdeS digestion, CpB digestion, and DTT reduction

For C-terminal lysine removal, IdeS digestion, and DTT reduction, the protocol was similar. For each vial, recombinant rat carboxypeptidase B (CpB, Prospec, Ness Ziona, Israel) and IdeS enzymes were added, and the digestions proceeded concomitantly. 90 µg of the monoclonal antibody provided by Genentech, Inc. was incubated with 90 units of IdeS and 0.12 units CpB (0.68 µg) in 50 mM Tris buffer, pH 8. The unit definition for CpB as provided by the manufacturer is as follows: one unit hydrolyzes one µmol of hippuryl-L-arginine per minute at 25 °C, pH 7.65. The antibody concentration was 8.4 mg/mL for the digestions. The incubation proceeded at 37 °C for 30 minutes. For reduction, 2 µL of 500 mM DTT was added and incubation continued at 37 °C for 15 minutes. After adding the DTT, the antibody concentration was 7.1 mg/mL.

4.3.2.3 Deglycosylated Fc study

For glycan cleavage, the enzymes were added concurrently and digested overnight. 90 µg of the monoclonal antibody provided by Genentech, Inc. was incubated with 90 units of IdeS (1.3 µL at 30 mg/mL), 0.5 µL CpB and 0.5 µL PNGase F. In the morning, the DTT reduction proceeded as normal and stored at 4 °C until ready to use.

4.3.3 HILIC and HILIC-MS

For UHPLC, a Waters Acquity I-Class UHPLC system was used (Waters Corporation, Milford, MA) with UV absorbance detection at 215 nm. Ultrapure water (80 MΩ cm) and HPLC grade acetonitrile were used. Solvent A was H₂O + 0.1% TFA and solvent B was acetonitrile + 0.1% TFA. The gradient was 75-65% B over 20 minutes, the flow rate was 100 µL/min and the column temperature were 30°C. The column was equilibrated with the starting mobile phase composition for 15 minutes before each run. For UHPLC-MS analysis, the Waters Acquity I-Class UHPLC system was used with a Thermo LTQ Velos mass spectrometer. Solvent A was H₂O with 0.1% FA + 0.025% TFA and solvent B was acetonitrile with 0.1% FA + 0.025% TFA. The gradient was 80-70% B over 20 minutes. The flow rate was 100 µL/min. The column temperature was

30°C. The sample is best injected in a solvent as similar as possible to the HILIC starting run conditions to avoid precipitation or early elution.⁴⁸ Therefore, the sample was prepared by diluting digested IgG1 in 75% ACN + 0.2% TFA to 1 mg/mL. Note that room temperature is best for solubility of the IgG1 tested, considering the high organic in the sample solvent.

For the HILIC-MS, the chromatographic method was the same, but a different UHPLC instrument was used: an UltiMate 3000 RSLC (Thermo Fisher Scientific) LC system. This was configured with HPG-3400RS binary gradient pump with a 400 μ L static mixer, WPS-3000TRS thermostatted split loop autosampler, TCC-3000RS thermostatted column compartment, and DAD-3000RS diode array detector with a semi-micro flow cell (2.5 μ L, 7 mm). Control of the system was via DCMSlink through Xcalibur software also provided by Thermo Fisher Scientific. The HPLC was coupled to a Thermo Exactive Plus EMR Orbitrap instrument (Thermo Fisher Scientific). The samples were analyzed using the following parameters for data acquisition: 3.90 kV spray voltage; 325 °C capillary temperature; 100 S-lens RF level; 15 sheath gas flow rate and 4 AUX gas flow rate in ESI source; 1500 to 6000 m/z scan range; desolvation, in-source CID 100 eV, CE 0; resolution of 17500 at m/z 200; positive polarity; 10 microscans; 3×10^6 AGC target; 25 V source DC offset; 8 V injection flatapole DC; 7 V inter flatapole lens; 6 V bent flatapole DC; 0 V transfer multipole DC tune offset; 0 V C-trap entrance lens tune offset; and trapping gas pressure setting of 2.

The mass spectrum deconvolution was performed with Thermo Protein Deconvolution 4.0 under the following parameters: 3-10 minimum adjacent charges, 95% confidence noise rejection, 1500-6000 m/z range, 20 ppm mass tolerance, and 1-100 charge state range. The relative quantification was based on the intensity reported by Protein Deconvolution 4.0 of each individual peak versus total summed intensities.

4.4 Results and Discussion

4.4.1 Necessity of digestion and reduction

In order to find the fastest assay possible, we injected whole therapeutic IgG1 and performed a separation to compare with the digested and reduced chromatogram. The

whole IgG1 does not separate well, and glycoforms are indistinguishable (Figure 4.4). There are two potential reasons for this, perhaps even compounding issues. First, molecular dynamics studies show that IgG1's Fc domain is highly dynamic, and the attached glycan itself is movable.⁴⁹ Second, the crystal structure of IgG1 molecules place the glycans in between the Fc fragments, making a stationary phase interaction difficult.⁵⁰ Thus, at least digestion is necessary for the stationary phase to access the glycan for a separation.

However, it was then considered whether reduction is necessary. After all, the DTT reduction only breaks apart the Fab fragment, but not affecting the Fc or its attached glycans. Therefore, we explored potential chromatographic changes with reduction. Figure 4.5 shows relative peak area recovery of IgG1 Fc glycoforms in HILIC-HPLC-UV. It was found that a 15-minute reduction of IgG1 provides a 4x greater recovery of the Fc glycoforms than the unreduced IgG1, despite both being cleaved from the Fab fragment by IdeS. It was decided that reduction would remain part of the protocol to maintain high peak recovery.

4.4.2 Digestion and reduction time optimization

The speeds of the IdeS and DTT reactions were studied to determine how fast the glycan assay could be completed. The results thus far used a 30-minute IdeS reaction time and a 15-minute DTT reduction time, as mentioned earlier. The possibility of shortening these times further was investigated. The IdeS digestion was investigated for a reaction time as little as 5 minutes, with the DTT reduction for 15 minutes. Peak areas were used for quantitation, separated with HILIC, and detected via UV absorbance for three replicate reactions. The data are presented in Figure 4.6A, where the error bars represent 95% confidence intervals. The results show that the IdeS reaction times do not affect glycosylation ratios, with a 5-min reaction time giving areas for all eight peaks that agree with the peak areas measured for the recommended 30-minute IdeS reaction time. The IdeS reaction is confirmed to be complete because the peak due to intact mAb is absent, as shown in the supporting information.

The possibility of shortening the DTT reduction time was investigated for the IdeS digestion time of 30 minutes. Again, three replicate reactions were run. The data are

presented in Figure 4.6B. The behavior of the highest peak, which is peak 3, suggests that a 5-minute reduction time might not be quite sufficient for reduction, whereas peak 6 suggests it is sufficient. Conservatively, 10 minutes is sufficient for quantitative reproducibility for all eight glycoform peaks in the chromatogram. In principle, the reduction step is not needed for the assay because the Fab fragment elutes well beyond the last glycan, but it extends the time needed to elute all fragments. It is noted that Fab fragments are sometimes glycosylated, in which case it would be advised to omit the reduction step since the glycosylated fragments would be similar in size to Fc/2 fragments. In this case, Fab would be even more strongly retained, avoiding overlap but increasing chromatographic run time.

4.4.3 PAAm column and necessity of TFA

Figure 4.3 shows chromatograms of IgG1 fragments separated on the PAAm column with varying amounts of TFA in the mobile phase – comparing 0.1% TFA, 0.1% FA + 0.025% TFA, and 0.5% FA. Despite a high percentage of acid in the mobile phase, 0.5% FA shows no selectivity among the glycans. However, 0.1% TFA and 0.1% FA + 0.025% TFA produce very similar profiles. This means that the FA + TFA solvent can be used when MS-compatibility is needed while still providing excellent resolution.

4.4.4 HILIC separation and MS peak identification

To characterize the chromatography and identify the peaks, the manufacturer's recommended reaction times were used: 30 minutes for IdeS digestion and 15 minutes for DTT reduction.²² It was confirmed that the intact mAb peak and the Fab peak were absent from the HILIC chromatogram. Figure 4.7 shows the chromatogram for HILIC of the Fc/2 fragments of IgG1, comparing a commercial HILIC column with the HILIC column made of the polyacrylamide brush layer and used in this work. The comparison shows that the resolution is higher for the HILIC columns used in this work. In particular, the second and third most abundant glycans, peaks 6 and 7, are strongly overlapped for the conventional column but are baseline resolved for the new column. The higher resolution is more evident with the chromatograms plotted on a 10-fold more sensitive scale. For example, it is easier to see that peak 5 is much more resolved for the

polyacrylamide column, and peak 4 is a shoulder, whereas the commercial column only shows peak 5 and it is just a shoulder. Peaks 1 and 2 are one symmetric peak for the commercial column, as illustrated by the dotted vertical line, whereas these are beginning to separate for the polyacrylamide column.

The peaks were identified using HILIC-MS, with the TIC chromatogram shown in Figure 4.8A. For this LCMS, 0.1% TFA was used to preserve the HILIC resolution. The high sensitivity of the Orbitrap mass spectrometer enables identification despite the ion-suppression caused by TFA in the mobile phase. The S/N is not as high in MS compared to UV absorbance, therefore, some of the smaller peaks are lost. In an assay, once the peaks have been identified by mass spectrometry, UV absorbance can be used to gain high S/N, as well as save expense and allow for ease of operation. The peak identifications are marked on the chromatogram. The raw ESI mass spectra for all eight peaks are provided in the supplemental material. The deconvoluted mass spectra for all peaks except for 4 and 5 are shown in Figure 4.8B. The G0F and two isomers of G1F are expected to be the main peaks, and the MS confirms the identities. The deconvoluted mass spectra indicate that these peaks have little overlap from other protein peaks. For monitoring the manufacturing of mAbs, these are the most important glycans to monitor. Peak 1 is shown to be from G0, giving a clean deconvoluted mass spectrum, and peak 2 is identified as G0F-N, showing overlap with peak 1. Peak 8 is well separated from other Fc/2 glycans, and its deconvoluted mass spectrum shows it to be G2F.

Peaks 4 and 5 in the chromatogram of Figure 4.8 are strongly overlapped, and one can see that these are distinct in the expanded scale of

Figure 4.7D. The deconvoluted mass spectrum for the two peaks together is given in Figure 4.11A, and it consists of three species. These include a high abundance peak for G0F due to the overlap with intense peak 3, as expected. Masses are also shown that correspond to G0F+Lys (i.e., G0F having a C-terminal lysine) and Man5. The C-terminal lysine assignment is based on the mass being shifted up by 128 Da from that of peak 4 for G0F. To confirm this assignment, Figure 4.11B shows the chromatogram before and after enzymatic treatment to clip the C-terminal lysine from the fragment. The results confirm that there is a significant amount of G0F+Lys. The Man5 peak is considered a critical quality attribute for mAb therapeutics because it affects clearing time.⁵¹ Removal of the C-terminal lysine would help in the detection of the Man5 peak, and the enzymatic cleavage can be performed during the IdeS cleavage to conserve the speed of analysis.

The glycan structures for all peaks, as assigned by mass spectrometry, are summarized in Table 1. The first entry (“no glycan”) is the known mass of the Fc/2 fragment without glycosylation, enabling calculation of glycan masses. The data show that the masses of the glycans recovered from the deconvoluted mass spectra are in good general agreement with the expected masses.

4.4.5 Deglycosylated Fc peak

In order to determine the amount of deglycosylated Fc, we first needed to find where it elutes. To accomplish this, in addition to treating IgG1 with IdeS and DTT, PNGase F was also used to cleave the glycan from the Fc fragment. In Figure 4.12, a comparison is made between A) the sample with PNGase F treatment and B) the sample without treatment. A new peak appears at the same time the glycosylated Fc peak shrinks, evidence of the new peak being deglycosylated Fc. The deglycosylated Fc elutes slightly after the light chain and is not totally resolved. Furthermore, there appears to be very little deglycosylated Fc in the sample without PNGase added, so we did not continue determining the amount of deglycosylated Fc. Another method such as RPLC may be helpful in resolving the two peaks, but this was not tested.

MS analysis was also performed on the deglycosylated sample, where we found the new peak to have a mass of 23783 Daltons. Since the Fc with G0 glycan weighs 25198 Da, the weight of the glycan alone was found to be 1425 Da. Likewise, since the Fc with

attached G1 glycan weighs 25386 Da, the weight of G1 alone is 1603 Da. Figure 4.13 shows the TIC chromatogram of the HILIC separation of PNGase-treated IgG1.

4.4.6 Implementation

A simple method for purification and analysis is envisioned to use the assay at the manufacturing site (Figure 4.14). First, the raw material is sampled from the bioreactor. Next, the antibody is removed from the matrix via affinity purification. The antibody is then digested with IdeS and reduced with DTT before separation of the glycoforms via HILIC HPLC. This short analysis allows the manufacturing site to check glycosylation during production and adjust as needed.

4.5 Conclusions

Combining the shortest IdeS digestion time and the shortest DTT reduction time gives a total reaction time of only 15 min for the assay of the glycosylation using the Fc/2 fragments. Relative peak heights for the G0F glycans are $64.6 \pm 0.2\%$ and for the G1F isomers, $14.1 \pm 0.2\%$ and $6.1 \pm 0.2\%$, which indicates the assay is sufficiently precise to monitor the variability of major glycans in mAb manufacturing. The high resolution of the HILIC column and its ability to be used for HILIC-MS is enabling for this application. Given that the chromatographic separation is complete in 20 minutes, and the column requires 15 minutes of re-equilibration with the mobile phase before the next run, which can be done during the time that the reactions are run, then the total assay time including sample preparation is typically 35 minutes. In addition, the labor is minimal and amenable to automation. Higher speed and less labor make this method feasible for monitoring the manufacturing of mAbs in real-time.

4.6 References

1. Köhler, G. & Milstein, C. Continuous cultures of fused cells secreting antibody of predefined specificity. *Nature* **256**, 495–497 (1975).
2. Liu, H., Gaza-Bulseco, G., Faldu, D., Chumsae, C. & Sun, J. Heterogeneity of Monoclonal Antibodies. *Journal of Pharmaceutical Sciences* **97**, 2426–2447 (2008).
3. Guo, D. *et al.* Mechanisms of unintended amino acid sequence changes in recombinant monoclonal antibodies expressed in Chinese Hamster Ovary (CHO) cells. *Biotechnology and Bioengineering* **107**, 163–171 (2010).
4. Guidance for Industry: Q8(R2) Pharmaceutical Development.
5. Jefferis, R. Glycosylation as a strategy to improve antibody-based therapeutics. *Nature Reviews Drug Discovery* **8**, 226–234 (2009).
6. Deisenhofer, J. Crystallographic refinement and atomic models of a human Fc fragment and its complex with fragment B of protein A from *Staphylococcus aureus* at 2.9- and 2.8-Å resolution. *Biochemistry* **20**, 2361–2370 (1981).
7. Krapp, S., Mimura, Y., Jefferis, R., Huber, R. & Sondermann, P. Structural Analysis of Human IgG-Fc Glycoforms Reveals a Correlation Between Glycosylation and Structural Integrity. *Journal of Molecular Biology* **325**, 979–989 (2003).
8. Suzuki, M., Kato, C. & Kato, A. Therapeutic antibodies: their mechanisms of action and the pathological findings they induce in toxicity studies. *Journal of Toxicologic Pathology* **28**, 133–139 (2015).
9. van Sorge, N. M., van der Pol, W.-L. & van de Winkel, J. G. J. FcγR polymorphisms: Implications for function, disease susceptibility and immunotherapy. *Tissue Antigens* **61**, 189–202 (2003).
10. Arnold, J. N., Wormald, M. R., Sim, R. B., Rudd, P. M. & Dwek, R. A. The Impact of Glycosylation on the Biological Function and Structure of Human Immunoglobulins. *Annual Review of Immunology* **25**, 21–50 (2007).
11. Higel, F., Seidl, A., Sörgel, F. & Friess, W. N-glycosylation heterogeneity and the influence on structure, function and pharmacokinetics of monoclonal antibodies and Fc fusion proteins. *European Journal of Pharmaceutics and Biopharmaceutics* **100**, 94–100 (2016).
12. Hooker, A. D. & James, D. C. Analysis of glycoprotein heterogeneity by capillary electrophoresis and mass spectrometry. *Mol Biotechnol* **14**, 241–249
13. Gennaro, L. A., Salas-Solano, O. & Ma, S. Capillary electrophoresis–mass spectrometry as a characterization tool for therapeutic proteins. *Analytical Biochemistry* **355**, 249–258 (2006).

14. Melmer, M. *et al.* HILIC analysis of fluorescence-labeled N-glycans from recombinant biopharmaceuticals. *Analytical and Bioanalytical Chemistry* **398**, 905–914 (2010).
15. Liu, B. *et al.* The availability of glucose to CHO cells affects the intracellular lipid-linked oligosaccharide distribution, site occupancy and the N-glycosylation profile of a monoclonal antibody. *Journal of Biotechnology* **170**, 17–27 (2014).
16. St. Amand, M. M., Radhakrishnan, D., Robinson, A. S. & Ogunnaike, B. A. Identification of manipulated variables for a glycosylation control strategy: Identifying Manipulated Variables for Glycosylation Control. *Biotechnology and Bioengineering* **111**, 1957–1970 (2014).
17. Fan, Y. *et al.* Amino acid and glucose metabolism in fed-batch CHO cell culture affects antibody production and glycosylation: Process-Dependent IgG Glycosylation. *Biotechnology and Bioengineering* **112**, 521–535 (2015).
18. Kildegaard, H. F., Fan, Y., Sen, J. W., Larsen, B. & Andersen, M. R. Glycoprofiling effects of media additives on IgG produced by CHO cells in fed-batch bioreactors: Glycoprofiling Effects of Media Additives on IgG. *Biotechnology and Bioengineering* **113**, 359–366 (2016).
19. Tharmalingam, T., Wu, C.-H., Callahan, S. & T. Goudar, C. A framework for real-time glycosylation monitoring (RT-GM) in mammalian cell culture: A Framework for Real-time Glycosylation Monitoring. *Biotechnology and Bioengineering* **112**, 1146–1154 (2015).
20. Villiger, T. K. *et al.* Controlling the time evolution of mAb N-linked glycosylation, Part I: Microbioreactor experiments: Biotechnol. Prog. *Biotechnology Progress* **32**, 1123–1134 (2016).
21. Karst, D. J., Steinebach, F., Soos, M. & Morbidelli, M. Process performance and product quality in an integrated continuous antibody production process: Integrated Continuous Antibody Production Process. *Biotechnology and Bioengineering* **114**, 298–307 (2017).
22. Periat, A. *et al.* Potential of hydrophilic interaction chromatography for the analytical characterization of protein biopharmaceuticals. *Journal of Chromatography A* **1448**, 81–92 (2016).
23. Cook, K. S., Bullock, K. & Sullivan, T. Development and qualification of an antibody rapid deglycosylation method. *Biologicals* **40**, 109–117 (2012).
24. Lauber, M. A. *et al.* Rapid Preparation of Released N-Glycans for HILIC Analysis Using a Labeling Reagent that Facilitates Sensitive Fluorescence and ESI-MS Detection. *Analytical chemistry* **87**, 5401–9 (2015).


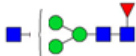

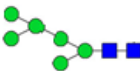




25. Flynn, G. C., Chen, X., Liu, Y. D., Shah, B. & Zhang, Z. Naturally occurring glycan forms of human immunoglobulins G1 and G2. *Molecular Immunology* **47**, 2074–2082 (2010).
26. Huckabee, A. G. *et al.* In-column bonded phase polymerization for improved packing uniformity. *Journal of Separation Science* **40**, 2170–2177 (2017).
27. Zhang, Z., Wu, Z. & Wirth, M. J. Polyacrylamide brush layer for hydrophilic interaction liquid chromatography of intact glycoproteins. *Journal of Chromatography A* **1301**, 156–161 (2013).
28. Cai, J. *et al.* A polyacrylamide-based silica stationary phase for the separation of carbohydrates using alcohols as the weak eluent in hydrophilic interaction liquid chromatography. *Journal of Chromatography A* **1524**, 153–159 (2017).
29. D'Atri, V., Fekete, S., Beck, A., Lauber, M. & Guilleme, D. Hydrophilic Interaction Chromatography Hyphenated with Mass Spectrometry: A Powerful Analytical Tool for the Comparison of Originator and Biosimilar Therapeutic Monoclonal Antibodies at the Middle-up Level of Analysis. *Analytical Chemistry* **89**, 2086–2092 (2017).
30. Tetaz, T., Detzner, S., Friedlein, A., Molitor, B. & Mary, J.-L. Hydrophilic interaction chromatography of intact, soluble proteins. *Journal of Chromatography A* **1218**, 5892–5896 (2011).
31. Schachner, L. *et al.* Characterization of Chain Pairing Variants of Bispecific IgG Expressed in a Single Host Cell by High-Resolution Native and Denaturing Mass Spectrometry. *Analytical Chemistry* **88**, 12122–12127 (2016).
32. Yin, Y. *et al.* Precise quantification of mixtures of bispecific IgG produced in single host cells by liquid chromatography-Orbitrap high-resolution mass spectrometry. *mAbs* **8**, 1467–1476 (2016).
33. Ehkirch, A. *et al.* An Online Four-Dimensional HIC×SEC-IM×MS Methodology for Proof-of-Concept Characterization of Antibody Drug Conjugates. *Analytical Chemistry* **90**, 1578–1586 (2018).
34. Beck, A., Wagner-Rousset, E., Ayoub, D., Van Dorsselaer, A. & Sanglier-Cianférani, S. Characterization of Therapeutic Antibodies and Related Products. *Analytical Chemistry* **85**, 715–736 (2013).
35. Zhang, B., Rempel, D. & Gross, M. Protein Footprinting by Carbenes on a Fast Photochemical Oxidation of Proteins (FPOP) Platform. *Journal of The American Society for Mass Spectrometry* **27**, 552–555 (2016).
36. Tian, Y. & Ruotolo, B. T. The growing role of structural mass spectrometry in the discovery and development of therapeutic antibodies. *The Analyst, Analyst* **143**, 2459–2468 (2018).

37. Zhang, H. M. *et al.* Structural and Functional Characterization of a Hole-Hole Homodimer Variant in a ‘Knob-Into-Hole’ Bispecific Antibody. *Analytical Chemistry* **89**, 13494–13501 (2017).
38. Heck, A. J. R. Native mass spectrometry: a bridge between interactomics and structural biology. *Nature methods* **5**, 927–33 (2008).
39. Chen, Z., Wang, Z., Ren, J. & Qu, X. Enzyme Mimicry for Combating Bacteria and Biofilms. *Accounts of chemical research* **51**, 789–799 (2018).
40. Ayoub, D. *et al.* Correct primary structure assessment and extensive glyco-profiling of cetuximab by a combination of intact, middle-up, middle-down and bottom-up ESI and MALDI mass spectrometry techniques. *mAbs* **5**, 699–710 (2013).
41. Yang, Y., Wang, G., Song, T., Lebrilla, C. B. & Heck, A. J. R. Resolving the micro-heterogeneity and structural integrity of monoclonal antibodies by hybrid mass spectrometric approaches. *mAbs* **9**, 638–645 (2017).
42. Berkowitz, S. A., Engen, J., Mazzeo, J. & Jones, G. B. Analytical tools for characterizing biopharmaceuticals and the implications for biosimilars. *Nature Reviews Drug Discovery* **11**, 527–540 (2012).
43. Beck, A., Sanglier-Cianféran, S. & Van Dorsselaer, A. Biosimilar, biobetter, and next generation antibody characterization by mass spectrometry. *Analytical chemistry* **84**, 4637–46 (2012).
44. Zauner, G. *et al.* Glycoproteomic Analysis of Antibodies. *Molecular & Cellular Proteomics* **12**, 856–865 (2013).
45. Zhang, H., Cui, W. & Gross, M. Mass spectrometry for the biophysical characterization of therapeutic monoclonal antibodies. *Febs Letters* **588**, 308–317 (2014).
46. Song, T., Ozcan, S., Becker, A. & Lebrilla, C. B. In-Depth Method for the Characterization of Glycosylation in Manufactured Recombinant Monoclonal Antibody Drugs. *Analytical Chemistry* **86**, 5661–5666 (2014).
47. Vincents, B., von Pawel-Rammingen, U., Björck, L. & Abrahamson, M. Enzymatic Characterization of the Streptococcal Endopeptidase, IdeS, Reveals That It Is a Cysteine Protease with Strict Specificity for IgG Cleavage Due to Exosite Binding [†]. *Biochemistry* **43**, 15540–15549 (2004).
48. Ruta, J., Rudaz, S., McCalley, D. V., Veuthey, J.-L. & Guilleme, D. A systematic investigation of the effect of sample diluent on peak shape in hydrophilic interaction liquid chromatography. *Journal of Chromatography A* **1217**, 8230–8240 (2010).

49. Lee, H. S. & Im, W. Effects of N-Glycan Composition on Structure and Dynamics of IgG1 Fc and Their Implications for Antibody Engineering. *Scientific Reports* **7**, (2017).
50. Saphire, E. O. Crystal Structure of a Neutralizing Human IgG Against HIV-1: A Template for Vaccine Design. *Science* **293**, 1155–1159 (2001).
51. Goetze, A. M. *et al.* High-mannose glycans on the Fc region of therapeutic IgG antibodies increase serum clearance in humans. *Glycobiology* **21**, 949–959 (2011).

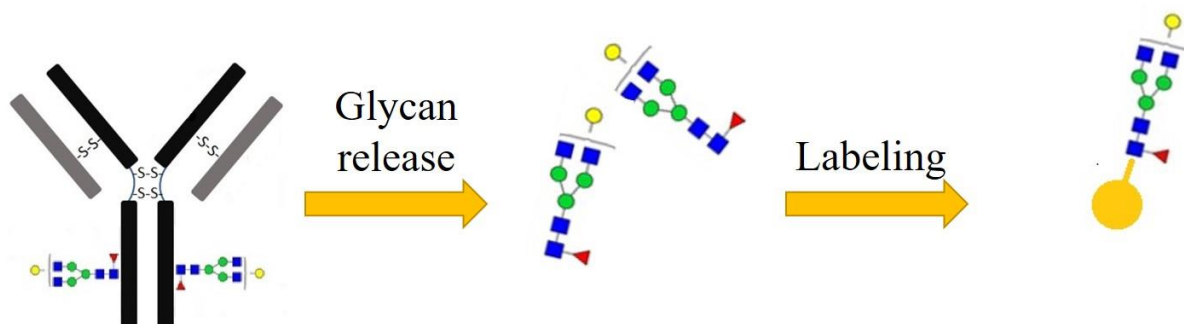
4.7 Figures and Table

Table 4.1: Peak identification by HILIC-MS. The glycan structures and expected masses, in addition to the observed masses of the Fc/2-glycan fragments are detailed.

Peak	Glycan	Structure	Glycan Mass (Da)	Expected Mass (Da)	Observed Mass (Da)	Delta Mass (Da)
	no glycan			23655.8		
1	G0		1299.2	24955.0	24953.9	1.1
2	G0F-N		1242.1	24897.9	24897.2	0.7
3	G0F		1445.3	25101.1	25100.1	1.0
4	M5		1217.1	24872.9	24871.8	1.1
5	G0F+Lys		1445.32 (G0F) +128 (Lys) = 1573.3	25229.1	25228.8	0.3
6	G1F		1607.5	25263.3	25262.3	1.0
7	G1F isomer		1607.5	25263.3	25262.3	1.0
8	G2F		1769.6	25425.4	25424.3	1.1

A) “Gold standard”

1.5 days

**B) Middle-down**

< 30 min

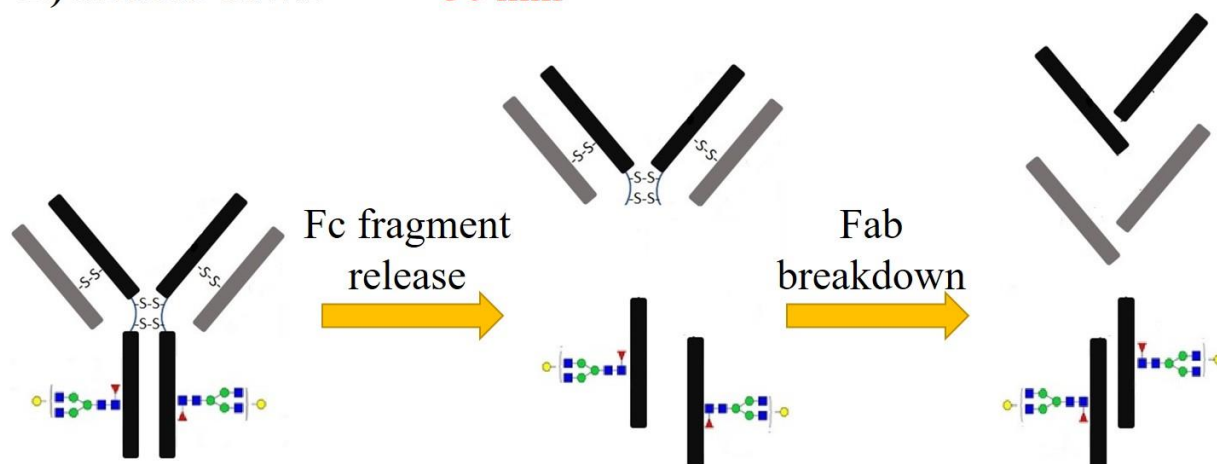


Figure 4.1: Scheme comparing middle-down vs the gold standard of glycosylation analysis. A) In the gold standard, the enzymatic glycan release is slow, followed by labeling before fluorescence or MS detection. B) In the middle-down approach, releasing the Fc subunit is fast, needs no labeling, and can be detected via UV or MS immediately after digestion.

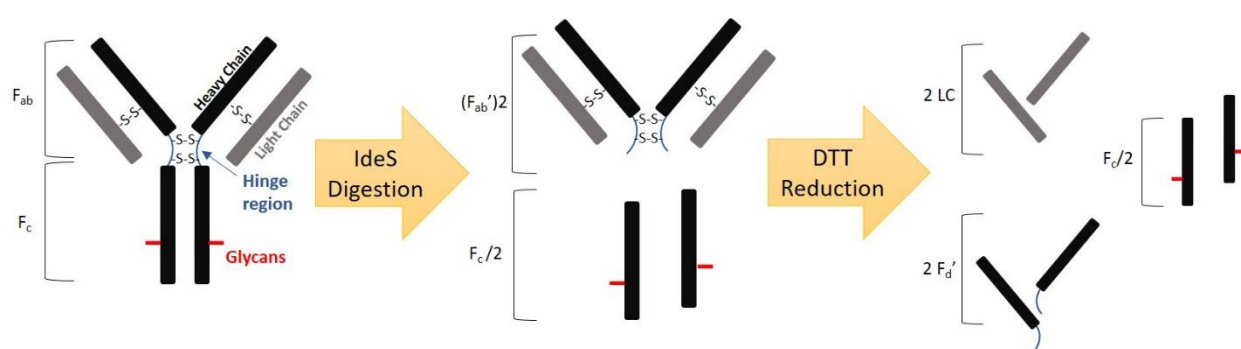


Figure 4.2: A more detailed scheme for middle-down production of IgG1 subunits. Fragments are generated by IdeS digestion below the hinge region, followed by DTT reduction of disulfide bonds. The released $F_c/2$ fragments bearing glycans are then ready for HILIC analysis.

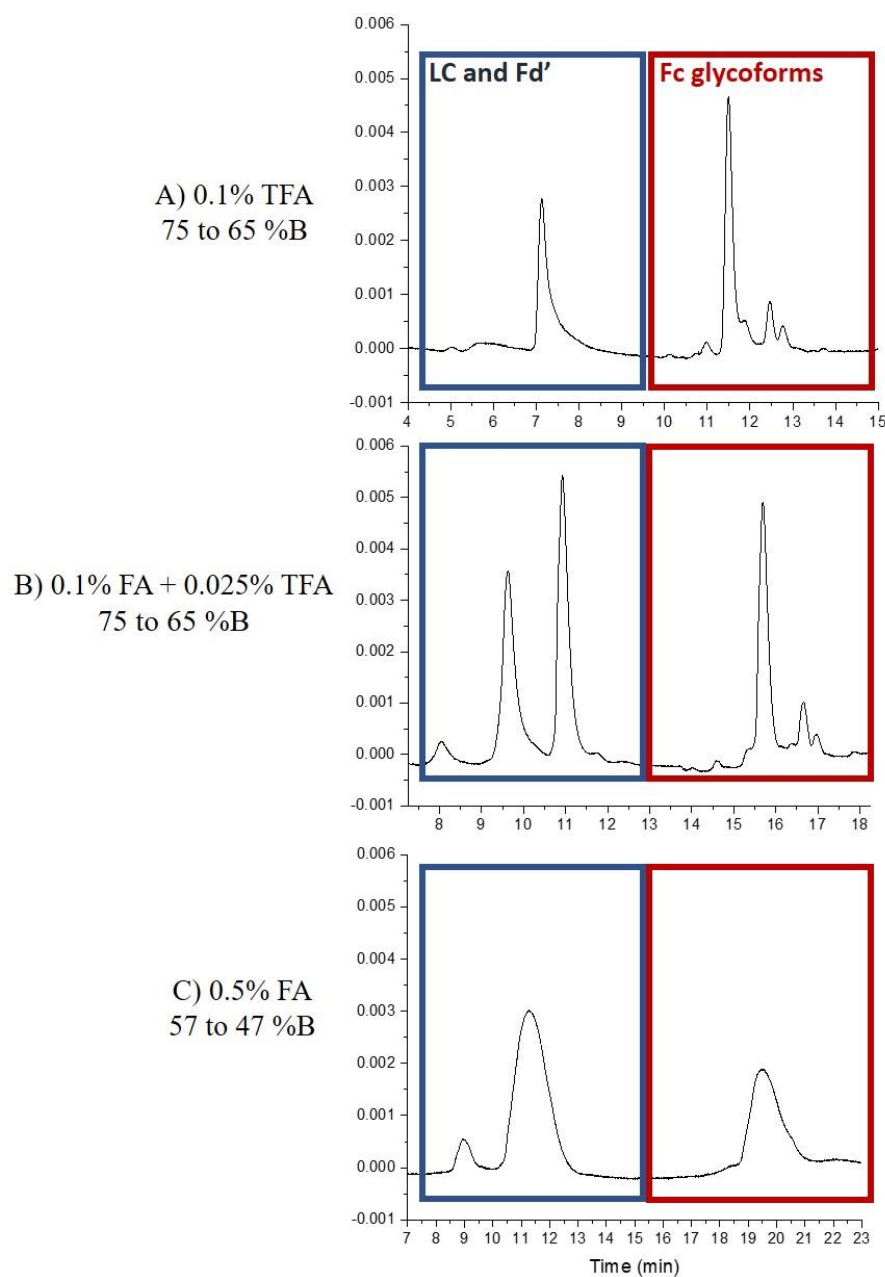


Figure 4.3: Comparison of varying acid modifiers in separation of digested and reduced IgG1 on long-chain polyacrylamide column. A) 0.1% TFA, 75 to 65 %B. B) 0.1% FA + 0.025% TFA, 75 to 65 %B. C) 0.5% FA, 57 to 47 %B. All run conditions were 10% Δ B in 20 min, 70 μ L/min, 0.5 μ g IgG1 digested and reduced injected in starting gradient, detection at 280 nm. Column was a 1 μ m dp in-situ polyacrylamide HILIC column produced with a 70 min reaction time.

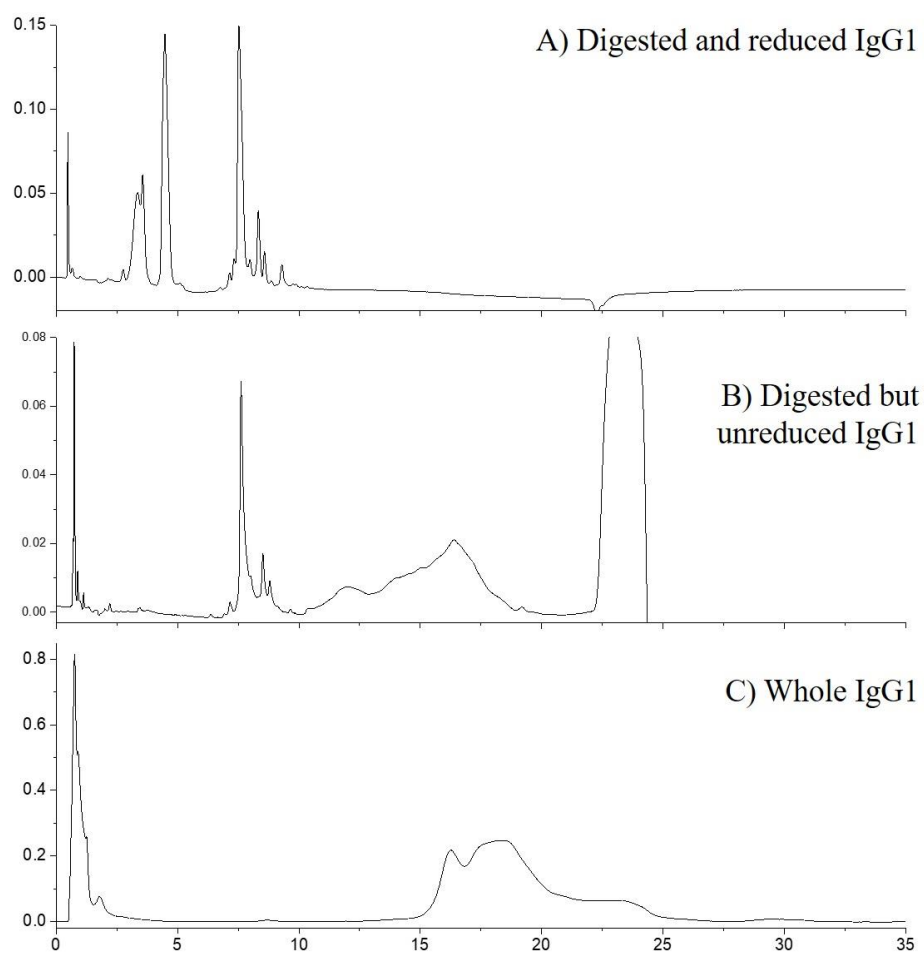


Figure 4.4: Comparison of digested and reduced IgG1 to unaltered IgG1 shows the latter elutes far after the subunits. A) Digested and reduced IgG1 B) Whole IgG1. Column is of a different particle size from the rest of the paper, $d_p = 620$ nm. Conditions 75 to 60% ACN in 20 min at 30°C, 1.4 μ g injection, 100 μ L/min, UV detection 215 nm.

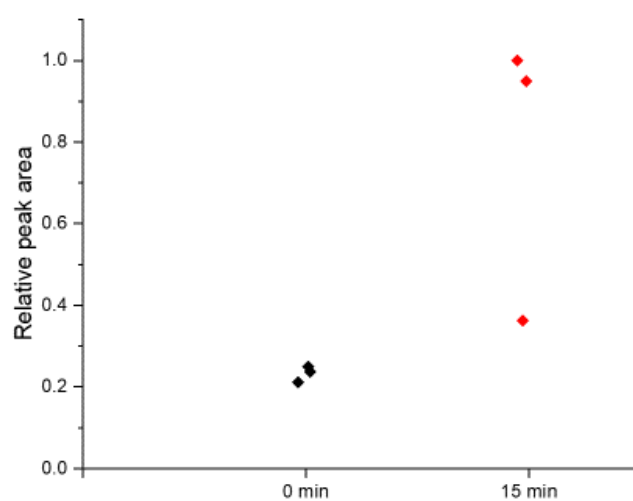


Figure 4.5: Relative peak area recovery of IgG1 Fc glycoforms in HILIC-HPLC-UV. A 15 min reduction of IgG1 provides 4x greater recovery than the unreduced IgG1, despite both being cleaved from the Fab fragment by IdeS. Note that the reduced IgG1 has an outlier of low recovery; this outlier is the first run of the set which seems to be causing the low recovery.

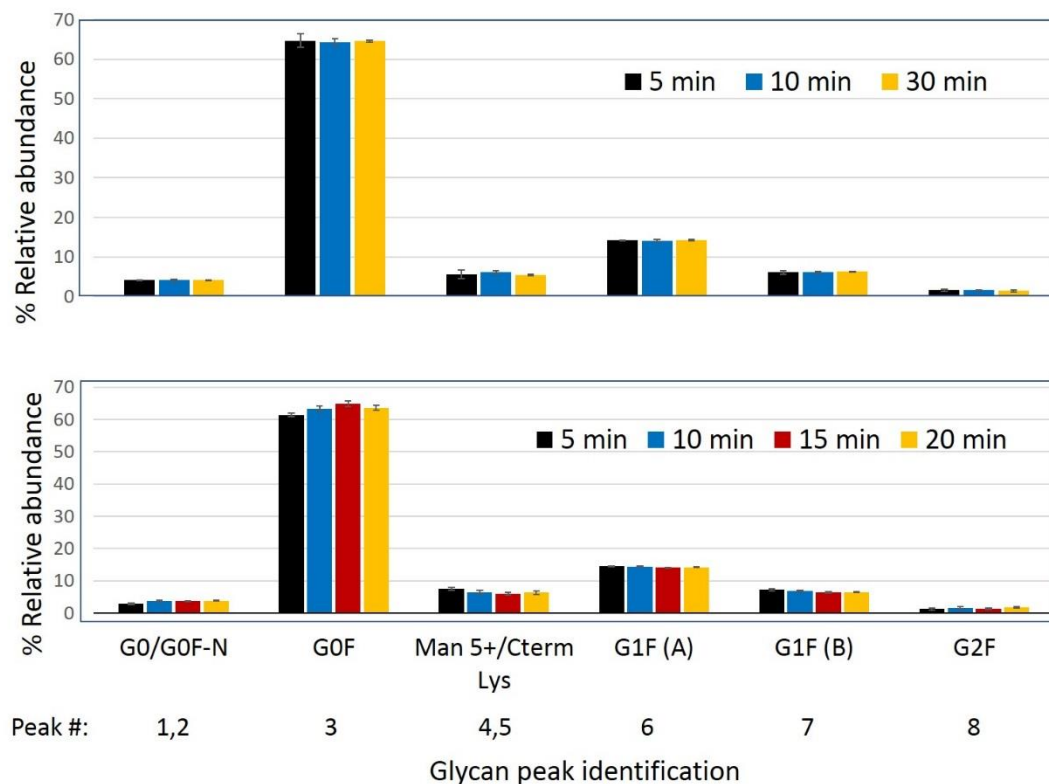


Figure 4.6: A) Peak heights and errors for varying times of digestion with IdeS. B) Peak heights and errors for varying times of reduction with DTT, after digestion with IdeS. The peaks are as labeled in Figure 3A. The height of each peak is represented as the percentage of total Fc/2 glycoforms in the sample. The error bars represent the 95% CI based on three replicate reactions, each followed by HILIC separation and quantitation by peak area.

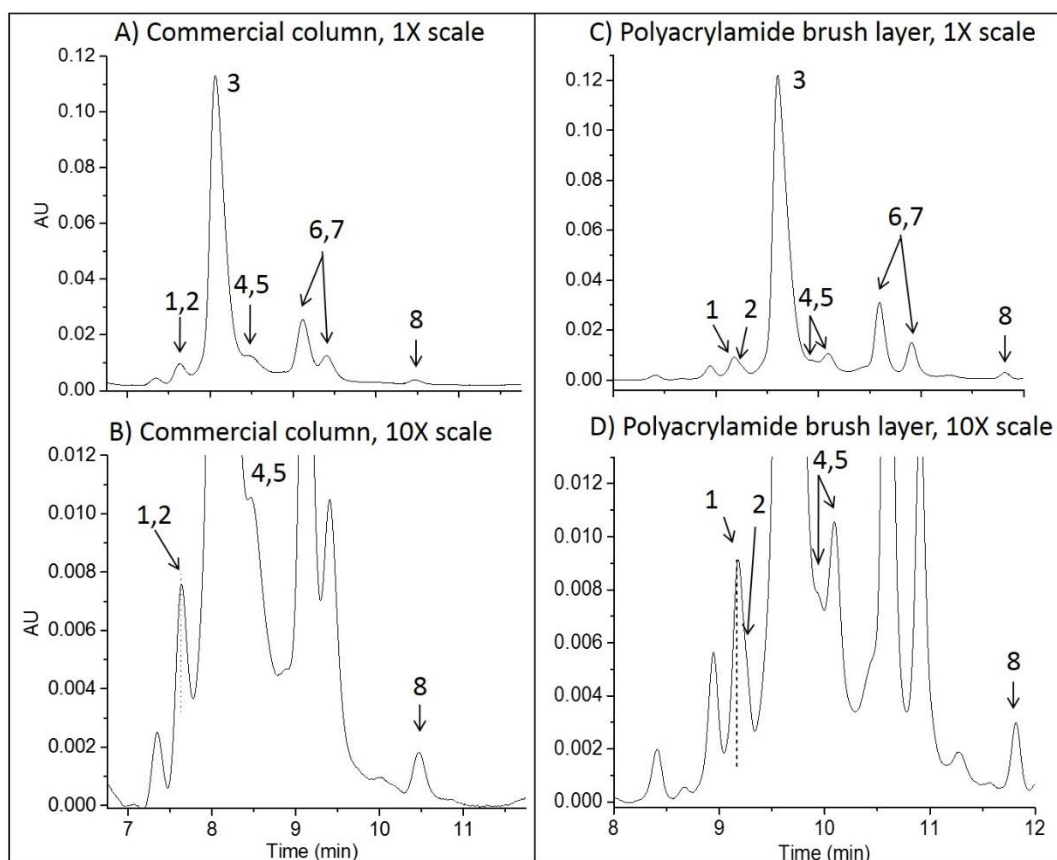


Figure 4.7: HILIC chromatograms using UV detection at 215 nm for IgG1 Fc/2 fragments prepared as in scheme from Figure 1 A) Commercial column (Waters Acquity Amide Glycoprotein 2.1 mm x 150 mm), with conditions 70 to 63% ACN in 20 min at 30°C, 4 μ g injection, 200 μ L/min. B) Same as panel A but absorbance is zoomed 10x. C) Polyacrylamide brush layer HILIC column (2.1 mm x 5 mm), with conditions 75 to 65% ACN in 20 min at 30°C, 1 μ g injection, 100 μ L/min. D) Same as panel C but absorbance is zoomed 10x. For both columns, 0.1% TFA was used as the mobile phase additive.

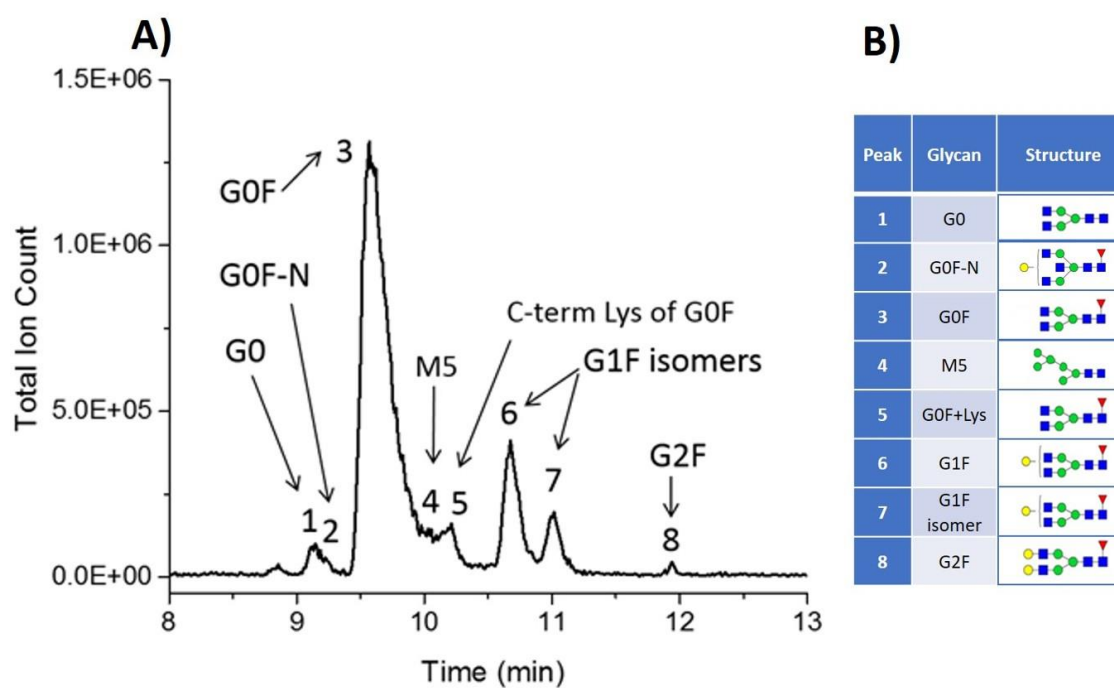


Figure 4.8: A) HILIC-MS of the Fc/2 glycoforms of the pharmaceutical grade IgG1 using the polyacrylamide brush layer HILIC column, with the labels identifying each of the glycans. B) Discovered glycan structures based on MS identification.

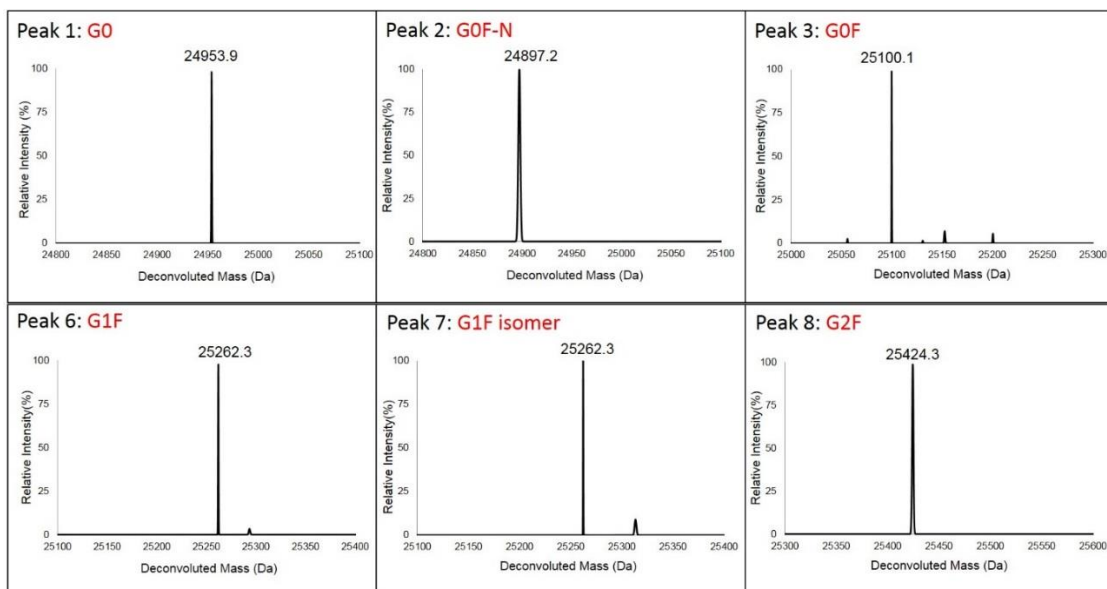


Figure 4.9: The deconvoluted mass spectra for all peaks labeled in the chromatogram of Figure 4.8A, except for peaks 4,5.

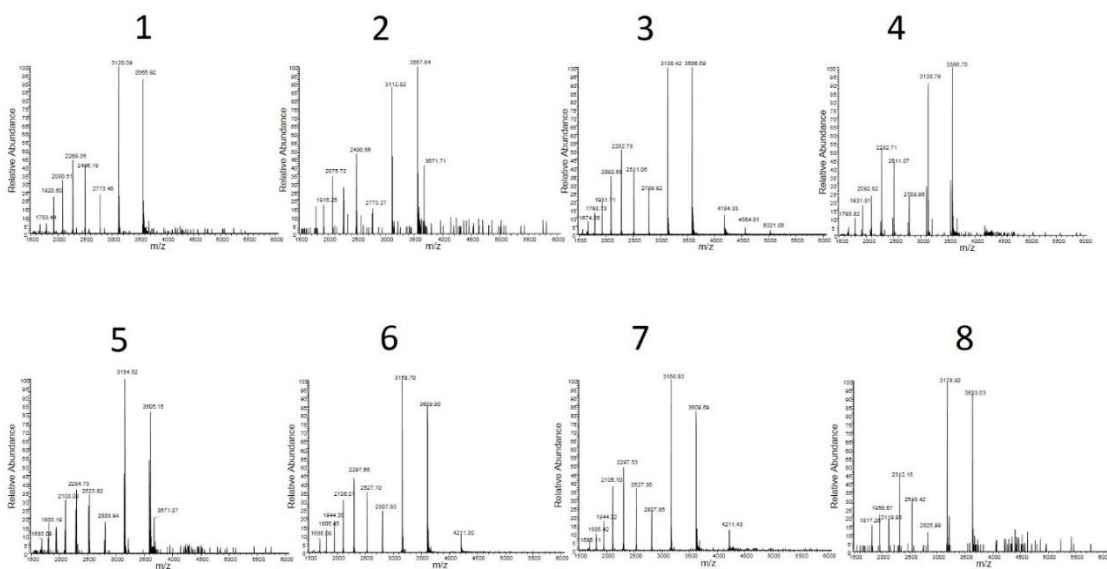


Figure 4.10: Raw mass spectra of the 8 peaks, separated via HILIC as seen in the chromatogram of Figure 4.8A, showing the charge distributions and their m/z range from the electrospray process. These were used to generate the deconvoluted mass spectra presented in the paper.

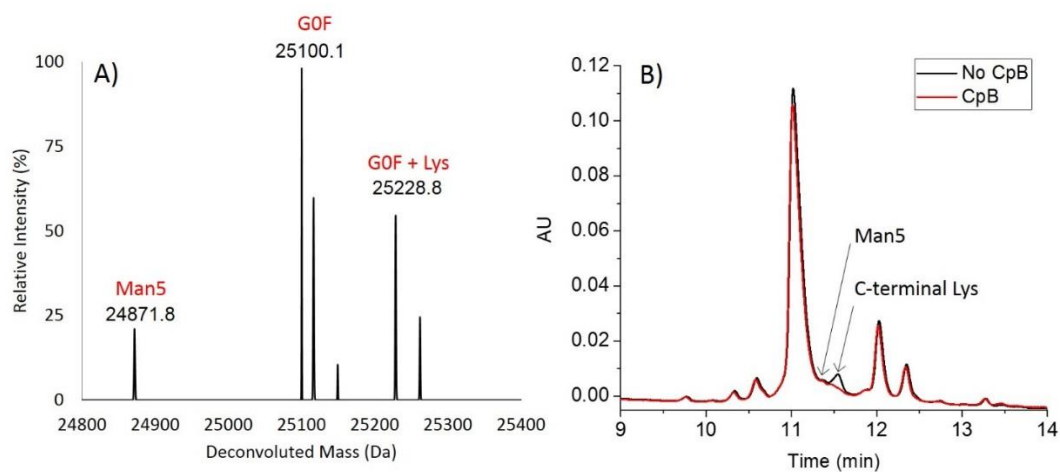


Figure 4.11: A) Deconvoluted mass spectrum for overlapped peaks 4 and 5, showing presence of the expected Man5 peak and a GOF peak with a C-terminal lysine. The overlap with peak 3 gives the large single from GOF. B) Initial chromatogram (black) and chromatogram after enzymatic removal of the C-terminal lysine using CpB (red), confirming the presence of GOF+Lys in the initial chromatogram at this peak position.

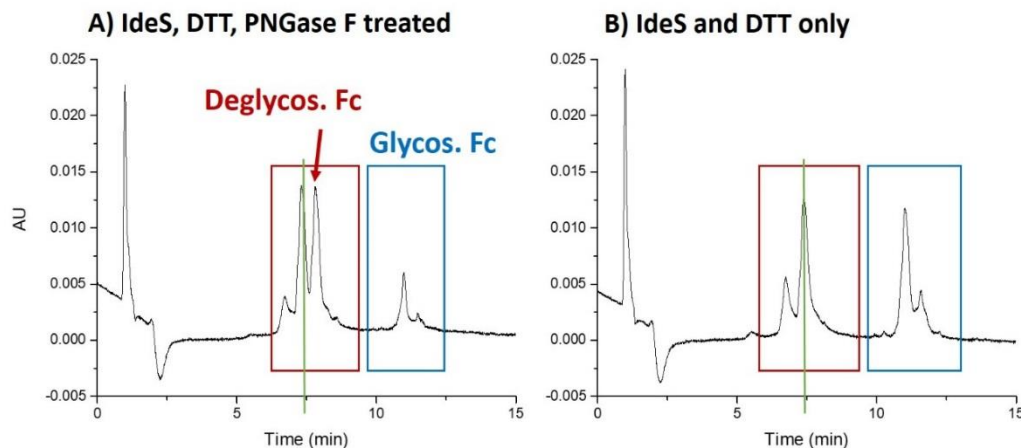


Figure 4.12: Digested and reduced IgG1 separated in HILIC, with A) treated with PNGase F to remove the glycosylation from the Fc fragment and B) no treatment with PNGase F. In the PNGase F treated chromatogram, the deglycosylated Fc elutes as a separate peak. The glycosylated Fc has not disappeared entirely from the chromatogram, indicating an incomplete digestion.

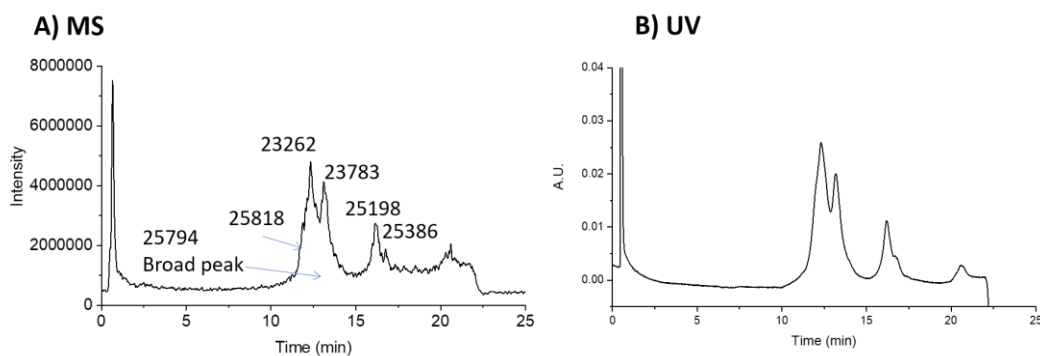


Figure 4.13: HILIC chromatograms of IdeS and PNGase F digested and DTT reduced IgG1 with A) MS and B) UV detection. The difference in weight between 23783 and 25198 is consistent with the G0 glycan which confirms the loss of the glycan.

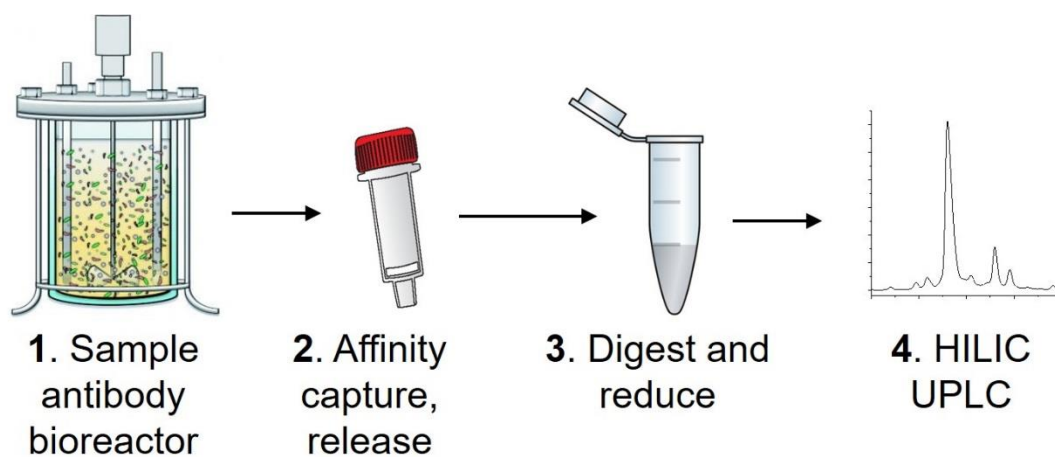


Figure 4.14: Scheme depicting a rapid, automated workflow for on-site analysis during biomanufacture to ensure correct glycosylation.

CHAPTER 5. GLYCOPEPTIDE BIOMARKERS ENRICHED AND SEPARATED WITH HILIC

5.1 Introduction

5.1.1 Usefulness of AFP glycan determination in hepatocellular carcinoma

Aberrant glycosylation profiles are one of the basic signs of a malignant cell, but cancer diagnosis and therapeutics does not use this to its full potential.¹ In fact, a majority of cancers exhibit an increase in both fucosylation and sialylation of N-glycans.² Given this finding, new approaches are currently being designed that use the glycan epitope as biomarkers.^{3–6} These approaches value non-invasive sampling techniques (i.e. serum), rapid analysis, and high-throughput capability.

In 2006, AFP-L3 was approved by the FDA for early detection of hepatocellular carcinoma (HCC). This test is based on the fraction of glycosylated AFP that is well-retained by the *Lens culinaris* agglutinin (LCA) lectin. It was discovered that the glycosylation profile sees an increase in fucosylation when HCC is present, but not for other liver diseases. From the original study, the AFP-L3 test detects 73% of HCC cases, all before HCC could be detected via imaging.³ The LCA lectin binds strongly to the AFP-L3 glycoforms (multiple glycoforms) due to the additional α 1,6-fucose bound to N-acetylglucosamine at the glycan base. However, my hypothesis is that by looking at individual glycan structures, it may be possible to increase the percentage of HCC cases detected. This requires the ability to separate and quantify the individual structures.

The proposed method for quantifying individual structures is to digest AFP into peptides, enrich for glycopeptides with HILIC-SPE, then separate the glycoforms via HILIC HPLC. The initial glycoform assignments can be determined with inline MS, then the assay can be used with HPLC in a diagnostic environment. To optimize the workflow and practice my technique, I started with Ribonuclease B as a test glycoprotein as it is less expensive and has fewer glycoforms.

5.1.2 Solid phase extraction (SPE) HILIC with nonporous particles

Solid phase extraction (SPE) is a sample preparation technique that is useful in removing matrices^{7,8}, exchanging buffers⁹, isolating analytes^{10,11}, concentrating sample^{12–}

¹⁴, and minimizing noise¹⁵ (these are of course not mutually exclusive). SPE is a type of chromatography with an “all-or-nothing” twist. To perform SPE, first the sample solution is mixed with the solid extraction support. The compound of interest binds to the solid support, whether through affinity, adsorption, or ionic interactions. The unretained matrix is then washed away, leaving a “clean” sample on the solid support. Then, the elution buffer is added to elute the analyte from the solid support into solution. The final step is removing the dissolved sample in the solution from the solid support, through centrifugation and decanting or a spin filter. This removal often requires multiple wash steps to completely remove the sample and is known for not being quantitative. In a work by Li *et al* for example, a method to quantify cotinine metabolites in rat plasma and brain tissue using SPE resulted in 15% RSD, despite the use of isotope-labeled internal standards minimizing the influence of recovery and matrix effects.¹⁶

This inconvenience is in part due to the solid support’s inherent porosity. Generally, these solids are made of similar material to chromatography columns such as silica or polymer spheres/beads. As such, analytes will diffuse into the pores and become difficult to completely remove, even with multiple wash steps. Even more disappointing, the multiple wash steps dilute the sample, requiring users to decide whether a “complete” extraction of sample or a concentrated analyte is more important.

Nick Sortedahl, Brian (Pei-Hsun) Wei, and Edwin Alzate in our lab have worked on this problem by looking to silica nanoparticles. Nonporous particles were polymerized with epoxide to covalently bind a mAb specific to the protein of interest for extraction. However, their work has only focused on affinity extraction. Other chromatographic modes can be used to bind and elute, such as HILIC, RPLC, or ion-exchange. Given the problem of low sample concentration, and a relatively hydrophilic analyte, HILIC SPE beads can be produced with the polyacrylamide stationary phase already used in our lab and can be compared with the porous silica SPE supports currently on the market (ZIP-TIP, iHILIC, ZIC-HILIC, Oasis, etc).

5.2 Method

5.2.1 Production of HILIC-SPE beads

Producing HILIC-SPE beads was performed similarly to free particles for column packing. 350 nm calcined, annealed, and rehydroxylated nonporous particles were used for this process. 1.3 g particles were silanated with 100 mL dry toluene, 3 mL mBC, and 100 μ L butylamine for 1.5 hours under nitrogen, reflux, and stirring. The particles were rinsed 3x with dry toluene and dried overnight under vacuum at 60 °C. The AGET ATRP produced PAAm chains on the surface. A 3:1 solution of water: isopropyl alcohol (IPA) was prepared. In a round bottom flask (RBF), 4.4 grams of acrylamide and 0.5 grams of mBC particles were suspended in 21 mL water/IPA solution. A septum was placed over the top of the reaction and the solution was purged of nitrogen. Two solutions were then prepared in separate 1-dram vials. Solution A contained 40.0 mg copper (II) chloride solid in 2 mL water/IPA, with 80 μ L (Tris[2(dimethylamino)ethyl]amine) added. Solution B contained 20.0 g sodium ascorbate in 2 mL water/IPA. When particles were fully suspended, solution A was added to the flask followed by solution B via syringe. Immediately after solution B was added, the reaction timer began for 55 minutes. After the reaction, the mixture was poured into a 50 mL conical tube and rinsed three times with water. The HILIC-SPE beads produced were dried under vacuum at room temperature.

5.2.2 Preparation of Ribonuclease B peptides

Ribonuclease B was used as a model glycoprotein for producing peptides since it is less expensive and complex than AFP. To make the sample, Ribo B was reduced with DTT, alkylated with IAA, and digested with high specificity α -chymotrypsin (G-Biosciences, St. Louis, MO). Ribo B was purchased as a solid protein from Sigma Aldrich and prepared at a concentration of 6.7 mg/mL in 2 M urea and 50 mM ammonium bicarbonate, pH 7.8. DTT was added to a final concentration of 8 mM and incubated 15 min at 50 °C. The solution was cooled to room temperature, then IAA was added to a concentration of 16 mM. The reaction was incubated at room temperature in the dark for 15 min. After alkylation, the reaction was quenched with another 8mM DTT (final concentration). The reaction was diluted 5x by adding 50 mM ammonium

bicarbonate buffer without urea (to reduce the concentration of urea to a level that will allow α -chymotrypsin to react). 50 μ g α -chymotrypsin was added to the reaction and incubated at 30 °C overnight. In the morning, the peptides were desalted (Thermo Zeba spin desalting column, 2 mL) and suspended in 80% ACN, 20% H₂O + 0.1% TFA for either injection or SPE. This reaction produced peptides at a concentration of 0.4 mg/mL in 80% ACN.

5.2.3 Preparation of AFP peptides

To make the sample, AFP was reduced with DTT, alkylated with iodoacetamide (IAA, Thermo Fisher), and digested with trypsin. The original AFP sample was purchased from Lee Biosolutions (Maryland Heights, MO) at a concentration of 1.6 mg/mL. 125 μ L of AFP was added to 71 μ L Tris buffer (50 mM Tris, pH 8) and 2 μ L of 500 mM DTT. The reaction proceeded at 60 °C for 1 hour. The DTT reduction breaks the disulfide bonds in the protein. Next, 8 μ L of 500 mM IAA is added and alkylation proceeds at room temperature in the dark for 30 min. The alkylation reaction is quenched with 4 μ L DTT (500 mM). Finally, the protein is digested with 2 μ g trypsin and the reaction is incubated overnight at 37 °C. In the morning, the sample is removed from heat and stored at -20 °C.

5.2.4 Enrichment of peptides with HILIC-SPE

The glycopeptide was then selected for with lab-produced HILIC-SPE beads. A peptide solution was diluted into 80% ACN + 0.1% TFA. 2.5 mg of dry HILIC-SPE beads were weighed in a microcentrifuge tube and conditioned at 80% ACN + 0.1% TFA for 10 minutes. The conditioning solution was decanted. The diluted peptide sample in 80% ACN + 0.1% TFA was then added to the HILIC-SPE beads in the microcentrifuge tube. The beads were suspended via vortexing and sonication before shaken end-over-end for 30 seconds. Then, the beads were centrifuged and rinsed one time with 80% ACN + 0.1% TFA. To elute, beads were suspended in 80 μ L 50% ACN + 0.1% TFA and shaken 5 minutes. The tube was centrifuged and peptide solution was decanted into a new tube. Peptide solution was diluted to a final ratio of 80% ACN + 0.1% TFA for HILIC-UHPLC analysis.

5.2.5 Separation and detection of AFP glycopeptides with HILIC-UV and HILIC-MS

HILIC separations were performed using 750 nm dp PAAm columns prepared as in Chapter 2. The Waters Acquity UPLC Glycoprotein Amide 300Å 1.7 µm 2.1 x 100 mm column was used for comparison. The instrument used for the UV detection was a Waters Acquity I-Class UPLC. Gradients for both columns were 95% to 60% ACN in 40 min unless otherwise noted, 30°C column temperature, 50 µL/min (PAAm) or 100 µL/min (Waters) flow rate. The gradient stacked the peptide at the head of the column for 1 min at 95% ACN before starting and rinsed at 60% ACN until all the glycopeptides were eluted (5-10 minutes). Comparisons were made for both 0.1% TFA and 0.1% FA + 0.025% TFA in both A and B for mobile phase additives.

For LCMS, a Waters Acquity H-Class UPLC with online Waters ESI ZSpray SQD2 mass spectrometer was used. Source voltage for the capillary was 3.50 kV for the PAAm column and 2.5 kV for the Waters column. The cone voltage was 60 V for both. The source temperature was 150°C, and the desolvation temperature was 350°C. The source gas flow rate was 300 L/h. The cone gas flow was 1 L/h. The MS inlet flow rate was 100 µL/min.

5.3 Results and discussion

5.3.1 HILIC separation of Ribonuclease B peptides

After the successes with intact glycoproteins using our lab-produced column, we decided to compare the results with the Waters Acquity Glycoprotein column. Figure 5.1 is the HILIC separation using the lab-produced PAAm column and either 0.1% TFA or 0.1% FA + 0.025% TFA in the mobile phase. Resolution worsens with the reduction in TFA. Figure 5.3 is the HILIC separation using the Waters column under similar conditions and either 0.1% TFA or 0.1% FA + 0.025% TFA. Again, resolution worsens with the reduction of TFA. However, comparing Figure 5.2A to Figure 5.3A, the Waters column appears to separate almost all of the glycopeptides to baseline resolution, which was not accomplished with the lab-produced PAAm column. Both columns were used for LCMS analysis as well to determine peak purity.

5.3.2 HILIC-MS of Ribonuclease B peptides

The PAAm and Waters column provided similar resolution using 0.1% FA + 0.025% FA (Figure 5.4A and Figure 5.5A/Figure 5.2), so both were tested for peak purity. Interestingly, the two columns have different selectivity for the earlier and later eluting peaks that have mixed peaks. In Figure 5.4B which is the lab-produced separation, the mass spectra are shown by individual peak. Peak 2 is the composite of peak 2A and 2B in the figure; similarly peak 3 is the composite of peak 3A and 3B. Peaks 2 and 3 were noticeably splitting in the chromatogram, and the MS confirmed different species in earlier and later eluting portions (“peak 2A” vs “peak 2B”, and “peak 3A” vs “peak 3B”). However, looking at Figure 5.5A, only peak 5 is able to begin splitting (and is denoted as “peak 5A” and “peak 5B”). The masses were calculated for each peak, and it was determined that the arbitrarily labels of peaks 0-6 on each chromatogram match to the other column’s separation.

It is well-documented that Ribonuclease B has 5 major glycoforms, consisting of GlcNAc₂ (the chitobiose core, two N-Acetylglucosamine monomers) and a branching structure of 5-9 Man (mannose) groups.¹⁷ The ladder of glycoforms differing by a single mannose group were assigned as peaks 1-5, with the number of mannose monomers increasing with retention time. Isomers of each glycoform are also found in Ribonuclease B, which were seen especially well in the Waters glycopeptide separation (Figure 5.3A). Table 5.3 shows the theoretical and experimental masses of the glycopeptides. Most of the glycopeptides were found as both triply and quadruply charged. Peaks 0 and 6 are trickier to identify, however. These two peaks are 17-18 Da lighter than the Man₅ glycopeptide, but due to the mass accuracy of the instrument it is not clear what has been lost. One possibility is the loss of a hydroxyl group through rearrangement. Tandem MS would be necessary to determine location of the hydroxyl as well. Further work includes determining the identity of these peaks.

5.4 Conclusion and future work

So far, I have successfully digested ribonuclease B into peptides, produced and tested HILIC-SPE particles, and identified Ribonuclease B’s 5 major glycosylated

peptide species via HILIC-MS. I will be continuing this project after the thesis is deposited. The next steps can be broken down into three main areas: HILIC-SPE bead characterization, assignment of Ribonuclease B minor peaks, and developing the assay for use as a HCC biomarker with AFP. The HILIC-SPE beads introduced in this chapter must be tested for capacity and recovery to determine if they are an improvement over commercial SPE for specific applications. While the beads proved successful in enriching the glycopeptides and reducing the amount of noise in the chromatogram, it is valuable to quantify this further.

Next, the minor peaks in the glycopeptide chromatogram (Figure xxx, peaks 0 and 6) were both shown to be 17-18 Da lower mass than the lightest known glycoform. In order to determine what atoms specifically are being lost, it is necessary to use a higher resolution MS than the single quadrupole walk-up instrument. Furthermore, tandem MS may be useful in determining where the loss occurs. Both are included in my further plans to better characterize the ribonuclease B glycopeptides.

Finally, the original intent of developing this workflow is to use it as a diagnostic tool for HCC. By the time we reach this stage, the legwork will be done in developing the assay. However, the protocols will need to be converted and optimized for the new glycoprotein. Potential difficulties may include the increased number of glycoforms (around 15 for AFP compared to 5 for Ribo B), the larger protein which results in more nonglycosylated peptides, and the smaller glycosylated peptide (8 amino acids for AFP vs 21 for Ribo B). That being said, the assay development challenges should not be insurmountable and have partially been accounted for with the addition of SPE.

5.5 Tables and figures

Table 5.1: PeptideCutter output showing peptide sequence from Ribonuclease B digestion with high specificity α -chymotrypsin.^{18,19} In bold, red type is the glycosylated asparagine (N) at position 60.

Position of cleavage site	Resulting peptide sequence	Peptide length [aa]	Peptide mass [Da]
34	MALKSLVLLSLLVLVLLLVRVQP SLGKETAAAKF	34	3635.580
51	ERQHMDSSTSAASSSNY	17	1857.883
72	CNQMMKSR N LTkDRCKPVNTF	21	2514.980
99	VHESLADVQAVCSQKNVACKNG QTNCY	27	2910.244
102	QSY	3	396.400
123	STMSITDCRETGSSKYPNCAY	21	2314.542
141	KTTQANKHIIIVACEGNPY	18	1987.261
146	VPVHF	5	597.715
150	DASV	4	390.393

Table 5.2: PeptideCutter output showing peptide sequence resulting from AFP digestion with trypsin.^{18,20,21} In bold, red type is the glycosylated asparagine (N) at position 251. Note that this peptide has only 8 amino acids on the chain. Table continues on next page as well.

Position of cleavage site	Resulting peptide sequence	Peptide length [aa]	Peptide mass [Da]
2	MK	2	277.382
19	WVESIFLIFLLNFTESR	17	2114.472
23	TLHR	4	525.608
61	NEYGASILDSYQCTAEISL ADLATIFFAQFVQEATYK	38	4235.729
65	EVSK	4	461.516
68	MVK	3	376.515
102	DALTAIEKPTGDEQSSGCL ENQLPAFLEELCHEK	34	3717.091
107	EILEK	5	630.739
121	YGHSDCCSQSEEGR	14	1557.586
129	HNCFLAHK	8	969.129
155	KPTPASIPLFQVPEPVTSC EAYEEDR	26	2904.241
161	ETFMNK	6	768.883
168	FIYEIAR	7	911.068
184	RHPFLYAPTILLWAAR	16	1925.310
187	YDK	3	424.454
194	IIPSCCK	7	762.981
205	AENAVECFQTK	11	1239.366
211	AATVTK	6	589.690
214	ELR	3	416.478
228	ESSLLNQHACAVMK	14	1530.777
233	NFGTR	5	593.640
242	TFQAITVTK	9	1008.183
246	LSQK	4	474.558
249	FTK	3	394.471
257	VNFTEIQK	8	978.113
271	LVLDDVAHVHEHCCR	14	1630.903
283	GDVLDCLQDGEK	12	1291.395
298	IMSYICSQQDTLSNK	15	1730.968
304	ITECCK	6	695.847
310	LTTLER	6	731.847

Table 5.2 continued on next page

Table 5.2 continued

Position of cleavage site	Resulting peptide sequence	Peptide length [aa]	Peptide mass [Da]
332	GQCIIHAENDEKPEGLSPNLNR	22	2434.666
337	FLGDR	5	606.679
347	DFNQFSSGEK	10	1158.189
360	NIFLASFVHEYSR	13	1582.779
372	RHPQLAVSVILR	12	1388.679
375	VAK	3	316.401
383	GYQELLEK	8	979.098
396	CFQTENPLECQDK	13	1554.710
403	GEEELQK	7	831.878
413	YIQESQALAK	10	1150.297
414	R	1	174.203
421	SCGLFQK	7	781.925
437	LGEYYLQNAFLVAYTK	16	1893.169
438	K	1	146.189
452	APQLTSSELMAITR	14	1517.761
453	K	1	146.189
468	MAATAATCCQLSEDK	15	1542.757
487	LLACGEGAADIIGHLCIR	19	1938.333
508	HEMTPVNPVGVCCTSSYANR	21	2251.492
530	RPCFSSLVVDETYVPPAFSDDK	22	2472.752
535	FIFHK	5	690.843
549	DLCQAQGVALQTMK	14	1505.767
558	QEFLINLVK	9	1103.327
581	QKPQITEEQLEAVIADFSGLLEK	23	2586.922
598	CCQGQEQEVCFAEEGQK	17	1916.082
602	LISK	4	459.586
604	TR	2	275.308
609	AALGV	5	429.517

Table 5.3: Comparison of theoretical and experimental glycopeptide masses of Ribonuclease B chymotrypsin digest, including glycan composition.

Peak #	Glycan Composition	Theoretical glycan mass	Peptide mass	Theoretical glycopeptide mass	Experimental glycopeptide mass	Δ Mass
0					3831.3	
1	Man ₅ GlcNAc ₂	1217.1	2629.08	3847.2	3849.0	1.8
2	Man ₆ GlcNAc ₂	1379.2	2629.08	4009.3	4010.7	1.4
3	Man ₇ GlcNAc ₂	1541.4	2629.08	4171.5	4173.3	1.8
4	Man ₈ GlcNAc ₂	1703.5	2629.08	4333.6	4335.3	1.7
5	Man ₉ GlcNAc ₂	1865.7	2629.08	4495.8	4496.4	0.6
6					3832.2	

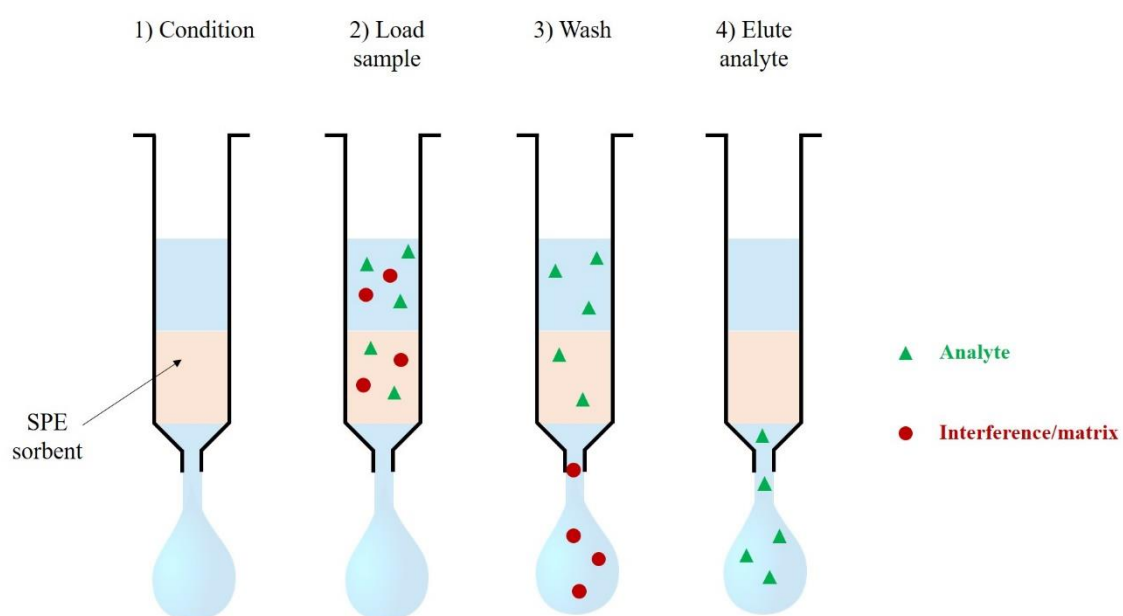
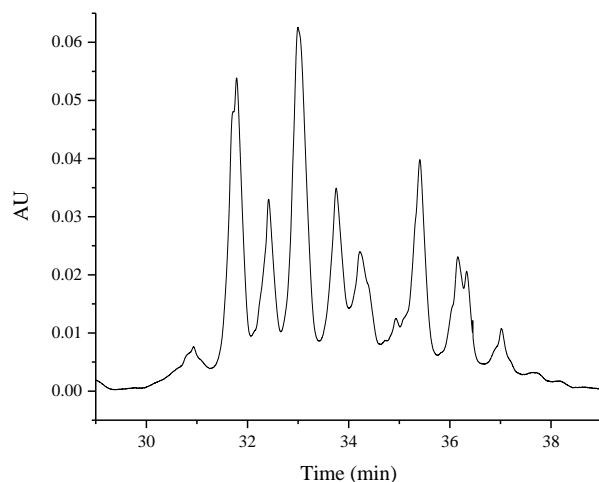


Figure 5.1: Depiction of a procedure used for cartridge SPE.

A) UV, 0.1% TFA



B) UV, 0.1% FA + 0.025% TFA

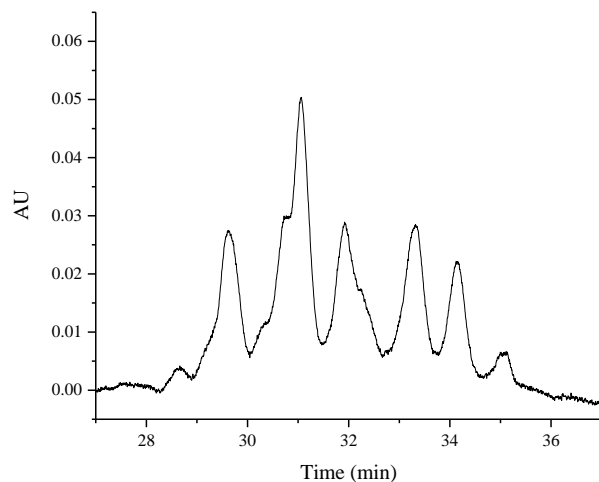
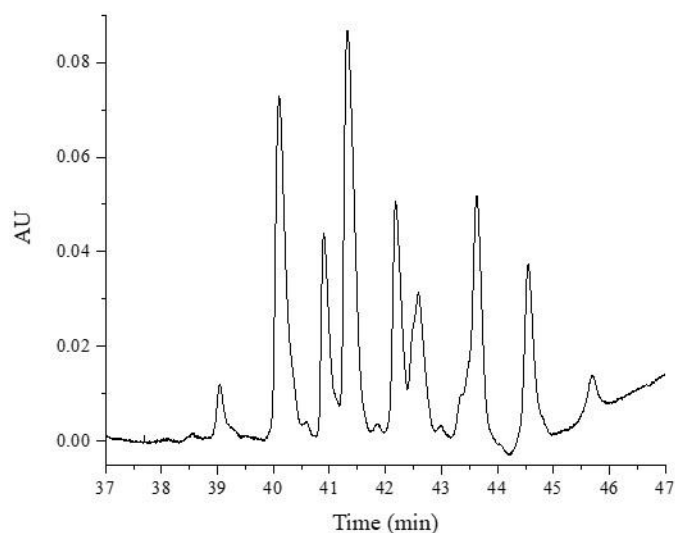


Figure 5.2: HILIC separations of ribonuclease B glycopeptides varying solvent modifier. PAAm 750 nm dp lab-produced column was used for separations. A) UV Absorbance at 215 nm wavelength, 0.1% TFA. B) UV absorbance at 215 nm, 0.1% FA + 0.025% TFA. Gradient stacked for 1 min at 95% ACN, then 95-60% ACN in 40 minutes, then 5 minutes of rinsing at 60% ACN before returning to 95% ACN for reconditioning. Flow rate was 50 μ L/min for both separations.

A) UV, 0.1% TFA



B) UV, 0.1% FA + 0.025% TFA

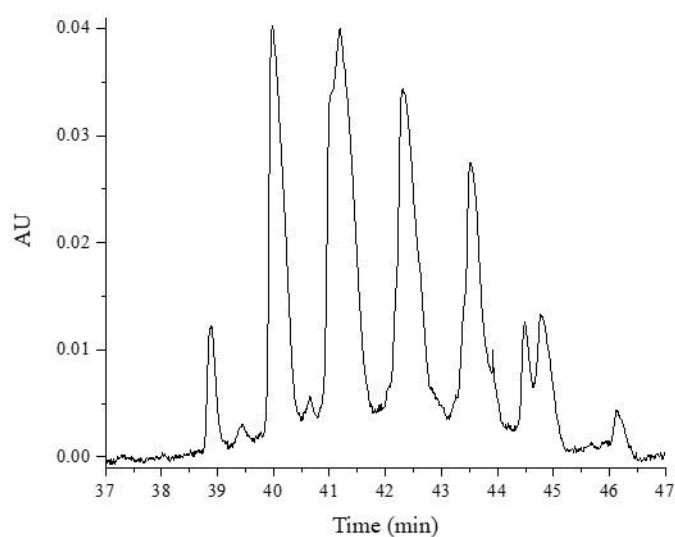


Figure 5.3: HILIC separations of Ribonuclease B glycopeptides varying solvent modifier. Waters Acquity Glycoprotein 100 mm HILIC column was used for separations. A) UV Absorbance at 215 nm wavelength, 0.1% TFA. The reason for the baseline increase at the end of the run is the change in UV absorbance at the end of the gradient. Later experiments the time was extended to circumvent this issue. B) UV absorbance at 215 nm, 0.1% FA + 0.025% TFA. Gradient stacked for 1 min at 95% ACN, then 95-60% ACN in 40 minutes, then 5 minutes of rinsing at 60% ACN before returning to 95% ACN for reconditioning. Flow rate was 100 μ L/min for both separations.

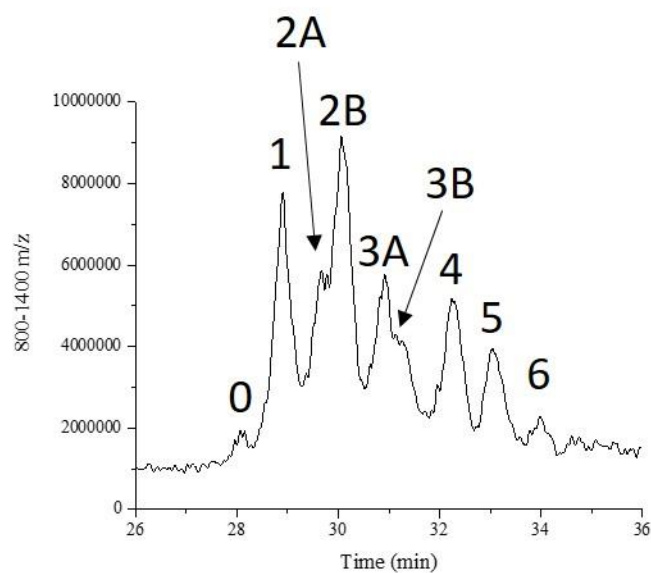


Figure 5.4A: HILIC-MS of ribonuclease B glycopeptides by peak using the lab-produced PAAm column. MS TIC chromatogram from 800-1400 m/z, 0.1% FA + 0.025% TFA, 95-60% ACN in 40 minutes, 50 μ L/min.

Figure 5.4B (next pages): MS spectra of labeled peaks in Figure 5.4A. Peak 2 is the composite of peaks 2A and 2B, since a clear delineation between the splitting peak is not possible as seen on the TIC chromatogram. Peak 3 is the composite of peaks 3A and 3B as well.

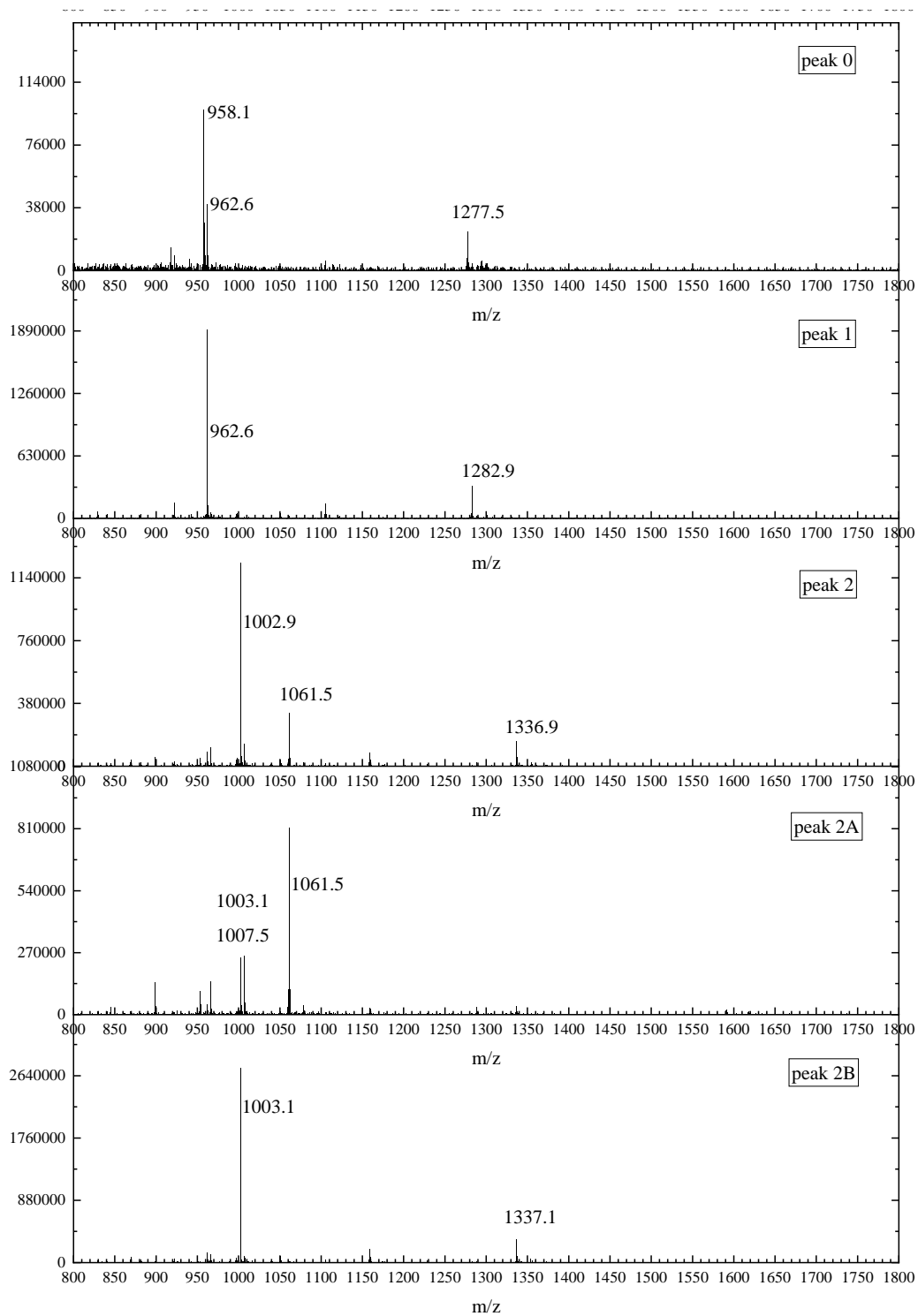


Figure 5.4B continued

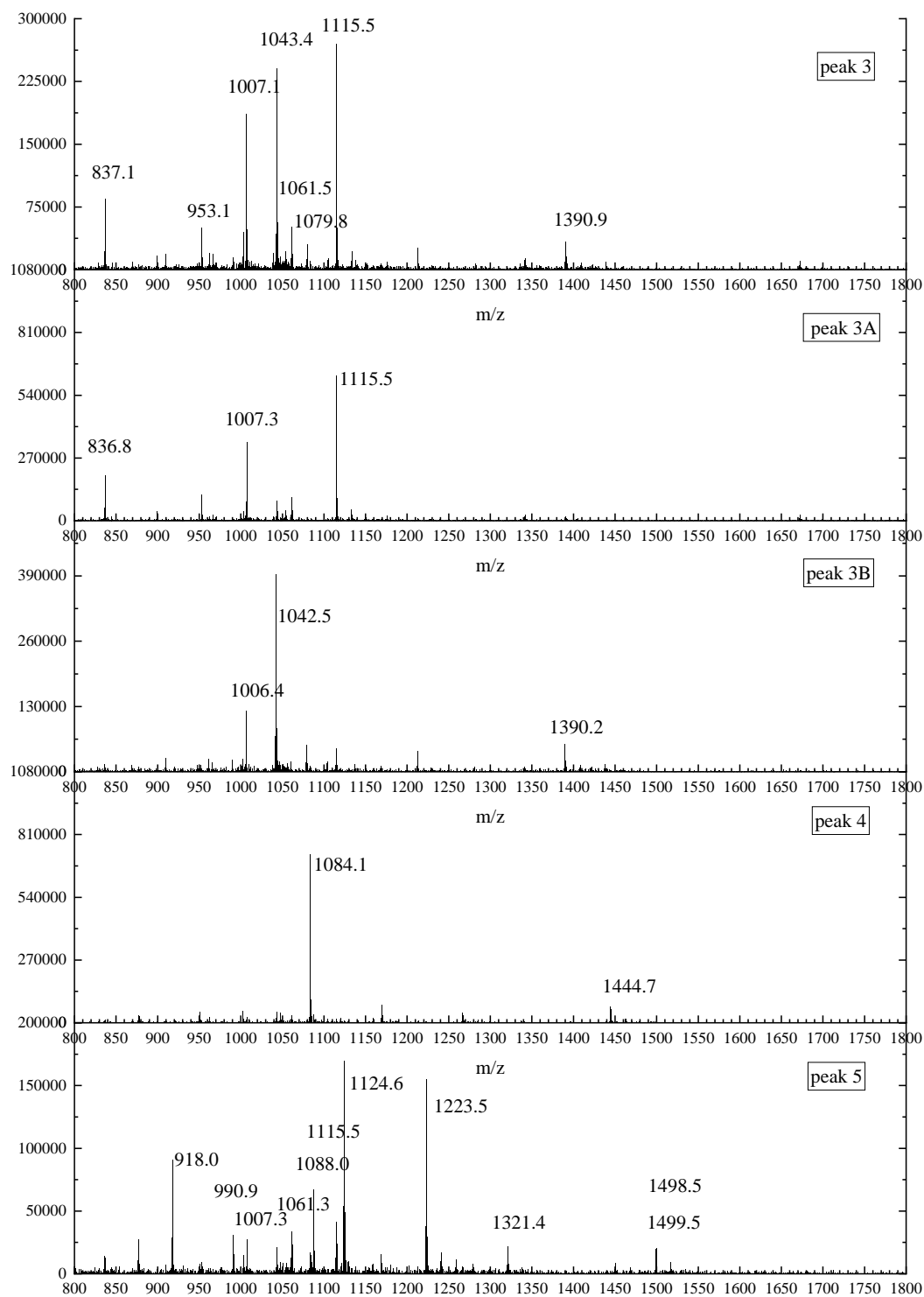
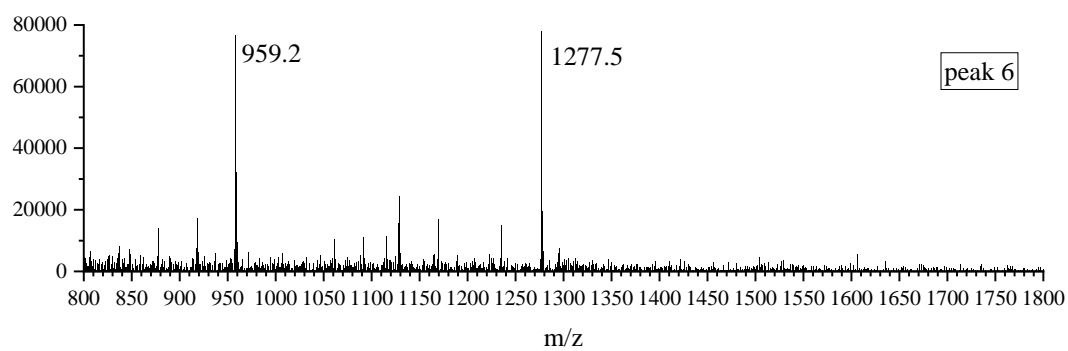


Figure 5.4B continued



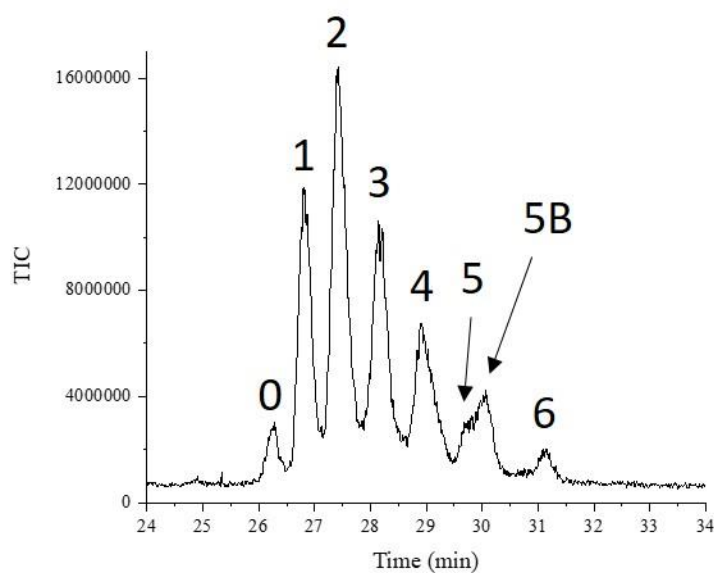


Figure 5.5A: HILIC-MS of ribonuclease B glycopeptides by peak using the Waters Acquity column. A) MS TIC chromatogram from 800-1400 m/z, 0.1% FA + 0.025% TFA, 95-60% ACN in 40 minutes, 100 μ L/min.

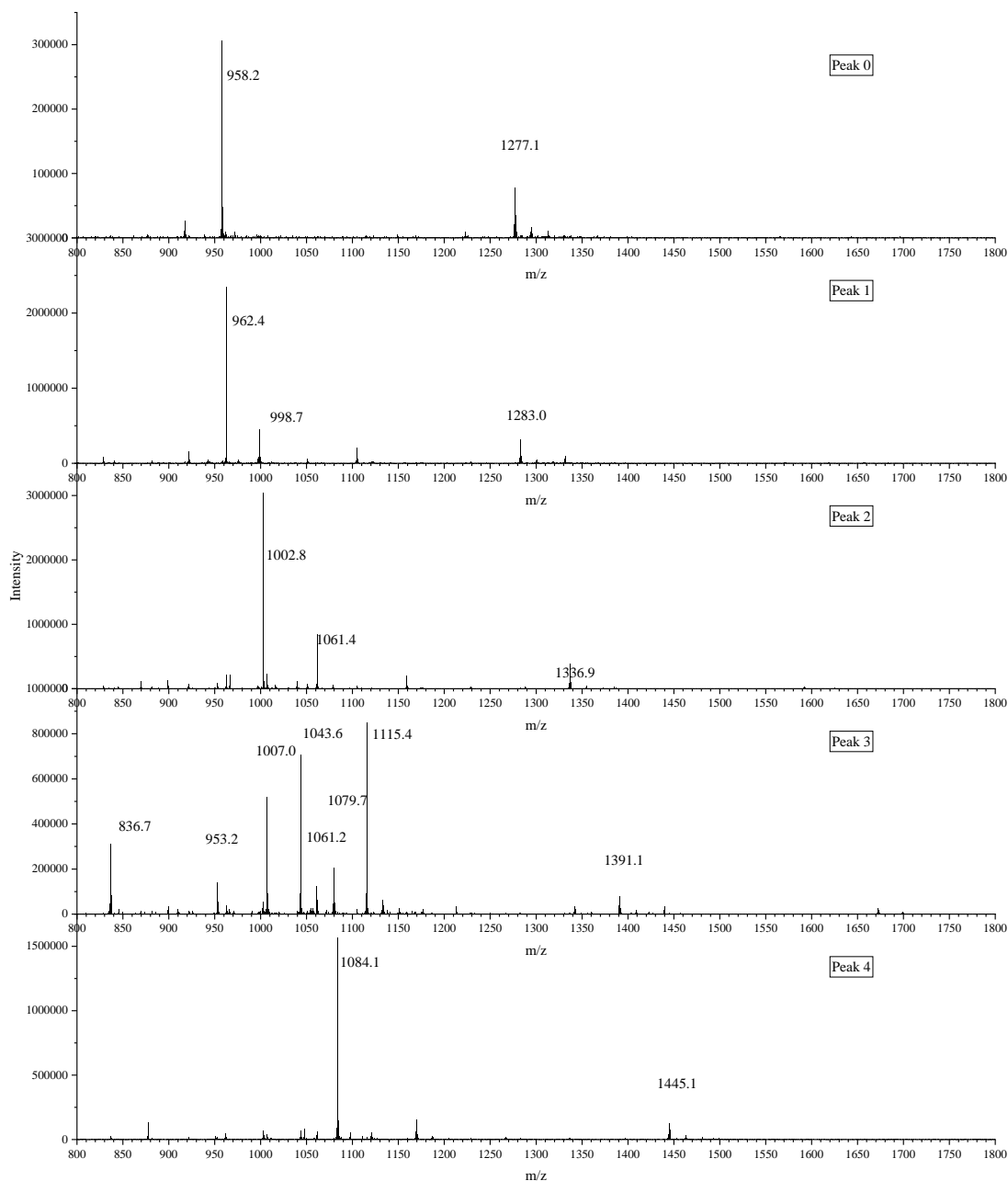
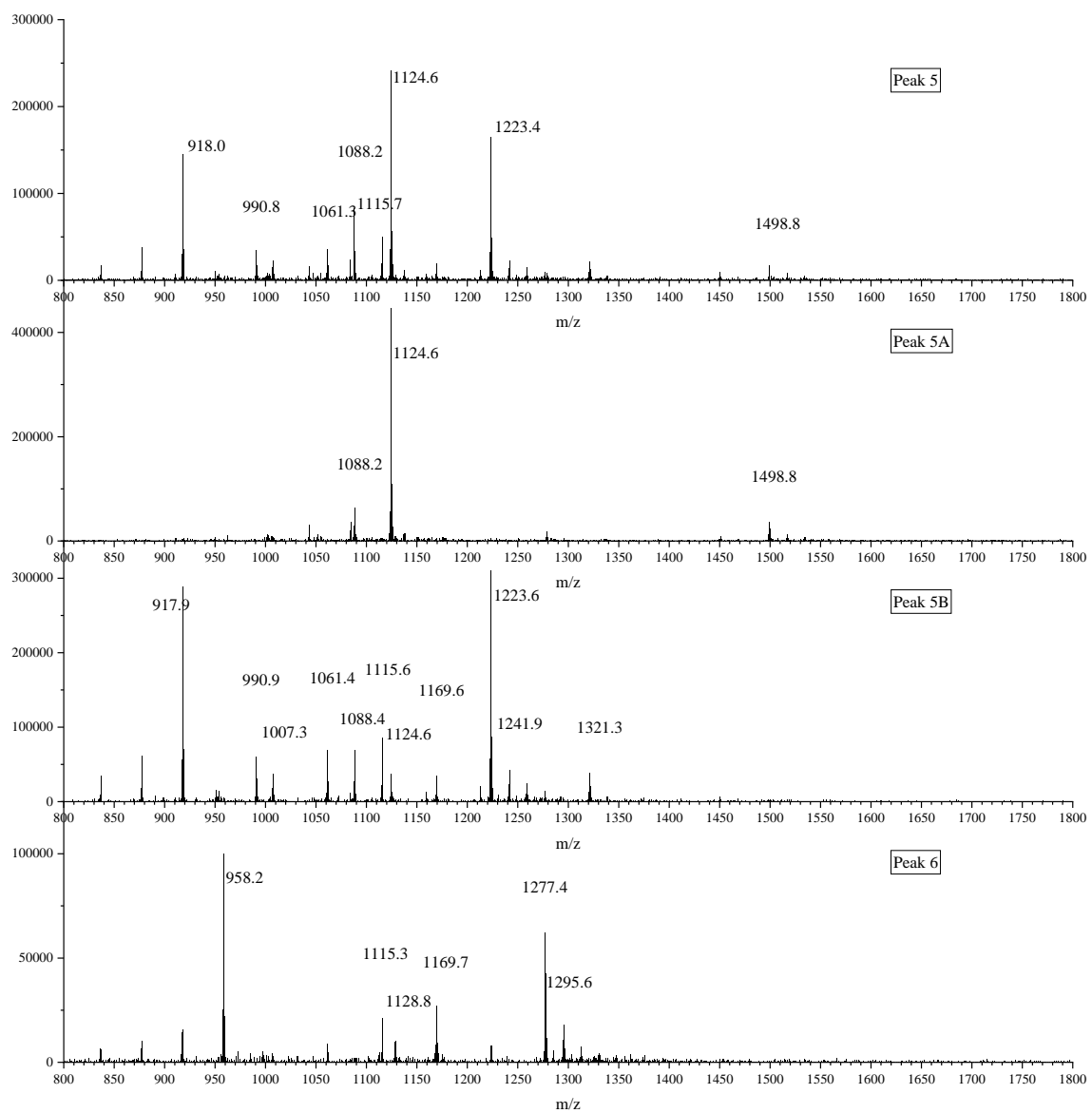


Figure 5.5B: MS spectra of labeled peaks in Figure 5.5A. Peak 5 is the composite of peaks 5A and 5B, since the peak was broad and appeared to be breaking into multiple peaks. A clear delineation between the splitting peak is not possible as seen on the TIC chromatogram. Continued on next page.

Figure 5.5B continued



5.6 References

1. Pearce, O. M. T. Cancer glycan epitopes: biosynthesis, structure and function. *Glycobiology* (2018). doi:10.1093/glycob/cwy023
2. Adamczyk, B., Tharmalingam, T. & Rudd, P. M. Glycans as cancer biomarkers. *Biochimica et Biophysica Acta (BBA) - General Subjects* **1820**, 1347–1353 (2012).
3. Sato, Y. *et al.* Early Recognition of Hepatocellular Carcinoma Based on Altered Profiles of Alpha-Fetoprotein. <http://dx.doi.org.ezproxy.lib.purdue.edu/10.1056/NEJM199306243282502> (2010). doi:10.1056/NEJM199306243282502
4. Llop, E. *et al.* Improvement of Prostate Cancer Diagnosis by Detecting PSA Glycosylation-Specific Changes. *Theranostics* **6**, 1190–1204 (2016).
5. Gilgunn, S., Conroy, P. J., Saldova, R., Rudd, P. M. & O’Kennedy, R. J. Aberrant PSA glycosylation—a sweet predictor of prostate cancer. *Nat Rev Urol* **10**, 99–107 (2013).
6. Ohyama, C., Koie, T., Yoneyama, T. & Tobisawa, Y. Quantification of Prostate Cancer-Associated Aberrant Glycosylation of Prostate-Specific Antigen. in *Glycoscience: Biology and Medicine* (eds. Endo, T., Seeberger, P. H., Hart, G. W., Wong, C.-H. & Taniguchi, N.) 1–6 (Springer Japan, 2014). doi:10.1007/978-4-431-54836-2_186-1
7. Li, A. *et al.* Elucidation of matrix effects and performance of solid-phase extraction for LC-MS/MS analysis of β -N-methylamino-L-alanine (BMAA) and 2,4-diaminobutyric acid (DAB) neurotoxins in cyanobacteria. *The Analyst* **137**, 1210 (2012).
8. Hajšlová, J. & Zrostlíková, J. Matrix effects in (ultra)trace analysis of pesticide residues in food and biotic matrices. *Journal of Chromatography A* **1000**, 181–197 (2003).
9. Zhang, C. *et al.* Development of an automated mid-scale parallel protein purification system for antibody purification and affinity chromatography. *Protein Expression and Purification* **128**, 29–35 (2016).
10. Chen, D., Zhao, Y., Miao, H. & Wu, Y. A novel dispersive micro solid phase extraction using PCX as the sorbent for the determination of melamine and cyromazine in milk and milk powder by UHPLC-HRMS/MS. *Talanta* **134**, 144–152 (2015).
11. Oellig, C. & Schwack, W. Planar solid phase extraction clean-up for pesticide residue analysis in tea by liquid chromatography–mass spectrometry. *Journal of Chromatography A* **1260**, 42–53 (2012).

12. Castiglioni, S. *et al.* Identification and Measurement of Illicit Drugs and Their Metabolites in Urban Wastewater by Liquid Chromatography–Tandem Mass Spectrometry. *Analytical Chemistry* **78**, 8421–8429 (2006).
13. van Nuijs, A. L. N. *et al.* Analysis of drugs of abuse in wastewater by hydrophilic interaction liquid chromatography–tandem mass spectrometry. *Analytical and Bioanalytical Chemistry* **395**, 819–828 (2009).
14. Mysling, S., Palmisano, G., Højrup, P. & Thaysen-Andersen, M. Utilizing Ion-Pairing Hydrophilic Interaction Chromatography Solid Phase Extraction for Efficient Glycopeptide Enrichment in Glycoproteomics. *Analytical Chemistry* **82**, 5598–5609 (2010).
15. Duca, R.-C., Salquebre, G., Hardy, E. & Appenzeller, B. M. R. Comparison of solid phase- and liquid/liquid-extraction for the purification of hair extract prior to multi-class pesticides analysis. *Journal of Chromatography B* **955–956**, 98–107 (2014).
16. Li, P., Beck, W. D., Callahan, P. M., Terry, A. V. & Bartlett, M. G. Quantitation of cotinine and its metabolites in rat plasma and brain tissue by hydrophilic interaction chromatography tandem mass spectrometry (HILIC–MS/MS). *Journal of Chromatography B* **907**, 117–125 (2012).
17. Zhang, Z., Wu, Z. & Wirth, M. J. Polyacrylamide brush layer for hydrophilic interaction liquid chromatography of intact glycoproteins. *Journal of Chromatography A* **1301**, 156–161 (2013).
18. Artimo, P. *et al.* ExPASy: SIB bioinformatics resource portal. *Nucleic Acids Research* **40**, W597–W603 (2012).
19. RNASE1 - Ribonuclease pancreatic precursor - Bos taurus (Bovine) - RNASE1 gene & protein. Available at: <https://www.uniprot.org/uniprot/P61823>. (Accessed: 23rd October 2018)
20. Alpi, E. *et al.* Analysis of the tryptic search space in UniProt databases. *PROTEOMICS* **15**, 48–57 (2015).
21. AFP - Alpha-fetoprotein precursor - Homo sapiens (Human) - AFP gene & protein. Available at: <https://www.uniprot.org/uniprot/P02771>. (Accessed: 11th October 2018)

CHAPTER 6. FUTURE DIRECTIONS

6.1 New HILIC monomer for improved stability and altered functionality

Briefly mentioned in Chapter 3, polyacrylamide is not stable enough to be sold commercially. This is due to the hydrolysis of acrylamide monomer to acrylic acid while in polymer form on the surface (Figure 6.1). Unfortunately, there does not seem to be a simple solution for polyacrylamide. The best way to improve chemical stability would be to add stabilizing groups to the acrylamide monomer, such as a methyl group. Edwin Alzate is taking on this challenge and the continuation of HILIC surfaces in the Wirth lab by testing new hydrophilic polymers. One such monomer is N-hydroxymethylacrylamide, containing a secondary amine rather than a primary amine (Figure 6.2). This substitution makes the nitrogen-carbonyl bond less susceptible to hydrolysis, ultimately improving stability over time.

6.2 Increasing surface area in column to improve loading capacity

Nonporous particles such as the ones used for this thesis are known for having low capacity. I showed in Chapter 3 that increasing surface area provides a proportional increase to loading capacity. This gives an avenue for improvement in the future. Charlie Bupp is planning to continue testing increases in surface area, including widening and lengthening the column, and continuing testing conical column prototypes. Surface area improvements will be especially important for commercializing the nonporous HILIC columns in the future, likely with the N-hydroxymethylacrylamide monomer.

6.3 Ion-exchange on silica-polymer hybrid column with low silanol activity

It has been shown in this dissertation that silanol activity is minimized with the usage of silica-polymer hybrid HILIC columns. By minimizing the silanol activity, one less off-target site is available for the analyte to bind. Unfortunately, this activity cannot be eliminated completely by acidifying the mobile phase. Therefore, in separations where the analyte is heavily affected by silanols, such as polar and cationic molecules, or proteins with many of these residues, the resolution should improve with such columns.

One interesting application which has not been heavily researched in our lab is the use of ion-exchange polymer. This way, multiple “ion-exchange” sites will not be on the stationary phase. This should improve column-to-column reproducibility and lessen column broadening.

6.4 Elucidation of water layer surrounding HILIC stationary phase

Users of HILIC mode have postulated several potential mechanisms, which are likely multiple occurring during one separation.^{11–13} The most cited primary mode is due to a water-rich layer on the hydrophilic surface enabling liquid-liquid partitioning where the hydrophilic portion of a molecule is more readily dissolved in water than the ACN-rich bulk.¹⁴ Other mechanisms involved include hydrogen bonding, adsorption, and electrostatic interactions. This leads us to question more specifically how the stationary phase effects the extent of each mechanism, as well as characterizing the separation mechanism on polyacrylamide. The molecular dynamics simulations by Mountain¹⁵ and Melnikov (Tallarek)^{16,17} have given us a wealth of theoretical data regarding the water rich layer for diol and bare silica, which would be interesting to experimentally verify.

Most hydration shell research for water using vibrational spectroscopy is performed for solutes, not a surface’s interface. The reason for this is simple: in solution, it is easier to increase signal by increasing path length. However, this cannot be readily done at interfaces which are measured by surface area rather than volume. Special techniques and instrumentation must be devised to accommodate this.

Moving away from research on silica specifically used for chromatography stationary phases, there is a good amount of research for general silica-water interfaces that can be tapped. Sum frequency generation spectroscopy (SFG) is the most commonly seen technique in the literature for probing the interfacial water structure of silica,^{18–21} but dynamic nuclear polarization (DNP)²² and atomic force microscopy (AFM)²³ are also found as well. It is a nonlinear laser spectroscopy technique that can be used to determine orientation, composition, and structural information at various interfaces. SFG can be used in both IR and Raman modes to determine different properties.²⁴

These studies show that even comparing different bare silica production methods can result in widely different hydration layer attributes on the surface. Bringing this

knowledge back to chromatography, while chromatographers and column manufacturers are very much aware of the importance of silica purity and thermal treating, we must be careful when comparing literature from various sources. It will be crucial for future water layer studies that attempt to determine hydration on HILIC surfaces to use the exact stationary phase. It is unrealistic to assume all HILIC stationary phases hydrate in a similar manner, especially considering the many different potential mechanisms that different HILIC columns can exhibit in a separation.^{25,26} Given these variations, it would be valuable to consider the use of SFG for probing hydration layers in HILIC stationary phases.

6.5 Figures

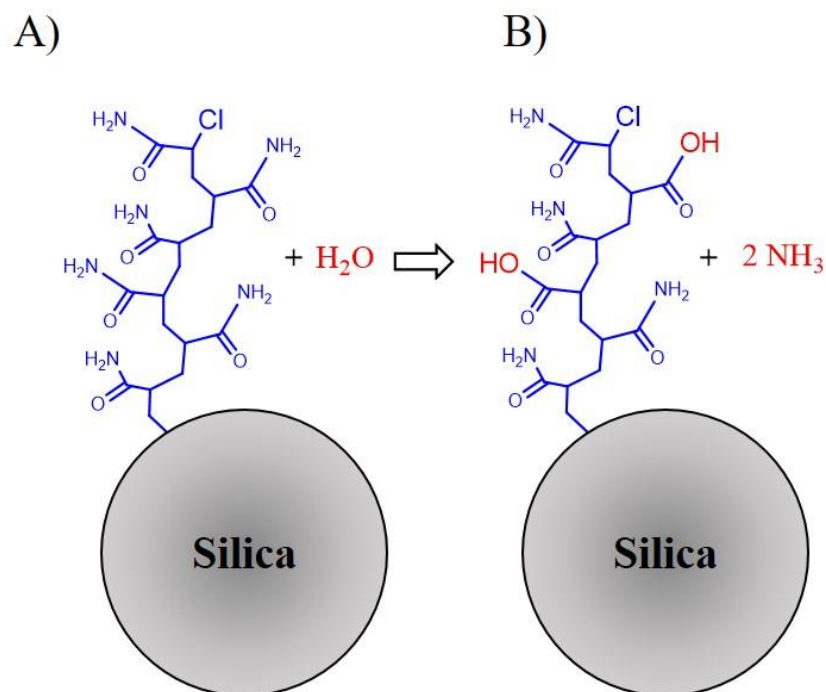


Figure 6.1: Scheme showing hydrolysis of polyacrylamide on silica surface. The amide group on polyacrylamide is hydrolyzed to a hydroxyl group, producing a copolymer of acrylamide and acrylic acid on the surface.

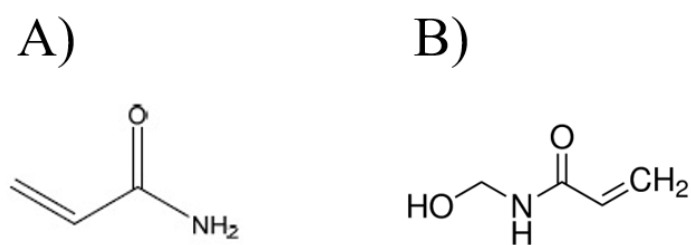


Figure 6.2: Comparison of the monomer used in this work and the new monomer currently being tested for improved stability in HILIC stationary phases. A) Acrylamide B) N-hydroxymethylacrylamide

6.6 References

1. Li, A. *et al.* Elucidation of matrix effects and performance of solid-phase extraction for LC-MS/MS analysis of β -N-methylamino-L-alanine (BMAA) and 2,4-diaminobutyric acid (DAB) neurotoxins in cyanobacteria. *The Analyst* **137**, 1210 (2012).
2. Hajšlová, J. & Zrostlíková, J. Matrix effects in (ultra)trace analysis of pesticide residues in food and biotic matrices. *J. Chromatogr. A* **1000**, 181–197 (2003).
3. Zhang, C. *et al.* Development of an automated mid-scale parallel protein purification system for antibody purification and affinity chromatography. *Protein Expr. Purif.* **128**, 29–35 (2016).
4. Chen, D., Zhao, Y., Miao, H. & Wu, Y. A novel dispersive micro solid phase extraction using PCX as the sorbent for the determination of melamine and cyromazine in milk and milk powder by UHPLC-HRMS/MS. *Talanta* **134**, 144–152 (2015).
5. Oellig, C. & Schwack, W. Planar solid phase extraction clean-up for pesticide residue analysis in tea by liquid chromatography–mass spectrometry. *J. Chromatogr. A* **1260**, 42–53 (2012).
6. Castiglioni, S. *et al.* Identification and Measurement of Illicit Drugs and Their Metabolites in Urban Wastewater by Liquid Chromatography–Tandem Mass Spectrometry. *Anal. Chem.* **78**, 8421–8429 (2006).
7. van Nuijs, A. L. N. *et al.* Analysis of drugs of abuse in wastewater by hydrophilic interaction liquid chromatography–tandem mass spectrometry. *Anal. Bioanal. Chem.* **395**, 819–828 (2009).
8. Mysling, S., Palmisano, G., Højrup, P. & Thaysen-Andersen, M. Utilizing Ion-Pairing Hydrophilic Interaction Chromatography Solid Phase Extraction for Efficient Glycopeptide Enrichment in Glycoproteomics. *Anal. Chem.* **82**, 5598–5609 (2010).
9. Duca, R.-C., Salquebre, G., Hardy, E. & Appenzeller, B. M. R. Comparison of solid phase- and liquid/liquid-extraction for the purification of hair extract prior to multi-class pesticides analysis. *J. Chromatogr. B* **955–956**, 98–107 (2014).
10. Li, P., Beck, W. D., Callahan, P. M., Terry, A. V. & Bartlett, M. G. Quantitation of cotinine and its metabolites in rat plasma and brain tissue by hydrophilic interaction chromatography tandem mass spectrometry (HILIC–MS/MS). *J. Chromatogr. B* **907**, 117–125 (2012).
11. Hemström, P. & Irgum, K. Hydrophilic interaction chromatography. *J. Sep. Sci.* **29**, 1784–1821 (2006).

12. Alpert, A. J. Effect of salts on retention in hydrophilic interaction chromatography. *J. Chromatogr. A* **1538**, 45–53 (2018).
13. Jandera, P. Stationary and mobile phases in hydrophilic interaction chromatography: a review. *Anal. Chim. Acta* **692**, 1–25 (2011).
14. Greco, G. & Letzel, T. Main Interactions and Influences of the Chromatographic Parameters in HILIC Separations. *J. Chromatogr. Sci.* **51**, 684–693 (2013).
15. Mountain, R. D. Molecular Dynamics Simulation of Water–Acetonitrile Mixtures in a Silica Slit. *J. Phys. Chem. C* **117**, 3923–3929 (2013).
16. Melnikov, S. M., Höltzel, A., Seidel-Morgenstern, A. & Tallarek, U. A Molecular Dynamics View on Hydrophilic Interaction Chromatography with Polar-Bonded Phases: Properties of the Water-Rich Layer at a Silica Surface Modified with Diol-Functionalized Alkyl Chains. *J. Phys. Chem. C* **120**, 13126–13138 (2016).
17. Melnikov, S. M., Höltzel, A., Seidel-Morgenstern, A. & Tallarek, U. Adsorption of Water–Acetonitrile Mixtures to Model Silica Surfaces. *J. Phys. Chem. C* **117**, 6620–6631 (2013).
18. Dalstein, L., Potapova, E. & Tyrode, E. The elusive silica/water interface: isolated silanols under water as revealed by vibrational sum frequency spectroscopy. *Phys. Chem. Chem. Phys.* **19**, 10343–10349 (2017).
19. Ostroverkhov, V., Waychunas, G. A. & Shen, Y. R. New Information on Water Interfacial Structure Revealed by Phase-Sensitive Surface Spectroscopy. *Phys. Rev. Lett.* **94**, (2005).
20. Shen, Y. R. & Ostroverkhov, V. Sum-Frequency Vibrational Spectroscopy on Water Interfaces: Polar Orientation of Water Molecules at Interfaces. *Chem. Rev.* **106**, 1140–1154 (2006).
21. Yamaguchi, S. & Tahara, T. $\chi(4)$ Raman Spectroscopy for Buried Water Interfaces. *Angew. Chem. Int. Ed.* **46**, 7609–7612 (2007).
22. Schrader, A. M. *et al.* Surface chemical heterogeneity modulates silica surface hydration. *Proc. Natl. Acad. Sci.* **115**, 2890–2895 (2018).
23. Morag, J., Dishon, M. & Sivan, U. The Governing Role of Surface Hydration in Ion Specific Adsorption to Silica: An AFM-Based Account of the Hofmeister Universality and Its Reversal. *Langmuir* **29**, 6317–6322 (2013).
24. Shen, Y. R. Surface properties probed by second-harmonic and sum-frequency generation. *Nature* **337**, 519–525 (1989).
25. Buszewski, B. & Noga, S. Hydrophilic interaction liquid chromatography (HILIC)—a powerful separation technique. *Anal. Bioanal. Chem.* **402**, 231–247 (2012).

26. Bell, D. S. Retention and Selectivity of Stationary Phases Used in HILIC. Available at: <http://www.chromatographyonline.com/retention-and-selectivity-stationary-phases-used-hilic>. (Accessed: 16th September 2018)

VITA

RACHEL ELIZABETH JACOBSON

EDUCATION

Purdue University

West Lafayette, IN

Doctor of Philosophy (PhD), Analytical Chemistry

2018

- GPA 3.4, Advisor: Dr. Mary Wirth

Wisconsin Lutheran College

Milwaukee, WI

Bachelor of Science (BS), Chemistry

2014

- GPA 3.6, Cum laude, Dean's List

RESEARCH EXPERIENCE

Research Assistant, Purdue University

2014 - current

Improved manufacturing method for proprietary LC columns as team member resulting in journal cover page and new patent

- Previously, stationary phase was prepared via radical polymerization before packing into column. We grew the stationary phase after packing particles inside LC column.
- Method became standard LC column production method in our lab
- Assisted with further improvements for commercialization at startup, BioVidria
- 4x more columns pass QC tests
- Packed bed lifetime improved >100%

Reduced analysis time of antibody drug glycosylation by 99% in partnership with Genentech (2 days to 35 min)

- UHPLC-MS assay allows us to reduce loss of high-value drug batches by changing growth conditions
- Managed project; collaborated with colleagues; held monthly meetings with external stakeholders

Held leadership roles within lab

- Onboarded, trained, and collaborated with grad student colleagues
- Supervised REU (NSF-funded summer research) and school-year undergraduates

Founder / Lab Manager of iGEM Team, Wisconsin Lutheran College

2011 - 2013

Founded genetic engineering team for competition sponsored by MIT.

- Wrote successful funding grant; procured lab space; collaborated on project design; recruited and trained new members

Presented talk and poster at North American competitions.

- 2012: Designed plasmid to transfect heart stem cell line to aid induction factor research
- 2013: Engineered probiotic to secrete cellulose-degrading enzymes, lowering livestock feed costs

Silver commendation awarded after only two years. Appeared on cover of university magazine.

Teaching Assistant, Purdue University 2014 - 2016

Part of teaching team for general and advanced analytical chemistry (including honors).

- Led recitation and lab sections of 24 students. Graded homework and proctored exams. Prepared unknowns and standards using wet chemistry techniques

Generac (Science) Hall Team Leader & Chemistry Stockroom Worker, Wisc. Luth. Coll. 2012 - 2014

Stockroom provides necessities for course labs, class demonstrations, and research projects.

- Followed SOPs, performed organic synthesis, prepared and distributed chemicals and glassware for labs, used autoclave and dishwasher, and assisted with lab cleanup and equipment maintenance

Promoted to team leader after one year.

- Validated time cards, maintained inventory, ordered/received chemicals and equipment, and transferred chemical database from MS Excel to new LIMS inventory system

Library Assistant, Purdue University Libraries 2016

- Researched and wrote webpage content and video script on electronic lab notebooks
- Prepared homework for library science course, including Web of Science, Scopus, Knovel, ChemBioDraw, and Reaxys

Field research at Discovery Bay Marine Laboratory, Jamaica - study abroad 2012

Shifts in water temperature, invasive species, and human agricultural practices are affecting the diverse ecosystems of the island country.

- Studied changes in ecosystems including mangrove swamp, coral reefs, and tide pools
- Interviewed locals to learn about culture and history of the island

Undergraduate Research, Wisconsin Lutheran College 2013, 2014

A new professor was custom-building a Raman spectrophotometer to investigate hydration interfaces.

- Set up instrument and presented at undergraduate research conference

PAPERS, PATENT, AND PRESENTATIONS

1. **Jacobson RE**, Zhou Y, Wei B, Han G, Zhang Y, Sandoval W, Wirth MJ. HILIC-MS for rapid middle-down assay of IgG1 Fc glycosylation. Poster presented at: HPLC 2018; 2018 Jul 29-Aug 2; Washington, DC.
2. Wirth MJ, **Jacobson RE**, Alzate EJ. Tricks of the trade-off. The Analytical Scientist. 2018 Jun 23.
3. **Jacobson RE**, Zhou Y, Wei B, Zhang Y, Wirth MJ. HILIC separation of IgG1 glycoforms. Poster presented at: PITTCO; 2018 Feb 25-Mar 1; Orlando, FL.

4. **Jacobson RE**, Zhou Y, Wei B, Zhang Y, Wirth MJ. HILIC separation of IgG1 glycoforms. Poster presented at: Iota Sigma Pi 32nd Triennial Convention; 2017 Jul 6-9; Indianapolis, IN.
5. Huckabee AG, Yerneni C, **Jacobson RE**, Alzate EJ, Chen T-H, Wirth MJ. In-column bonded phase polymerization for improved packing uniformity. *J Sep Sci.* 2017;40:2170–2177. **Cover page.**
6. Wirth, MJ, Huckabee AG, **Jacobson RE**, Chen T-H. Uniformly dense stationary phase for chromatography. Patent application. 2017.

COMMUNITY OUTREACH, LEADERSHIP, AND COMMUNICATION

PCHMS (Purdue Chemists Helping Manage Stress), Purdue University 2017, 2018
Served on committee for improving mental health among grad student community.

- Contributed a committee goal of connecting struggling students to campus resources
- Collaborated with campus mental health experts and set up committee training

Volunteer Judge, Lafayette Regional Science and Engineering Fair 2016, 2017
Judged special awards with cash prizes.

Peer mentor, eMentoring program 2017, 2018
Met with mentee weekly over coffee and gave advice about advisors, courses, and work/life balance

President and Founder, Biotechnology Club, Wisconsin Lutheran College 2012, 2013
Every campus organization performs one service project per year.

- Organized service project and mobilized members to clean up local park

Started a weekly Journal Club to discuss academic articles.

- Organized sessions and led two discussions on scientific articles

Research Officer, Student Organization for Undergrad Research Collab. Efforts 2013, 2014

Club needed visibility to gather new members, so we hosted a snack for the student body.

- Served liquid nitrogen ice cream and homebrew root beer

Our university was a small institution, which had few research projects. Furthermore, students wanted to learn techniques for the new genetic engineering team. We bridged the gap by holding “lab practicals.”

- Designed and taught experiment to isolate chloroplasts from spinach
- Prepared experiments for other club leaders’ sessions

AV Media Services Worker, Wisconsin Lutheran College 2010 - 2012

- Interfaced directly with presenters to provide audio/video support; recorded and live streamed events

AWARDS

Advanced Management Principles (AMP) Program

2018

Chosen to attend Krannert's "mini-MBA" course (5/10 chemistry PhD candidates selected)

R.D. and Linda Peters Scholarship

2012 - 2014

Merit-based scholarship based on high GPA and financial need

Presidential Scholarship

2010 - 2014

Most selective merit scholarship; awarded to <20% of incoming freshmen based on ACT scores, GPA, and class rank

MEMBERSHIP IN PROFESSIONAL SOCIETIES**American Chemical Society (ACS)**

2015 - current

Iota Sigma Pi (ISP)

2015 - current

National honor society for women in chemistry

PUBLICATIONS

ISSN 1615-9306 · JSSCJ 40 (10) 2081–2314 (2017) · Vol. 40 · No. 10 · May 2017 · D 10609

JSS

JOURNAL OF
SEPARATION
SCIENCE

10 | 17

VOLUME **40**

The diagram illustrates two methods of polymer growth on silica particles for chromatography. On the left, 'Ex situ polymer growth' shows a silica particle (represented by a grid of blue circles) that is 'Coated with polymer before packing'. A cross-section shows a thick, uniform red polymer layer. On the right, 'In situ polymer growth' shows a silica particle 'Coated with initiator before packing'. A cross-section shows a thin red layer. A label 'Silica, initiator, polymer' points to the red layer. A red arrow labeled 'Added to packed column' points to the in situ method. The background of the diagram is a colorful, abstract pattern.

Ex situ polymer growth

In situ polymer growth

Added to packed column

Silica, initiator, polymer

Coated with polymer before packing

Coated with initiator before packing

Methods
Chromatography · Electroseparation

Applications
Biomedicine · Foods · Environment

www.jss-journal.com

WILEY-VCH

In-column bonded phase polymerization for improved packing uniformity

Alexis G. Huckabee | Charu Yerneni | Rachel E. Jacobson | Edwin J. Alzate |
Tse-Hong Chen | Mary J. Wirth 

Department of Chemistry, Purdue University, West Lafayette, IN, USA

Correspondence

Dr. Mary J. Wirth, Department of Chemistry, Purdue University, 560 Oval Drive, West Lafayette, IN 47907, USA.
Email: mwirth@purdue.edu

It is difficult to pack chromatographic particles having polymeric-bonded phases because solvents used for making a stable slurry cause the polymer layer to swell. Growth of the polymer inside the column (in situ) after packing was investigated and compared with conventional, ex situ polymer growth. The method of activators generated by electron transfer, along with atom-transfer radical polymerization, enabled polymerization under ambient conditions. Nonporous, 0.62 μm silica particles with silane initiators were used. Polyacrylamide films with a hydrated thickness of 23 nm in 75:25 water/isopropanol grew in 55 min for both in situ and ex situ preparations, and the same carbon coverage was observed. Higher chromatographic resolution and better column-to-column reproducibility were observed for in situ polymer growth, as evaluated by hydrophilic interaction liquid chromatography for the model glycoprotein, ribonuclease B. In situ polymer growth was also found to give lower eddy diffusion, as shown by a narrower peak width for injected acetonitrile in 50:50 acetonitrile/water. When columns were packed more loosely, bed collapse occurred quickly for ex situ, but not for in situ, polymer growth. The higher resolution and stability for in situ polymer growth is explained by packing with hard, rather than soft, contacts between particles.

KEYWORDS

glycoproteins, hydrophilic interaction liquid chromatography, packing, polymer, stationary phases

1 | INTRODUCTION

Polymeric materials have long been a mainstay in protein chromatography, including gel filtration [1], ion-exchange [2], antibody affinity [3], and hydrophobic interaction [4] resins. More recently monolithic columns formed in situ by cross-linked polymers enable high performance chromatography [5], and molecularly imprinted polymers are used in SPE columns [6]. Grafted bonded phases of polymer chains onto polymer or silica beads are increasingly being used. These have been enabled by the development of solution-phase atom-transfer radical polymerization (ATRP) [7], which allows for controlled molecular weight of linear polymer chains. ATRP was first used to make bonded phases for LC by attaching a silane initiator to silica gel, giving

surface-confined growth of polymer chains, and this was demonstrated for size-exclusion chromatography of proteins [8]. Since then, a host of bonded phases have been made for protein chromatography using ATRP, including metal affinity chromatography [9], ion chromatography [10], hydrophobic interaction chromatography [11], hydrophobic charge induction chromatography [12], thermally responsive bonded phases [13], HILIC [14], and lectin affinity chromatography [15]. Furthermore, ATRP-generated polymer surfaces are utilized in other analytical separations and applications [16]. The versatility of ATRP has made polymeric-bonded phases of broad interest in protein chromatography.

Uniform packing of chromatography columns is a long-standing problem, as it has been well documented that columns have radial heterogeneity [17]. The introduction of sonication during slurry-packing for submicrometer particles provides high radial uniformity in capillaries by promoting rapid transverse transport of particles during packing, shown by an eddy diffusion term of less than 10 nm [18]. Extremely long LC columns, 1 m in length, have shown improved eddy diffusion using sonication during slurry packing of 2 μm particles, giving reduced plate heights on the order of unity and plate number in excess of 50 000 [19]. The challenge of

Abbreviations: AGET, activators generated by electron transfer; ATRP, atom-transfer radical polymerization; Me₆TREN, Tris[2-(dimethylamino)ethyl]amine

Conflict of interest: Dr. Mary J. Wirth has a financial interest in a company, bioVidria, Inc., which has licensed the polymer growth technology described in this manuscript.

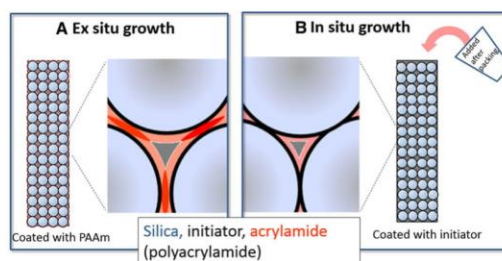


FIGURE 1 Depiction of the structural distinction between columns packed with particles that (A) had polymer grown before packing (ex situ) versus (B) particles containing initiator but no polymer, with the polymer subsequently grown on the particle surface inside the column (in situ)

uniform packing remains unmet for particles with polymer bonded phases. For example, 0.7 μm silica particles with bonded phases of linear polyacrylamide chains, when used for HILIC, gave a very high eddy diffusion term of 20 μm for a 2.1 mm I.D. column [14].

One reason for the difficulty in packing polymer-coated particles is a compromise in the choice of solvent for the slurry. A solvent that stably suspends the polymer-coated particles also causes the polymer layer to swell, which impedes tight packing because this layer must be compressed. This issue is illustrated in Fig. 1A. Decompression of the column after packing would cause the polymer layer at the contact points to re-swell, giving a lower packing density. Further, the cycling of swelling and contraction, due to pressurization/depressurization and cycling from the gradient, is possibly why columns with polymer-bonded phases have notoriously short lifetimes. The problems with polymer swelling would conceivably be avoided by first packing the particles when they have only the small-molecule initiator on the surface, then growing the polymer in situ by flowing the ATRP reagents through the packed column, as illustrated in Fig. 1B. For submicrometer particles, this would give the additional advantage of minimizing non-Newtonian rheology, which also impedes uniform packing. This can be understood from a study of slurries of 0.6 μm silica particles, which shows that these exhibit shear-thinning at high slurry concentration [20], which would augment transverse mass transport of the particles during packing for radial homogeneity. By contrast, when the same particles are coated with the hydrophilic polymer, PEG, these exhibit shear-thickening at high slurry concentration, which increases viscosity [20]. Both polymer swelling and increased slurry viscosity work against uniform packing of columns.

The purpose of this work is to test whether growth of the polymer-bonded phase inside the column, i.e., in situ, improves packing. In situ growth of an anionic copolymer on silica particles has very recently been used for capillaries, resulting in minimal swelling-shrinking behavior, a greater mechanical stability, and higher column efficiency than polymer-based monoliths [21]. The in situ and ex situ

columns are compared for the case of HILIC using a bonded phase of linear polyacrylamide chains. The previous method of ATRP for preparing HILIC columns [14], where a small amount of Cu(I) was used as catalyst, would be cumbersome for in situ polymer growth because oxygen-free conditions are required. In situ polymer growth is facilitated here by employing AGET ATRP (AGET is activators generated by electron transfer) [22]. AGET maintains a low concentration of Cu(I) through electrochemical reduction of Cu(II) by concentrated ascorbate, thereby buffering against loss of Cu(I) from atmospheric oxygen. Both in situ and ex situ polymer growth are carried out in this work using AGET ATRP with the same reagent composition and reaction time. The performance for each type of column packing is tested by HILIC of the model glycoprotein, ribonuclease B, which has a ladder of 5–9 mannose groups. Polymer growth, column variability and column stability are characterized, and the width of an unretained peak is monitored to assess packing homogeneity.

2 | MATERIALS AND METHODS

2.1 | Materials

Nonporous silica particles (750 nm) were purchased from Superior Silica (Mesa, AZ). Empty stainless-steel columns (2.1 mm I.D., 30 mm length), reservoirs (4.6 mm I.D., 150 mm), and frits (0.5 μm pore diameter) were purchased from Isolation Technologies (Middleboro, MA). Stainless-steel tubing, ferrules, and internal nuts were all purchased from Valco Instruments (Houston, TX). Methyltrichlorosilane and [(chloromethyl)phenylethyl]trichlorosilane (Gelest, Morrisville, PA), acrylamide, sodium ascorbate, Tris[2-(dimethylamino)ethyl]amine (Me_6TREN), acetonitrile, TFA, and Ribonuclease B (Sigma-Aldrich, St. Louis, MO), and copper(II) chloride (Acros Organics, Morris Plains, NJ) were used. All protein samples were prepared in ultrapure water at a concentration of 1.0 mg/mL.

2.2 | Silylation of particles

The silica particles were calcined at 600°C for 12 h, then annealed at 1050°C for 3 h, and rehydroxylated overnight in 0.1 M HNO₃. Particles were then rinsed in ultrapure water and dried in a 60°C vacuum oven. SEM showed that the particles decreased in diameter to 0.62 µm from the heating steps. The particles were suspended in dry toluene by sonication and modified with a 2% v/v [(chloromethyl)phenylethyl]trichlorosilane solution. The particles were allowed to react overnight and stirred with a stir bar. After reaction, the particles were rinsed three times with dry toluene, and then dried for 2 h in a 120°C oven to condense the siloxane bonds.

2.3 | Ex situ AGET ATRP

In a 25 mL round bottom flask, 500 mg of silylated particles and 4.4 g acrylamide were suspended together by sonication in 20 mL of 75:25 H₂O/IPA (v/v). Two other solutions were made: a copper solution containing, 40 mg copper(II) chloride and 80 µL Me₆TREN, and a solution containing 20 mg sodium ascorbate. These were also prepared in 2.5 mL of 75:25 H₂O/IPA. Afterwards, the copper/Me₆TREN solution was added to the suspension, followed by the sodium ascorbate solution; this vessel was left to react for 55 min under sonication. The particles were then rinsed three times with water and dried in a vacuum desiccator at room temperature to allow weighing. Finally, 154 mg of particles were suspended in 75:25 water/IPA and packed into 2.1 mm × 30 mm stainless-steel columns under sonication using a high pressure pump (Laboratory Alliance of Central New York, LLC, Syracuse, NY).

2.4 | In situ AGET ATRP

A solution containing the same reaction solution as for ex situ polymerization was prepared, but without the particles. The solution was poured into a plugged, 2.1 mm × 150 mm reservoir column. A 2.1 mm × 30 mm column was packed with silylated particles suspended in acetonitrile. The reservoir and column were connected in series. The reaction solution from the reservoir was pumped into the column starting at a high flow rate (200 µL/min) until the reaction mixture dripped from the end of the column. The flow rate was then lowered to 100 µL/min, and the polymerization reaction was allowed to proceed for the desired time period. After reaction, the column was rinsed with water for 10 min at 100 µL/min.

2.5 | Chromatography

HILIC separation of ribonuclease B was performed using a Waters Acquity UPLC I-Class system (Milford, MA) with UV absorbance detection. Solvent A was water with 0.1% TFA and solvent B was acetonitrile with 0.1% TFA. The gradient

was 75–60% B over 20 min. Absorbance wavelength was set to 215 nm. The flow rates were 100 µL/min and 150 µL/min. The column temperature was 30°C and the injection volume was 2 µL.

3 | RESULTS AND DISCUSSION

To monitor in situ polymer growth, the column backpressure was recorded as a function of time while the reagent solution of acrylamide monomer and catalyst were continuously flowed through the column. A plot of column backpressure versus time during polymer growth is provided in Fig. 2A. There is an initial dip because the initial flow rate was set to 200 µL/min to fill the entire length of the column quickly, and after 1 min, the flow rate was switched to 100 µL/min in anticipation of the increase in backpressure. Since the column dead volume is 50 µL, the reagent fills the column in only 15 s to give uniform reaction conditions along the length of the column during the 55 min growth time. The increase in backpressure over the course of the 55 min reaction time is shown to be considerable, changing from 10 000 to 17 000 psi. The 55 min reaction time is the same as that used for the particles coated ex situ. Columns were made for varying reaction time, and the HILIC separation of the ribonuclease B glycoforms is shown for the cases of 20, 40, and 55 min reaction times in Fig. 2B, C and D, respectively. These establish that significantly shorter reaction times are not feasible. Consistent with previous results, a sufficiently thick polymer is needed [14].

The backpressure increase in Fig. 2A is a consequence of the decrease in porosity caused by the growth of the polymer. One can calculate this decrease in porosity over time using the Kozeny–Carman equation.

$$\frac{P}{L} = \frac{180 \cdot \eta}{d_p^2} \cdot \frac{(1 - \epsilon)^2}{\epsilon^3} \cdot \frac{Q}{\pi r^2} \quad (1)$$

The porosity is ϵ , the volume flow rate is Q , the column radius is r , and all other variables have their usual meanings. The viscosity of the 75:25 water/IPA (v/v), which converts to a mole fraction of 0.925 water, is 1.1 mPa·s [23]. Equation (1) is strictly true if the particles are spheres of diameter, d_p , which is not exactly the same as spheres of d_p with a thin coating, so it is assumed that the polymer is thin compared to the particle diameter. Figure 3A gives a plot of the calculated porosity as a function of time, showing that it decreases from an initial value of 0.36 to 0.31 at the end of the reaction.

The decrease in porosity for the growing polymer can be used to estimate the polymer thickness through the relation between the hydrodynamic radius of the fluid channel and the porosity.

$$r_{\text{hyd}} = \frac{d_p}{3} \cdot \frac{\epsilon}{(1 - \epsilon)} \quad (2)$$

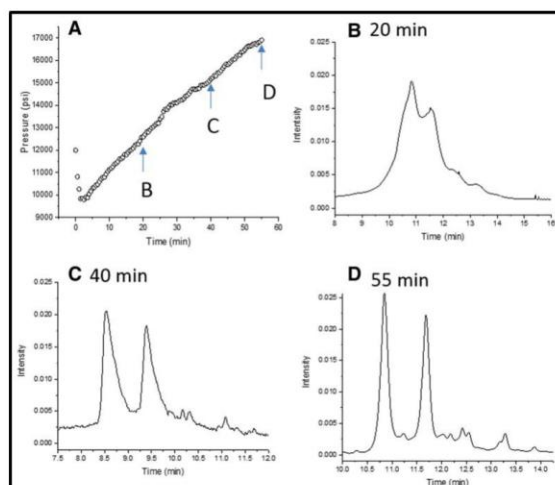


FIGURE 2 Effect of polymer growth time on the HILIC chromatogram of ribonuclease B. (A) Increase in backpressure during in-column polymer growth over 55 min. Pressure drop over the first 2 min is caused by a step-decrease in flow rate from 200 $\mu\text{L}/\text{min}$, for filling the column with reagent, to 100 $\mu\text{L}/\text{min}$ during the reaction. The solvent is 25:75 IPA/water. (B, C, D) Chromatograms for growth times of 20, 40 and 55 min, respectively. The gradient 75–60% acetonitrile in water, with 0.1% TFA, over 20 min at 100 $\mu\text{L}/\text{min}$, 30°C, injection volume 2 μL , and detection at 215 nm

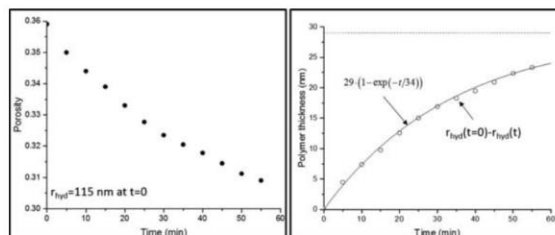


FIGURE 3 (A) Calculated porosity and (B) calculated polymer thickness during in situ growth. These graphs are derived from the pressure versus reaction time data in Fig. 2A through the Kozeny–Carman and hydrodynamic radius equations in the text

The initial hydrodynamic radius, i.e., before polymer growth, is 115 nm. After the polymer has grown for 55 min, the final hydrodynamic radius is calculated to be 92 nm. The difference between the two numbers is the polymer thickness. Figure 3B shows the increase in calculated polymer thickness with reaction time, reaching a thickness of 25 nm after 55 min. This is less than 10% of the particle radius, so the application of the model is reasonable. It is noted that the polymer thickness would change with solvent. Since the AGET ATRP reaction is conducted in more aqueous conditions, the polymer is expected to be more swollen, giving a higher backpressure compared to the less aqueous conditions of HILIC.

Microanalysis of the packing media showed that the carbon loading by mass is 2.0% for both ex situ and in situ polymerization. This means that materials with the same surface

coverage are being compared. One can estimate the density of silica on the surface for the in situ polymer growth. Since SEM showed the silica particles to have a final diameter of 0.62 μm after processing, and the coverage of nitrogen, which neglects the initiator layer, is $0.53 \pm 0.01\%$, then the molar coverage of acrylamide monomer is 86 $\mu\text{mol}/\text{m}^2$, based on a density of 2.2 g/cm^3 for silica. This is 23% of the density of liquid acrylamide. Since non-cross-linked polyacrylamide can swell in water to as much as 10 times its volume in methanol [24], one can presume that water takes account for the large hydrated volume of the polymer layer. The nonlinearity of the polymer growth in Fig. 3B is thus not attributed to steric hindrance; instead, it is owed to radical termination, which is likely from the high catalyst concentration. Whether a more linear polymer growth, or a longer growth

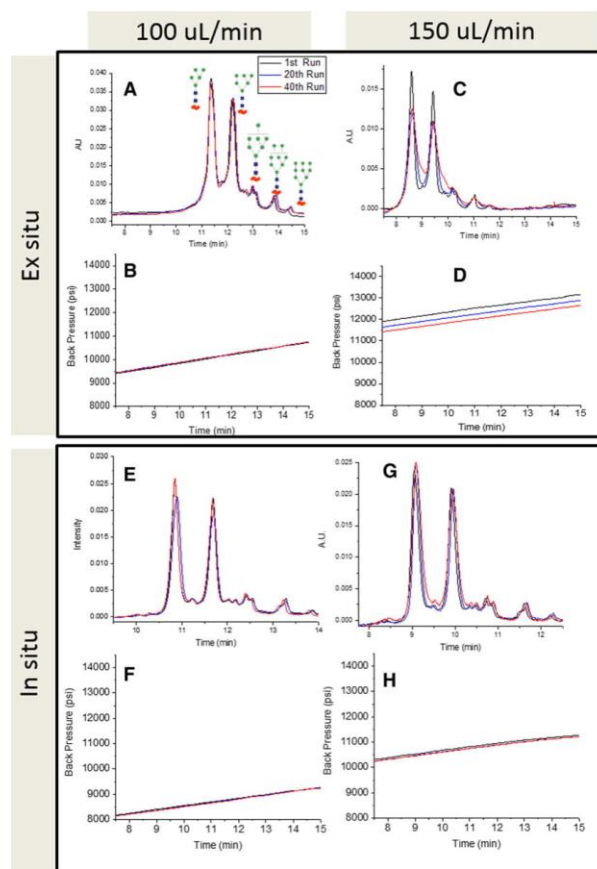


FIGURE 4 HILIC data for ribonuclease B and the corresponding plots of backpressure during the gradient elutions. 40 runs were done for each panel, which show the runs for the 1st, 20th, and 40th runs. The flow rates listed regard the chromatographic separations. (A) HILIC for ex situ growth with a flow rate of 100 $\mu\text{L}/\text{min}$ and (B) the corresponding backpressure. (C) HILIC for ex situ growth with a flow rate of 150 $\mu\text{L}/\text{min}$ and (D) the corresponding backpressure. (E) HILIC for in situ growth with a flow rate of 100 $\mu\text{L}/\text{min}$ and (F) the corresponding backpressure. (G) HILIC for in situ growth with a flow rate of 150 $\mu\text{L}/\text{min}$ and (H) the corresponding backpressure. The gradient was the same as in Fig. 2

time, improvements in HILIC will be investigated in subsequent work, but the quality of the separation in Fig. 2D is comparable to previous results.

Among the multiple columns produced by ex situ growth conditions, more variability in resistance to flow was exhibited compared to in situ grown columns. Columns with lower resistance exhibited less long-term stability for the ex situ case, but not for the in situ case. This is illustrated in Fig. 4. This figure has a high information content, and the first feature to be considered is that most columns were tightly packed, limiting the flow rate to 100 $\mu\text{L}/\text{min}$. More tightly packed columns could not reach as high of a flow rate and

had a shorter t_0 . Tight versus loose packing seems to be happenstance. For one such column, the HILIC chromatogram for ribonuclease B is shown in panel A for ex situ polymerization, showing a good quality separation. The five glycoforms are clearly visible, and the resolution is competitive or better than the commercial columns studied previously [14]. This same panel shows a sampling of replicates: the 1st, 20th, and 40th runs, and these line up well, revealing that the stability exceeds 40 runs. A graph of the column backpressure during the gradient is provided below in panel B, establishing that column resistance is constant from run to run. Backpressure rises during the HILIC separation as the increasing

proportion of water increases the viscosity of the mobile phase. The chromatogram for a more loosely packed column made by *ex situ* polymerization is shown in panel C, where the flow rate was 150 $\mu\text{L}/\text{min}$. The data show that the quality of the separation was initially high, but the quality degraded significantly over the course of 40 runs. Panel D shows the backpressure during the gradient elution. The entire curve also dropped over the course of the 40 runs. The column failure is thus associated with decreasing resistance to flow. This indicates bed collapse, i.e., the particles moved to open lower resistance channels or some polymer was lost to increase porosity. The two columns initially gave similar resolution, they differed only in how tightly the particles were packed. It is noted that the more loosely packed columns did not fail over these time frames at the lower flow rate and pressure, hence it is a combination of loose packing and high compression that causes column failure. Tighter packing helps stability, presumably by locking the particles in place.

Figure 4 also presents HILIC data for *in situ* polymer growth. Panels E and F show, respectively, the chromatograms for the more tightly packed column and the backpressure versus time during the gradient separation. The chromatograms and backpressure curves again line up for the 40 runs. For the more loosely packed column made by *in situ* polymerization, the stability is now shown to be higher. Panels G and H show that there is minimal degradation of the quality of separation after 40 runs, and the backpressure did not change over 40 runs. This indicates that the bed and the polymer remain intact despite the loose packing for the case of *in situ* polymerization. This supports the notion that solid contacts between particles, depicted in Fig. 1, enhance column stability.

One way of interrogating bed collapse for loosely packed columns is to measure the profile of an unretained peak. This was done by injecting acetonitrile into 50:50 water/acetonitrile and eluting isocratically. The refractive index change gives a negative going peak. Figure 5 provides the results. In Fig. 5A, the unretained peak profile is shown for the *in situ* polymerization, but before the polymer is grown. This allows a subsequent determination of how much the polymer affects uniformity of the flow paths through the

column. Figure 5B shows that the peak width, measured by the full-width at half-maximum (FWHM) is the same before and after *in situ* polymerization, 7 μL , indicating that the polymer growth does not significantly affect uniformity of flow through the column. Comparing panels 5A and B also shows that the mobile phase volume decreased with polymerization, as expected. Panel B shows that the mobile phase volume increased slightly, by 3 μL , after 40 runs, perhaps due to loss of polymer, but the peak width remained the same, indicating that the flow paths remained homogeneous. For the case of *ex situ* polymerization, panel C shows, for the first run, the mobile phase volume was virtually identical to that of *in situ* polymerization, but the peak width was somewhat wider, 9 μL . This is a manifestation of the difficulty in packing particles after they have been polymerized. Panel C also shows that after the 40 runs, the peak width became significantly wider, 13 μL , indicating that the flow paths became more heterogeneous. The mobile phase volume becomes smaller, indicating that wider channels were opened. This interpretation is supported by the column backpressure dropping, as was shown in Fig. 4D. The smaller mobile phase volume and greater heterogeneity of flow paths signal the onset of bed collapse, consistent with the degradation of the chromatographic behavior for this column. Minimizing bed collapse may be achieved by lowering the flow rate for loosely packed *ex situ* columns.

To assess column-to-column reproducibility of the *in situ* versus *ex situ* polymerization, eight columns were made by each method. A different batch of particles was used for each *ex situ* column presented here. Studies (not shown) of columns made with the same batch of particles showed as much variability. The chromatographic behavior of the 16 columns is shown in Fig. 6. In Fig. 6A and B, the best three columns are compared for *ex situ* and *in situ* polymer growth. This shows that the *in situ* growth results in better resolution. The widths of the unretained peaks, discussed earlier, are much narrower than the protein peaks, hence the packing homogeneity is not responsible for the improved resolution. It is possibly due to the polymer density being uniform for *in situ* growth, as opposed to the compressed polymer layer near particle contacts for *ex situ* growth. Figure 6C and D compare the other five columns. For *ex situ* growth, three of the five

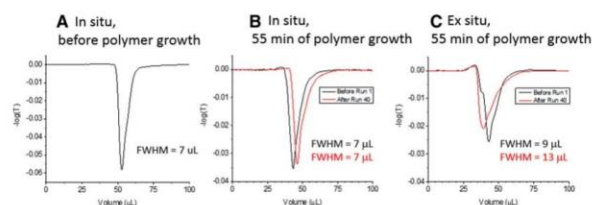


FIGURE 5 Profiles of unretained peaks for three different columns (A) column packed with particles bearing only initiator, (B) same column as A but after 55 min of polymer growth, also same column as in Fig. 4G, and (C) column packed with particles polymerized *ex situ* for 55 min, also same column as in Fig. 4C. In each case, 2 μL of pure acetonitrile was injected into a mobile phase of 50:50 acetonitrile/water and eluted isocratically, with a flow rate 150 $\mu\text{L}/\text{min}$

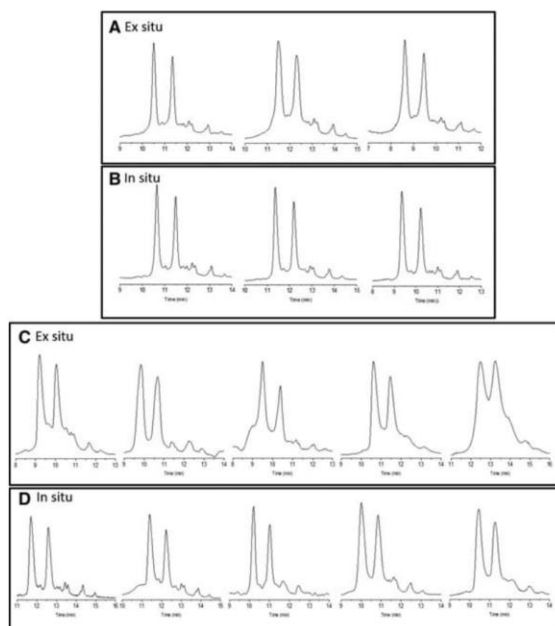


FIGURE 6 Chromatograms of ribonuclease B for the best three of eight columns made by (A) ex situ and (B) in situ polymer growth. Chromatograms for the remaining five of eight columns made by (C) ex situ and (D) in situ polymer growth. The gradient was the same as in Figs. 2 and 4

columns in Fig. 6C have unacceptably low resolution. These show that the quality is more variable for the ex situ growth. For the in situ growth, the worst column is comparable to the commercial columns previously studied [14]. Improvements can be made for the in situ growth, which gives a 50% yield, with four of the eight columns giving high resolution. Most notably, optimization of the packing process, as well as the AGET ATRP conditions, might improve resolution.

4 | CONCLUDING REMARKS

The problem of preparing stable, reproducible columns with a polyacrylamide bonded phase for HILIC of intact proteins is addressed by growing the polymer-bonded phase in the column after the solid particles are packed. This in situ growth is shown to give a better HILIC stationary phase, in addition to improvements in stability and reproducibility. The use of the AGET ATRP reaction scheme facilitates in situ growth by removing the necessity of maintaining an oxygen-free environment for the Cu(I) catalyst. The inherent slowness of the reaction is overcome by use of a higher Cu(I) concentration. This gives some radical termination, but is able to generate a polymer thickness estimated to be 23 nm in 75:25 v/v water/IPA after a 55 min reaction time. The methodology can

presumably be adapted to other types of polymeric-bonded phases made by radical polymerization.

ACKNOWLEDGMENT

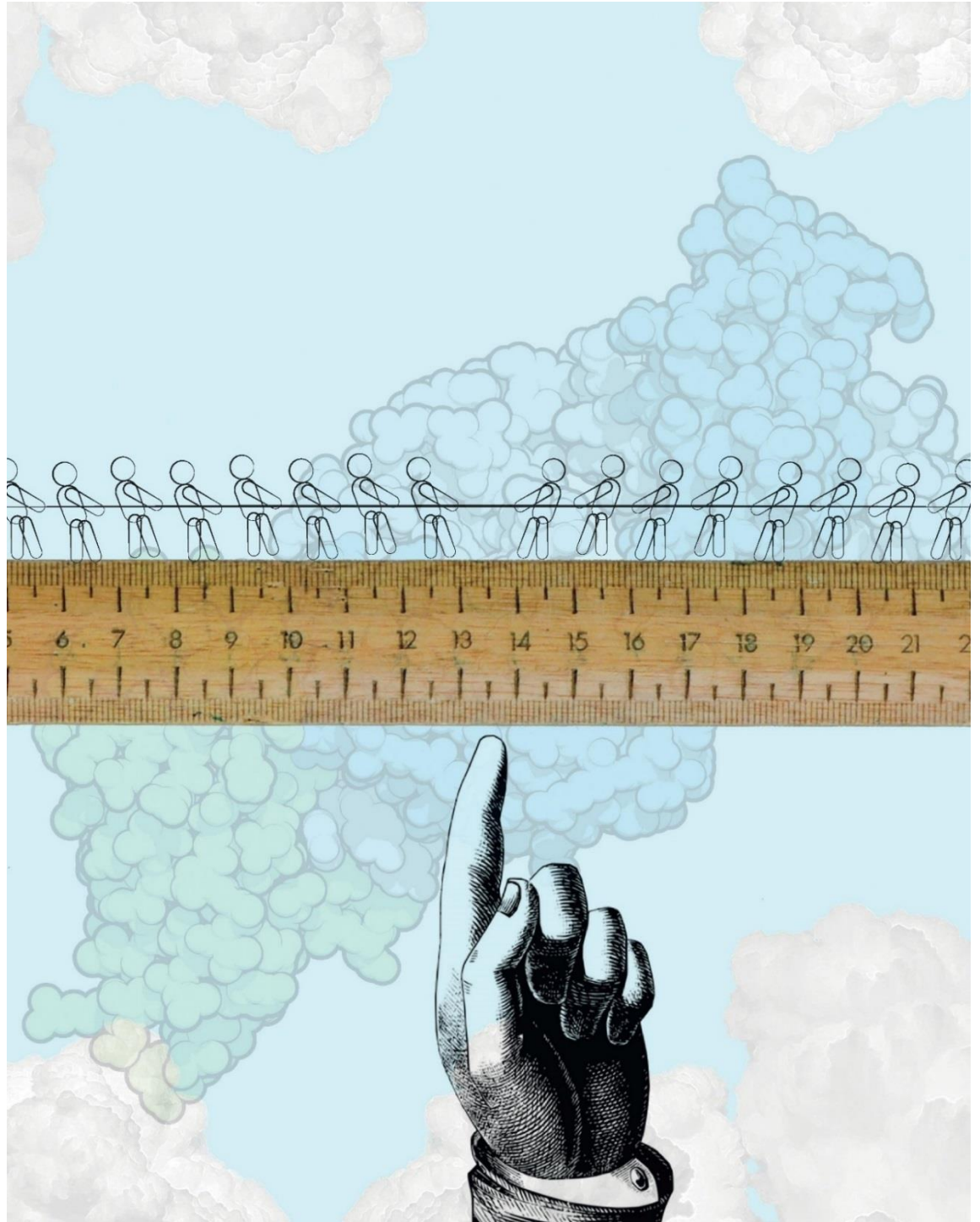
This work was supported by NIH under grant R01GM101464.

REFERENCES

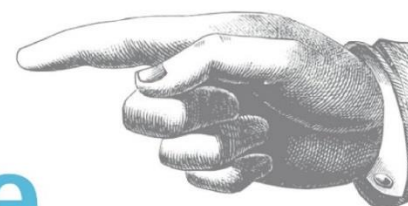
- Williams, T., Gel permeation chromatography: a review. *J. Mater. Sci.* 1970, 5, 811–820.
- Stein, A., Kiesewetter, A., Cation exchange chromatography in antibody purification: pH screening for optimised binding and HCP removal. *J. Chromatogr. B Analyt Technol. Biomed. Life Sci.* 2007, 848, 151–158.
- Fahrner, R. L., Blank, G. S., Zapata, G. A., Expanded bed protein affinity chromatography of a recombinant humanized monoclonal antibody: process development, operation, and comparison with a packed bed method. *J. Biotechnol.* 1999, 75, 273–280.
- Mata-Gomez, M. A., Yaman, S., Valencia-Gallegos, J. A., Tari, C., Rito-Palmares, M., Gonzalez-Valdez, J., Synthesis of adsorbents with dendronic structures for protein hydrophobic interaction chromatography. *J. Chromatogr. A* 2016, 1443, 191–200.
- Svec, F., Quest for organic polymer-based monolithic columns affording enhanced efficiency in high performance liquid chromatography separations of small molecules in isocratic mode. *J. Chromatogr. A* 2012, 1228, 250–262.
- Sarafraz-Yazdi, A., Razavi, N., Application of molecularly-imprinted polymers in solid-phase microextraction techniques. *TrAC Trends Anal. Chem.* 2015, 73, 81–90.

7. Patten, T. E., Xia, J. H., Abernathy, T., Matyjaszewski, K., Polymers with very low polydispersities from atom transfer radical polymerization. *Science* 1996, 272, 866–868.
8. Huang, X. Y., Wirth, M. J., Surface-initiated radical polymerization on porous silica. *Anal. Chem.* 1997, 69, 4577–4580.
9. McCarthy, P., Chattopadhyay, M., Millhauser, G. L., Tsarevsky, N. V., Bombalski, L., Matyjaszewski, K., Shimmin, D., Avdalovic, N., Pohl, C., Nano-engineered analytical immobilized metal affinity chromatography stationary phase by atom transfer radical polymerization: separation of synthetic prion peptides. *Anal. Biochem.* 2007, 366, 1–8.
10. Schwellenbach, J., Kosiol, P., Solter, B., Taft, F., Villain, L., Strube, J., Controlling the polymer-nanolayer architecture on anion-exchange membrane adsorbers via surface-initiated atom transfer radical polymerization. *React. Funct. Polym.* 2016, 106, 32–42.
11. Shen, Y., Qi, L., Wei, X. Y., Zhang, R. Y., Mao, L. Q., Preparation of well-defined environmentally responsive polymer brushes on monolithic surface by two-step atom transfer radical polymerization method for HPLC. *Polymer* 2011, 52, 3725–3731.
12. Liu, T., Lin, D. Q., Wu, Q. C., Zhang, Q. L., Wang, C. X., Yao, S. J., A novel polymer-grafted hydrophobic charge-induction chromatographic resin for enhancing protein adsorption capacity. *Chem. Eng. J.* 2016, 304, 251–258.
13. Kanazawa, H., Okano, T., Temperature-responsive chromatography for the separation of biomolecules. *J. Chromatogr. A* 2011, 1218, 8738–8747.
14. Zhang, Z., Wu, Z., Wirth, M. J., Polyacrylamide brush layer for hydrophilic interaction liquid chromatography of intact glycoproteins. *J. Chromatogr. A* 2013, 1301, 156–161.
15. Lazar, J., Park, H., Rosencrantz, R. R., Boker, A., Elling, L., Schnakenberg, U., Evaluating the thickness of multivalent glycopolymer brushes for lectin binding. *Macromol. Rapid Commun.* 2015, 36, 1472–1478.
16. Jain, P., Baker, G. L., Bruening, M. L., Applications of polymer brushes in protein analysis and purification. *Annu. Rev. Anal. Chem.* 2009, 2, 387–408.
17. Guiochon, G., Farkas, T., Guan-Sajonz, H., Koh, J. H., Sarker, M., Stanley, B. J., Yun, T., Consolidation of particle beds and packing of chromatographic columns. *J. Chromatogr. A* 1997, 762, 83–88.
18. Wei, B. C., Rogers, B. J., Wirth, M. J., Slip flow in colloidal crystals for ultraefficient chromatography. *J. Am. Chem. Soc.* 2012, 134, 10780–10782.
19. Godinho, J. M., Reising, A. E., Tallarek, U., Jorgenson, J. W., Implementation of high slurry concentration and sonication to pack high-efficiency, meter-long capillary ultrahigh pressure liquid chromatography columns. *J. Chromatogr. A* 2016, 1462, 165–169.
20. Zaman, A. A., Bjelopavlic, M., Moudgil, B. M., Effect of adsorbed polyethylene oxide on the rheology of colloidal silica suspensions. *J. Colloid Interf. Sci.* 2000, 226, 290–298.
21. Ren, H., Zhang, X., Li, Z., Liu, Z., Li, J., Silica-supported polymeric monolithic column with a mixed mode of hydrophilic and strong cation-exchange interactions for microcolumn liquid chromatography. *J. Sep. Sci.* 2017, 40, 826–833.
22. Jakubowski, W., Matyjaszewski, K., Activator generated by electron transfer for atom transfer radical polymerization. *Macromolecules* 2005, 38, 4139–4146.
23. Pang, F. M., Seng, C. E., Teng, T. T., Ibrahim, M. H., Densities and viscosities of aqueous solutions of 1-propanol and 2-propanol at temperatures from 293.15 K to 333.15 K. *J. Mol. Liq.* 2007, 136, 71–78.
24. Li, A., Ramakrishna, S. N., Kooij, E. S., Espinosa-Marzal, R. M., Spencer, N. D., Poly(acrylamide) films at the solvent-induced glass transition: adhesion, tribology, and the influence of crosslinking. *Soft Matter* 2012, 8, 9092–9100.

How to cite this article: Huckabee AG, Yerneni C, Jacobson RE, Alzate EJ, Chen T-H, Wirth MJ. In-column bonded phase polymerization for improved packing uniformity. *J Sep Sci.* 2017;40:2170–2177. <https://doi.org/10.1002/jssc.201601376>



Tricks of the Trade -Off



The detailed characterization of post-translational protein modifications relies on performance improvements in both HPLC and MS. But how do we strike a balance between LC resolution and MS sensitivity?

By Mary J. Wirth, Rachel E. Jacobson and Edwin Jhovany Alzate Rodriguez

It's an unfortunate fact that the best conditions for chromatographic resolution are those least conducive to high sensitivity in mass spectrometry. Specifically, ion-pairing agents or high salt concentrations are the basis for improved resolution in chromatography – but they are the bane of mass spectrometry. Reversed-phase liquid chromatography with mass spectrometry has arguably been the most successful

marriage between HPLC and MS, because acidic modifiers that avoid ion-pairing have been a tolerable compromise. Other separation modes fare worse, including hydrophilic interaction liquid chromatography (HILIC) and hydrophobic interaction chromatography (HIC). Here, we present new strategies that make HPLC-MS work with less compromise in HILIC and HIC modes.



HILIC into shape

HILIC (for the uninitiated, a type of normal-phase chromatography based on hydrophilicity, where the mobile phase is acetonitrile/water and the stationary phase is a hydrophilic layer [1]) has attracted increased interest in recent years due to its ability to characterize protein glycosylation (sugars are very hydrophilic so retention is longer when the glycan has more sugar groups). Why is glycosylation of such interest to bioanalytical chemists? Two reasons: first, many biological therapeutics are glycoproteins and their effectiveness relies on having the same glycan sequence as the native human protein (2); second, most of the human proteome is comprised of glycoproteins, and aberrant glycosylation is a hallmark of cancer (3). Thus, improvements in speed and sensitivity in characterizing protein glycosylation could have a broad impact in medicine.

HILIC has high efficiency and compatibility with MS for glycans but lower resolution and less MS compatibility for glycoproteins. The current workaround for characterizing protein glycosylation is to enzymatically release the glycans from the glycoproteins, label the glycans, and perform HILIC-MS. However, this process is slow and labor-intensive, and doesn't tell us where the glycan is attached.

We wanted to improve HILIC resolution for intact glycoproteins, and this led us to make a bonded phase that allows us to use HILIC-MS for the characterization of intact glycoproteins (Figure 1). In Figure 1a, conventional small-molecule bonded phases allow for electrostatic interactions between the positively charged protein and the negatively charged silanols on the silica surface. Our idea? We use a thick polymer layer to create a greater distance between the protein and the silica surface (Figure 1b). Since the electrostatic potential decays exponentially from the surface, distances longer than a few nanometers will screen the charge well. We have shown that this approach gives better resolution of an intact model glycoprotein, ribonuclease B, compared to commercial columns (4).

In making the bonded phase, the polymer layers are grown from the silica by atom-transfer radical polymerization. This technology was first demonstrated in 1997, where polymer chains were grown from surface-bound initiators on silica in a controlled way, largely avoiding polymer formation in solution (6).

A middle-down middle ground

The approach of using a thicker bonded phase allows the use of MS-compatible mobile phase modifiers. Trifluoroacetic

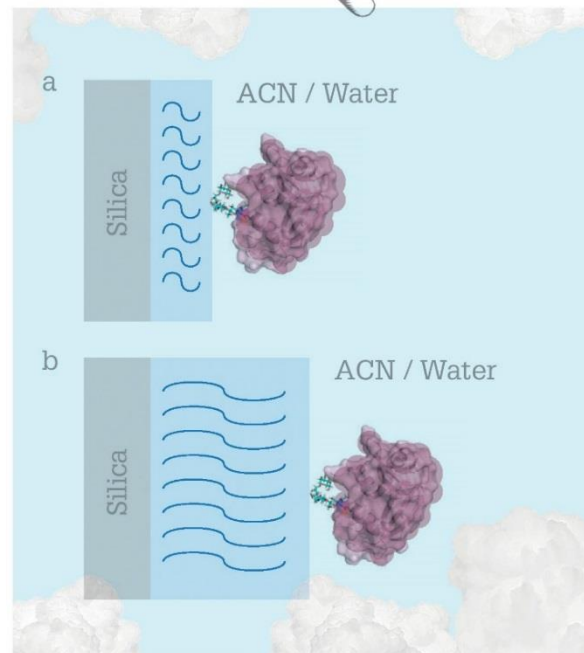


Figure 1. a) The conventional HILIC bonded phase is made of short, covalently bonded functional groups, and b) the co-polymeric bonded phase is thick enough to screen charges effectively. The glycan preferentially interacts with the hydrophilic bonded phase, as depicted. The structure of the glycoprotein, ribonuclease B, was adapted from Jayaprakash et al (7).

acid (TFA) is used as a mobile phase modifier for HILIC of glycoproteins because it is a strong enough acid to neutralize the most acidic silanols on the silica, but it greatly reduces sensitivity in MS because its anion forms adducts with proteins. Formic acid is compatible with mass spectrometry, but resolution in HILIC is lost because the pKa of formic acid is much higher than that of TFA, which makes the silica surface more charged. With a much thicker bonded phase, formic acid can be used with very little TFA because the surface charge is screened by the polymer.

To illustrate how much a polymeric bonded phase improves HILIC-MS, take a look at the chromatograms in Figure 2 for ribonuclease B. The change from 0.1 percent TFA to the MS-

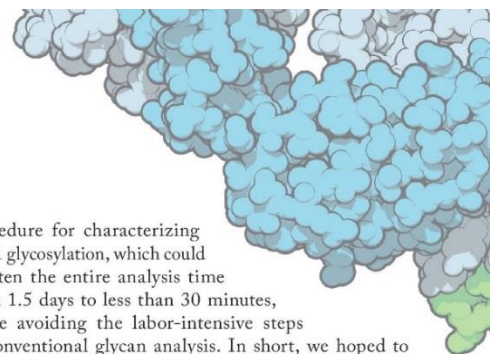
“The middle-down approach is performed in one vial, with fast reactions, and the contents can be directly injected into the column without further sample preparation”

compatible mobile phase of 0.1 percent formic acid plus 0.025 percent TFA results in a negligible change in resolution, but means that we can now consider using HILIC-MS on intact glycoproteins instead of the released glycans.

We collaborated with Genentech to test a middle-down

procedure for characterizing IgG1 glycosylation, which could shorten the entire analysis time from 1.5 days to less than 30 minutes, while avoiding the labor-intensive steps of conventional glycan analysis. In short, we hoped to enable rapid, automated monitoring of glycosylation during manufacturing, allowing for real-time adjustments (the two procedures are compared side-by-side in Figure 3). The middle-down approach is performed in one vial, with fast reactions, and the contents can be directly injected into the column without further sample preparation. Such an approach has been studied previously, but the HILIC separation did not provide sufficient resolution even with the use of TFA (5). Our HILIC columns provide the resolution needed to make this approach work (publication is pending so we can't share the data here) – and the resolution is maintained for 0.1 percent formic acid + 0.025 percent TFA.

In another application, we collaborated with scientists at Abbvie on HIC-MS of a model antibody–drug conjugate. This project might seem like an impossible dream, given that HIC



the micro-Chip Chromatography Company

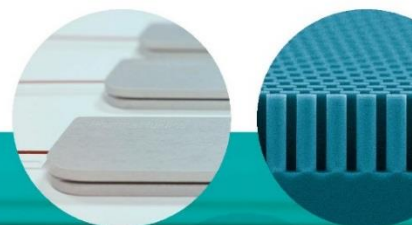
Changing the ART of analytical chromatography with μ PAC™ Pillar Array Columns:

These micro-Chip columns feature a perfectly-ordered separation bed of free-standing pillars ensuring:

- excellent separation power
- unprecedented reproducibility
- unrivalled robustness

Enhance the data productivity of your nano-LC/MS system for tiny, complex biological samples.

Discover our products on www.pharmafluidics.com or meet us at HPLC (July 29 - August 2, Washington DC, USA)



FOLLOW US

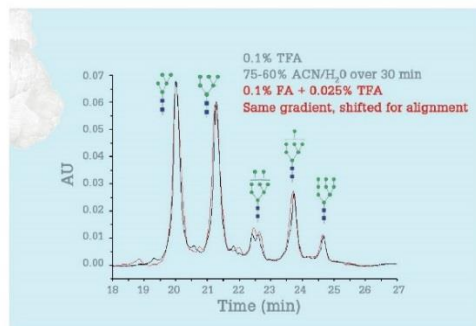

 42 Feature


Figure 2. HILIC separations using 0.1 percent TFA (black) and the MS-compatible modifier of 0.1 percent formic acid + 0.025 percent TFA (red).

“The most essential factor in commercialization is collaborating with potential customers.”

for such drugs currently requires a salt gradient containing a high concentration of sodium ions, but with the lessened electrostatic interactions, high resolution was maintained using low concentration ammonium formate for HIC-MS. We expect to publish on this soon, as well.

From collaboration to commercialization

We have commercialized this technology through bioVidria (www.biovidria.com), located in the Purdue Research Park. The HILIC and HIC columns, as well as RPLC column, are stainless steel, 50 mm × 2.1 mm, packed with 1.2 μm silica particles with the appropriate covalently bonded copolymer for the separation mode. The intellectual property is protected under an issued patent, US Patent 9,758,542, 2017, with international rights pending.

Commercializing the technology has been an adventure for us. Why? Academic research is directed toward the future, whereas commercialization has to survive in the present. To illustrate the dichotomy: the chromatographic resolution is better with submicron particles, but the variability of available frits prevents cost-effective production right now. Another illustration of the difference between academic research and commercial practicality? Polyacrylamide works great for HILIC-MS of intact proteins, but the acrylamide monomer is a neurotoxin that would have to be carefully weighed out in large quantities for reproducible and cost-effective bonded phases. Polyacrylamide swells, which gives high back-pressure and makes the particles fight back during high-pressure packing. It also degrades too fast for the customers' satisfaction. All of these problems matter little in basic research, but weigh heavily when bringing the technology to practice. The learning process has enabled us to develop a safe, cost-effective, high-performing copolymer for HILIC-MS.

The most essential factor in commercialization is collaborating with potential customers. Our collaborators at Genentech, Abbvie and Pfizer were valuable in developing our HILIC, HIC and RPLC columns, respectively.

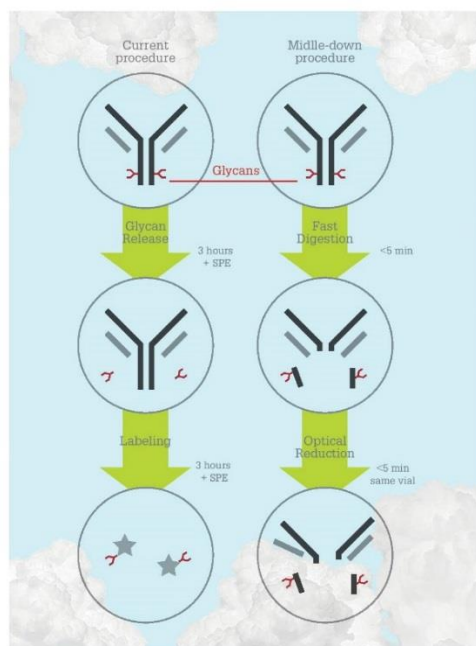
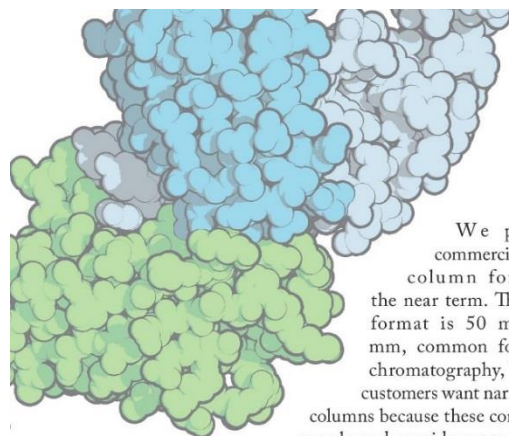


Figure 3. Comparing the current procedure for glycan analysis, where HILIC is performed on the released glycans, and the faster middle-down procedure where the Fc/2 fragment bearing glycans are generated simply by addition of reagents and separated by HILIC.

the Analytical Scientist



We plan to commercialize more column formats in the near term. The current format is 50 mm x 2.1 mm, common for protein chromatography, but many customers want narrower bore columns because these consume less sample and provide more sensitivity in mass spectrometry. We continue to explore new polymers and, on the basic research side, we are using capillaries and fluorescence imaging to understand the gradient elution process better, identifying where the broadening occurs so that we can design columns for even better separations in the future.

Mary J. Wirth is W. Brooks Fortune Distinguished Professor — Analytical Chemistry, and Rachel E. Jacobson and Edwin Alzate are doctoral candidates in the Department of Chemistry, Purdue University, Indiana, USA.

References

1. AJ Alpert, "Hydrophilic-interaction chromatography for the separation of peptides, nucleic-acids and other polar compounds", *J Chromatogr*, 499, 177–196 (1990).
2. A Zbigiang, "Therapeutic monoclonal antibodies: from bench to clinic", *J. Wiley & Sons: Hoboken, NJ*, (2009).
3. A Kirwan et al., "Glycosylation-based serum biomarkers for cancer diagnostics and prognostics", *Biomed Res Int*, [Epub] (2015).
4. Z Zhang et al., "Polyacrylamide brush layer for hydrophilic interaction liquid chromatography of intact glycoproteins", *J of Chromatogr A*, 1301, 156–161 (2013).
5. V D'Atri, "Hydrophilic interaction chromatography hyphenated with mass spectrometry: a powerful analytical tool for the comparison of originator and biosimilar therapeutic monoclonal antibodies at the middle-up level of analysis", *Anal Chem*, 89, 2086–2092 (2017).
6. XY Huang et al., "Surface-initiated radical polymerization on porous silica", *Anal Chem*, 69, 4577–4580 (1997).
7. NG Jayaprakash, A Surelia, "Role of glycosylation in nucleating protein folding and stability", *Biochem J*, 474, 2333–2347 (2017).





Sciencix

SERVING ROYALTY. EXCEEDING EXPECTATIONS. EVERY MOMENT.

- Provider of top brand HPLC instrumentation products
- Equivalent to corresponding OEM products
- Serving customers for over 30 years
- Reduce product repair expenses by 15% to 30%
- Lifetime Warranty on manufacturing defects

www.sciencix.com
800.682.6480
sales@sciencix.com

